UNIVERSITÉ DE STRASBOURG

MÉMOIRE

soumis en vue d'obtenir

L'HABILITATION À DIRIGER DES RECHERCHES

Spécialité : Physique Nucléaire

Présenté et soutenu publiquement

par

Kamila SIEJA

Le 08.12.2016

TITRE:

Shell model studies of exotic nuclei and their interest for nuclear astrophysics

devant le Jury composé de :

M. E. CAURIER	Garant	DRE CNRS	IPHC Strasbourg
M. B. GALL	Rapporteur	Professeur	Université de Strasbourg
Mme A. GARGANO	Rapporteur	Professeur	INFN Naples
M. S. HILAIRE	Examinateur	Expert Senior	CEA-DAM Arpajon
M. G. MARTINEZ-PINEDO	Examinateur	Professeur	TU Darmstadt
M. O. SORLIN	Rapporteur	DR CNRS	GANIL Caen

Contents

In this short synthesis, I present the research subjects I have explored after my PhD thesis, during two post-doctoral periods (GSI/TU Darmstadt, 2007-2009 and IPHC Strasbourg, 2009-2012) as well as during the four years of my work as chargeé de recherches CNRS (October 2012-present) in IPHC. It is during my first post-doc that I have begun to work on the physics of exotic nuclei using the large scale shell model techniques and I have started the collaboration with the shell model group in Strasbourg, as well as with the numerous experimental groups worldwide. I have continued these studies for the consecutive 9 years, mostly developing empirical effective interactions for shell model studies and exploring a wide range of nuclear structure subjects. In this synthesis I describe briefly only the major axes of the research of these recent years, leaving out some of the already accomplished projects (the complete list of publications is provided in Chapter 8) and preferring to give some room to unpublished results.

In the first chapter of this dissertation, to give a general view on the discipline and the related problems, I discuss the current status of the modern shell model and the recent progress in the microscopic derivations of effective interactions for such studies. Starting from Chapter 2, I make a concise review of my work concerning constructing empirical effective interactions in several model spaces and physics results that could have been obtained thanks to those developments. I discuss some of unpublished results and, in passing, ideas for future studies. This is the major part of my work which is illustrated by selected articles collected in Chapter 7.

In Chapter 3 I present major conclusions of different published studies based on the spin-tensor analysis of realistic and empirical effective interactions. Further, I discuss more widely the unpublished results concerning such analysis of both monopole and multipole Hamiltonians.

Finally, I present several SM applications of interest for astrophysics in Chapter 4, describing as before some of the unpublished observations and outlook for further studies in this direction.

More perspectives and ideas for future research are given in Chapter 5.

The document contains as well the complete list of publications (Chapter 8) and a detailed CV in Chapter 9.

Chapter 1

Current status of the modern shell model

Modern shell model, known as Configuration Interaction (CI) in quantum chemistry and condensed matter, is a way to find approximate solutions of the Schrödinger equation for a system with many interacting particles. The unknown wave function is approximated by a linear combination of many-body states (configurations) that are allowed to mix (interact) with each other in order to minimize energy. The solutions are obtained by diagonalization of the Hamiltonian matrix constructed in the many-body basis. The method provides the solutions to the Schrödinger equation to an arbitrary numerical precision. Its advantage with respect to other methods is that it is very general, can be applied to fermions and bosons, it gives the ground and excited states, is not limited to a single type of interaction. In practice however, the numerical complexity limits the usage of the shell model to systems with a restricted number of particles, i.e. $A \sim 12$ for the no-core shell model and several particles/holes in the core shell model approach in valence spaces above the pf-shell (for full space diagonalizations). As will be discussed in this synthesis, a lot of progress has been achieved recently in Strasbourg which allowed for the largest up-to-date diagonalizations of the SM Hamiltonian matrices. Historically, the Strasbourg shell model codes ANTOINE and NATHAN, conceived by Etienne Caurier, [1, 2] have opened new avenues for the diagonalization approaches. First diagonalizations in the full fp-shell have been achieved for the lower part of the shell using ANTOINE in Ref. [3], treating m-scheme dimensions of $\sim 2 \times 10^6$. Further, with the developments of the NATHAN code, all pf shell nuclei could have been calculated without truncation [4]. Nowadays, the non-public version of ANTOINE is the most powerful diagonalization code in our area. The largest diagonalizations have been attained recently in the Strasbourg group, in the studies of the island of inversion at $N = 40$ [5] using the $fpgd$ model space, light xenon isotopes in the gds model space [6] (matrices size in m-scheme $\sim 9 \times 10^9$) and recently, the deformed ^{72}Kr in the $fpgd$ valence space (unpublished, size of matrices $\sim 10^{10}$) on a single processor. Thanks to the work of Nowacki and Caurier, also parallel versions of these codes are used in the Strasbourg group [1, 5]. The pioneering no-core shell model calculations in very large spaces were as well achieved with the use of the ANTOINE code by Caurier et al.

[7]. The no-core version of ANTOINE is still used and appreciated, some developments of it (e.g. parallelization) have been also applied by the ab-initio community [8].

Since the appearance of the realistic nucleon-nucleon (NN) potentials, efforts have been made to use them in shell model calculations. As the high-precision NN potentials such as CD-Bonn [9] or Argonne [10] are strongly repulsive at short distances, in conventional approaches to shell model effective interactions, the strong-range repulsion was tamed by performing a ladder resummation of the NN potential to obtain a G-matrix [11]. Currently, the so-called V_{lowk} potentials are preferred [12], where the softening of the hard core is obtained by the decoupling of high and low modes in the momentum space. A recent review on the subject can be found in [13].

The advantage of the V_{lowk} over a conventional G-matrix for NN interactions is that it decouples the high- and low- energy modes and does not require inconvenient starting energy. In shell model practice however, as shown by Dufour and Zuker in [14] and again by Schwenk and Zuker in Ref. [15], there is no substantial difference in the final two-body matrix elements (TBME) to be used in actual calculations, independently on the starting potential (Bonn, Argonne, N3LO) and the method of renormalization (G-matrix, V_{lowk}). This is a good news as the link to phase shifts seems model independent and the many-body calculations give the same answer irrespective the details of the effective 2-body Hamiltonian. It is known from decades that microscopic effective Hamiltonians based on NN potentials do not provide correct saturation and fail to reproduce the spin-orbit closures (known as well as extruder-intruder (EI) shell closures, $N = 28, 50, 82, ...$) while may exaggerate the size of the harmonic oscillator ones. The blame for this was put on the absence of the three-nucleon (3N) forces. One can mention here the efforts of A.P. Zuker, who in Refs. [16, 17] proposed empirical ways to demonstrate the validity of such an assumption. With the arrival on the market of the no-core and Green-function calculations with 3N forces [18, 19] it has been proven in fully microscopic calculations that one has to go beyond the NN interaction.

The breakthrough in the treatment of 3N forces came with the developments of chiral Effective Field Theory (EFT). It has been realized that the scenario of low energy QCD is characterized by pions and nucleons interacting via a force governed by spontaneously broken approximate chiral symmetry. Thus chiral EFT allows for a systematic low momentum expansion known as chiral perturbation theory (ChPT). Contributions are analyzed in terms of powers of small momenta over a large scale $(Q/\Lambda_\chi)^\nu$, where Q is generic for a momentum (nucleon three-momentum or pion four-momentum) or pion mass and Λ_χ is the chiral symmetry breaking scale. The ChPT implies that nuclear forces emerge as a hierarchy controlled by the power ν of the expansion. The first non-vanishing 3N forces appear in this scheme at next-to-next-to leading order ($\nu = 3$), showing that they are weak compared to NN forces which start at $(Q/\Lambda_\chi)^0$.

The conventional approach of obtaining effective two-body shell model Hamiltonians in a valence space is the many-body perturbation theory (MBPT) which allows to include by perturbation the particle-hole excitations from the core to the valence space or scattering of the valence space particles to the orbitals outside the chosen model space (see Refs. [20, 21] for a review). In practice effective interactions are defined in terms of functions called Q-

boxes which contain all valence-linked diagrams of the perturbative expansion, typically up to second or third order. Iterative methods of Kuo-Kreciglowa [22] or Lee-Suzuki [23] are then used to determine the effective interaction.

Attempts to derive effective NN interactions for shell model studies with the contribution of chiral 3N forces using MBPT were undertaken recently [24], providing however not enough improvement with respect to the use of purely NN interactions, especially in the case of the pf-shell. The authors of. Refs. [25, 26] tried then to extend the classical model spaces to reach the agreement with experiment. This approach, however, is plagued by spurious center of mass (COM) excitations and an unphysical picture of nuclei emerges, where the 2^+ energies of closed shell nuclei arise in the absence of the shell gaps, due to the uncontrolled contributions of the COM Hamiltonian to the ground and to the excited states.

Only recently there has been some progress in the construction of effective interactions for SM calculations with 3N forces using non-perturbative methods. The first of such is the coupled cluster (CC) approach, which offers a resummation of MBPT diagrams, providing an infinite order approximation in selected cluster operators, usually single and double excitations (CCSD). Limiting the resummations to all terms that arise from single and double excitations, T_1 and T_2, defines the CC wave function $\psi_{CCSD} = exp(T_1+T_2)\psi_0$ which adds all the products like $T^2/2$ or T_1T_2 with respect to the shell model wave function. In fact, the CC theory at single and double excitation level contains contributions identical to those of second-order and third-order many-body perturbation theory. In a recent work an effective SM Hamiltonian with 3N forces has been obtained via CCSD resummation with perturbative corrections for the triple clusters [27]. The effective Hamiltonian obtained within CC approach with the inclusion of 3N components has been applied to oxygen and carbon nuclei, showing a fair agreement with data. However, there is so far no information on the rms deviation of such a Hamiltonian for the whole sd-shell and further improvements may be necessary in this scheme, e.g. incorporating the induced 3N forces.

The other promising approach is in-medium similarity renormalization group (IM-SRG). This method consist of a continuous unitary transformation $U(s)$, parameterized by a flow parameter s, that drives the Hamiltonian to the band- or block-diagonal form, which is accomplished by solving the flow equation. The in-medium approach means that the induced many-body operators are ordered with respect to a many-body reference state for each A-body system. In the case of SM interactions, a Hartree-Fock reference state is constructed for the core and the basis is split into particle and hole states. All matrix elements which couple core to excitations must be eliminated. The recent implementation of this method has been achieved with 3N forces at N2LO level and 3N forces induced by the evolution treated consistently [28]. Results have been presented for oxygen isotopes, showing that the IM-SRG Hamiltonian with the full 3N forces provides a good description of these nuclei.

Though the studies from Refs. [27, 28] are promising, they are still in the phase of developments and trials. Only sd-shell nuclei have been investigated so far and in practice, no effective Hamiltonians with the inclusion of 3N forces are available to the community. It seems as well that the chiral Hamiltonians, even with a proper inclusion of 3N forces,

fail to reproduce many-body observables without a readjustment of parameters in complex nuclei. For all that reasons, effective Hamiltonians based on NN interactions without 3N forces are still used in SM calculations, either with no further adjustments which works successfully in the vicinity of the closed cores, see e.g. Refs. [29, 30] or for deformed nuclei [31], or with empirical modifications to assure a proper propagation of s.p. energies with many-particle filling.

Since the appearance of the first shell model calculations, the experimental data were used to fit the sets of TBME, obtained e.g. with the surface δ interaction. Nowadays, to obtain high precision SM interactions, fits are performed starting from realistic NN potentials in which all TBME are treated as parameters using the linear combination (LC) method, see e.g. [32]. This way, the famous USD family of interactions was obtained [32, 33], as well as interactions for medium masses nuclei, like GXPF1A for the pf-shell [34], JUN45 for $f_{5/2}pg_{9/2}$ model space [35] or the unpublished GCN5082 in the gds model space from the Strasbourg group [36]. However, the Strasbourg group has been employing another approach to finding a suitable effective interaction. Thanks to the work of Dufour and Zuker [14, 37], it was understood that some TBME are more important than others and readjustments can be done in a way that keeps the starting NN interaction possibly close to its initial form. The decomposition into monopole Hamiltonian, which governs the shell evolution, and into multipole Hamiltonian (with the coherent terms shown to be the familiar pairing, quadrupole, octupole, etc.) allowed for readjustments of the Hamiltonians in regions where the numerical methods, such as LC method, are not feasible. Finding the physics behind the tables of numbers, that the shell model interactions are, revolutionized our understanding of physics and allowed a lot of insight into the mechanisms behind the shell evolution and established links between realistic Hamiltonian and the many-body observables. Applying monopole corrections to the realistic Hamiltonians effective interactions of high quality have been obtained for the pf-shell nuclei, i.e. KB3 [38] or more recently SDPF-U [39] in the $sd-pf$ shell, LNPS [5] in the $f_{5/2}pg_{9/2}d_{5/2}$ model space and the work continues for heavier and heavier systems, e.g. in the model spaces above ^{78}Ni [40] and ^{132}Sn [41] cores.

Currently one still has to rely on empirical, monopole tuned or entirely fitted interactions, and it will remain the method of choice for accurate studies of spectroscopy of exotic, open-shell nuclei at least for the next few years. It has been thus our purpose to provide realistic-based, high precision empirical Hamiltonians, without which the experimental results cannot be understood and which consist a precious benchmark for the ab-initio methods. In the next chapters of this dissertation I present shortly the recent progress in this domain and the wealth of physics results that could be obtained thanks to such developments, including a detailed analysis of realistic and adjusted interactions in terms of spin-tensor analysis (Chapter 3) and SM calculations of astrophysics interest (Chapter 4).

Chapter 2

Developments of empirical effective interactions for the LSSM studies of exotic nuclei

An important part of my research in nuclear structure has been devoted to derivations of empirical effective interactions for large scale shell model (LSSM) calculations and their applications to studies of shell evolution and structure of exotic nuclei, currently produced abundantly in the RIB facilities. Many of these subjects have been undertaken due to experimental needs and progress, and on the other hand, predictions have been made for the yet unobserved nuclei that wait for their confirmation in future experiments. As described in Chapter 1, the 2-body effective interactions based on realistic potentials fail to reproduce the observed monopole trends and shell closures. Therefore, an empirical approach has been engaged, where the monopole (and sometimes multipole) adjustments to the known data have been applied or the mechanisms known from other regions of nuclei have been incorporated to assure more viable monopole trends. Here I give a synopsis of the results obtained with such empirically-tuned interactions in several regions of nuclei. In the derivations of microscopic NN interactions the Oslo codes for renormalization and MBPT were employed [42] while ANTOINE and NATHAN Strasbourg codes were used for the many-body calculations throughout this work.

2.1 Initialization of calculations in the $r3g-r4h$ model space for exotic nuclei above ^{78}Ni

For the purpose of spectroscopic studies of exotic nuclei above ^{78}Ni core, I have developed an interaction in the valence space comprising proton $0f_{5/2}, 1p_{3/2}, 1p_{1/2}, g_{9/2}$ and neutron $1d_{5/2}, 2s_{1/2}, 1d_{3/2}, 0g_{7/2}, 0h_{11/2}$ orbitals outside the closed core of ^{78}Ni, which we denote hereafter $r3g-r4h$. It was based on the realistic CD-Bonn potential softened through the G-matrix approach and adapted to the model space by many-body perturbation techniques. The neutron-neutron and proton-proton parts were provided from the linear combination

fits to a large amount of data [36, 43] while the proton-neutron monopoles have been adjusted to reproduce the known trends in the shell evolution between ^{91}Zr and ^{101}Sn. An interesting aspect of this part of my work was to show, in Ref. [40], that the shell evolution between ^{91}Zr and ^{101}Sn is not given entirely by the tensor interaction, contrary to the earlier claims of Ref. [44]. Also our results of spin-tensor analysis of effective interactions in $sd-pf$ nuclei (discussed in the next Chapter) have shown that both the central and tensor parts are necessary to describe the evolution of spin-orbit gaps [45, 46]. The authors of Ref. [44] improved later their general monopole model by adding to it a Gaussian central part [47], which assured a better reproduction of the single-particle levels evolution, including those presented in Ref. [40].

The interaction has been conceived originally to the study of the mid-spin structures of neutron-rich fission products with $N = 54 - 56$: yttrium [48], strontium [49] and rubidium [50, 51] isotopes. It has further applied to the structure of zirconium isotopes [40] (see publications attached to the synthesis), demonstrating that for the description of these isotopes ^{78}Ni core is a much better choice than the previously used ^{88}Sr one. Recently, in collaboration with experimental groups in Germany and USA, we have also studied the transition from collectivity to single-particle modes in Zr and Sr chains from $N = 44$ to $N = 52$, via magnetic moments measurements. The interpretation I did showed that proton core excitations are important in ^{88}Sr, imposing it is a proton-soft core, probably even softer than ^{90}Zr. This work was highlighted as Editor's Suggestion in Phys. Rev. C [52].

Though the interaction was first built and tested for proton numbers around $Z = 38 - 40$, it appeared to be predictive also in very neutron rich nuclei close to the ^{78}Ni core. Recently, I have performed calculations for the $N = 53$ nuclei [53] where the theory could reproduce the systematics of their low lying states within dozens of keV agreement with experiment, predicting correctly the inversion of the $5/2^+$ and $3/2^+$ states in ^{89}Kr. A possible onset of deformation has been proposed as the origin of this behavior while a coexistence of collective and single-particle modes in ^{87}Se, similar to that known in neutron-rich copper isotopes [54], has been suggested by theory and awaits experimental confirmation. Also low lying structures of $N = 52 - 54$ isotones have been examined successfully in Refs. [55, 56, 57]. The calculations in Refs. [55, 56] have been performed by H. Sliwinska, PhD student in the shell model group in years 2013-2014. Those of Ref. [57] have been a part of the PhD project of K. Kolos (PhD in Orsay, 2012, currently post-doctoral researcher in USA) whom I tutored on shell model and guided for the theory part of her work.

Further refinement in the description of the nuclei above ^{78}Ni came with a new fit of the proton-proton part of the interaction which I have carried out recently to optimize it for the $N = 50$ isotones, including new EXIL data on ^{85}As [58] and a new estimation of the single-particle energies in ^{79}Cu [59]. The resulting interaction has been successfully applied to the study of low-spin level schemes of many nuclei, e.g., ^{86}Se and ^{88}Kr [60], where we could confirm some of the shell model predictions about the deformation and the role of non-axial degrees of freedom in $N = 52, 54$ isotopes, ^{88}Br [61] , ^{89,87}Br and ^{90}Rb [62].

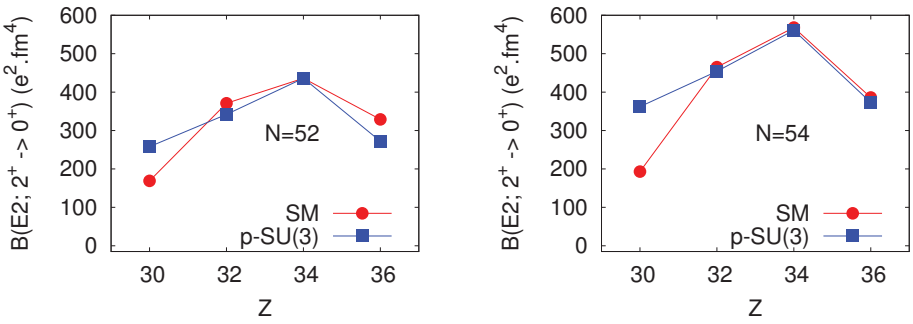

Figure 2.1: Reduced transition probabilities obtained in the SM diagonalizations versus the algebraic pseudo-SU(3) model.

2.1.1 Collective features of $N = 52 - 54$ isotones

Since the $r3g - r4h$ valence space contains the orbits forming the pseudo-SU(3) blocks (pseudo-sd for protons and pseudo-pf for neutrons), the collective features of the systems with valence nucleons filling these orbitals can be anticipated within the algebraic approach, as noticed before e.g. in [40] for the study of the deformation of zirconium isotopes. It was of interest to investigate what happens closer to the ^{78}Ni core. Approaching the SU(3) limit would require a degeneracy or a close proximity of the orbitals of interest. In the present SM framework, the $d_{5/2}$ and $s_{1/2}$ shells were assumed degenerate in the nickel core, and the proton $f_{5/2}$ and $p_{3/2}$ levels are known to cross with the filling of the $g_{9/2}$ orbit in the copper chain, thus should remain close at $N = 50$. We have thus explored in various theoretical approaches development of deformation in $N = 52 - 54$ isotones with proton numbers $Z = 30 - 36$ [63] (see publications attached). The algebraic pseudo-SU(3) approach appeared to give a very good estimate of collective properties in the proton mid-shell as compared to SM diagonalization results, see Fig. 2.1. The maximum of collectivity has been predicted in ^{88}Se, while all the models, including the particle and angular momentum symmetry conserving beyond mean-field with Gogny forces (calculations performed by T. R. Rodriguez, UAM Madrid), pointed to a triaxial deformation in ^{86}Ge. A beautiful coherence was found between SM diagonalization and the latter approach in ^{86}Ge, where the yrast bands have been predicted within several keV agreement between the models.

Some insight into the deformation properties of these nuclei have been however obtained already from the experiments performed in Ref. [57] on ^{84}Ge, where the second excited state has been assigned 2^+ spin/parity in accordance with SM predictions. Recently many more spectroscopic data in the $N = 52$ region have been collected by the Warsaw group. In particular, a good agreement has been obtained between SM and experiment for the excitation spectra of ^{86}Se, for both yrast and non-yrast states, where a candidate for the 3^+ state has been found [60], confirming further the theoretical predictions about the role of non-axial degrees of freedom in this region. Recent measurements of lifetimes of excited states in this nucleus from the Cologne group are also consistent with SM postulates. The

article presenting more results on collectivity of ^{86}Se, including the analysis of the intrinsic shape parameters (β, γ) from shell model, has been published recently [64].

2.2 Developments of effective interactions in the $fpgd$ valence space

2.2.1 Island of inversion at N=40

One of the goals of the nuclear structure theory, and of shell model in particular, is comprehension of phenomena appearing in nuclei from the point of view of the underlying shell structure, symmetries and other mechanisms governing those. It allows to predict the same scenarios in other regions of nuclei. An example is the *island of inversion* at $N = 40$, predicted in analogy to what was known at $N = 20$. In 1992 Alfredo Poves (UAM Madrid) presented his prediction of maximum of deformation in this region in ^{64}Cr based on a simple SU(3) analysis. Later, truncated calculations have been performed in the $fgpd$ model space outside the ^{48}Ca core [65, 66] confirming that prediction. Only recently, thanks to the developments of the ANTOINE code by E. Caurier, it has become possible to perform full space (or converged) diagonalizations in the $fpgd$ model space of the large set of deformed nuclei around $N = 40$.

In collaboration with F. Nowacki, A. Poves and S. Lenzi, we have derived an empirical Hamiltonian for this model space (fp orbits for protons and $f_{5/2}pg_{9/2}d_{5/2}$ orbits for neutrons) called LNPS and the largest to date calculations of $N = 40$ chain as well as isotopic chains with $Z = 20 - 28$ were carried out in Strasbourg. The pioneering work on the new island of inversion at $N = 40$ reported in Ref. [5] has been highlighted in Physics and became a reference work for this region of nuclei, cited already more than 130 times (see publications attached). Further developments of the interaction have been continued in Strasbourg for different purposes, some of them are summarized in the next paragraphs. The LNPS in its original or slightly revised version has been employed in a large number of theoretical interpretations of physics of nuclei in the island of inversion and I have carried out several such studies, e.g. [67, 68, 69, 70, 71, 72, 73]. The shape co-existence in ^{68}Ni has been also predicted with the LNPS interaction [5, 74]. ^{68}Ni became recently a hot subject in nuclear physics, new measurements of 0^+ energies have been performed as well as Monte Carlo Shell Model calculations appeared for this nucleus which allowed for a deeper interpretation of its intrinsic shapes [75].

2.2.2 Stability of the $Z = 28$ shell closure

The studies of low spin structures in $N = 49, 50$ and $Z = 29$ nuclei provide an opportunity to investigate the stability of shell gaps $N = 50$ and $Z = 28$ and the role of the cross-shell excitations on nuclear structure in this region. In this spirit, the studies of the copper isotopes [54, 76, 77, 78, 79], first in proton pf and neutron $f_{5/2}pg_{9/2}$ model space and then adding as well the $d_{5/2}$ neutron orbital, have been performed in recent years. In Ref. [54] we

have demonstrated that proton core excitations are indispensable to describe correctly the systematics of magnetic moments of copper isotopes between $N = 40$ and $N = 46$, which has not been possible within the $r3g$ model spaces (one proton only in the valence space). A slight reduction of the $Z = 28$ gap between ^{68}Ni and ^{78}Ni assumed in the model has been shown to be coherent with the observed trends in the copper isotopes (see publications in Chapter 7).

In the PhD work of P. Morfouace (IPN Orsay, 2014, currently post-doctoral researcher in USA) spectroscopic factors have been obtained from ^{72}Zn(d,^{3}He)^{71}Cu pick-up reaction for ^{71}Cu and from ^{70}Zn(d,^{3}He)^{69}Cu for ^{69}Cu. I have tutored P. Morfouace for the theory part of his thesis work and provided large scale $fpgd$ calculations with the LNPS interaction refined in its proton-neutron part to assure a proper evolution of the $Z = 28$ gap inferred from Refs. [54, 59]. We have found an overall agreement between theory and experiment for the single-particle strength distributions in ^{71}Cu, while in ^{69}Cu the $f_{7/2}$ centroid seemed to appear too high in the shell model calculations. In spite of minor discrepancies, these studies allowed to understand that the $f_{7/2} - f_{5/2}$ splitting remains constant with the increasing neutron number. An interesting point was determining the nature of the $7/2^-$ state at 981keV in ^{71}Cu, predicted previously in the particle-core coupling model to be a single hole state: this state was however not observed in the transfer reaction of Ref. [77] neither populated in Coulex [80] due to its low $B(E2)$ value. In the present shell model these two facts are explained, as the 981keV state comes out in the calculations as the $2^+_\nu \otimes \pi f_{5/2}$ structure and is thus connected via a very low $B(E2)$ rate to the ground state dominated by the $0_\nu \otimes p_{3/2}$ single-particle structure [77, 79].

Final validation of the model came from the data from RIKEN on ^{77,79}Cu nuclei [59]. In the case of ^{79}Cu, there is one to one correspondence and a good agreement in excitation energies between the observed and calculated spectra. These studies allowed to obtain a better constraint for the $f_{5/2} - p_{3/2}$ splitting of the proton orbitals in the ^{78}Ni core, which I have implemented recently in the new version of the $r3g - r4h$ interaction as described in Section 2.1.

2.2.3 Stability of the $N = 50$ shell closure

As for the $N = 50$ gap, I have started its investigations through the structures of $N = 50$ nuclei, where the $5^+, 6^+$ excited states have been observed at low energy, which might correspond to particle-hole excitations across the gap. In Ref. [81] we have shown that these states can be indeed interpreted as cross-shell excitations and that they are located on a parabola between $Z = 28$ and $Z = 36$, which is a well known effect of the many-body correlations. At the same time there is no reduction of the yet unknown $N = 50$ gap in ^{78}Ni with respect to its size in higher Z nuclei. The 2^+ energy in ^{78}Ni was predicted around 4MeV and its wave function dominated by a neutron excitation over the $N = 50$ gap (see Chapter 7). One should also note that the shell evolution due to the $T = 1$ part of the nuclear force between ^{68}Ni and ^{78}Ni resembles what was known before from oxygen and calcium chains, where the 3N forces were discussed to be responsible for the creation of the $N = 14$ and $N = 28$ gaps [24, 82, 83]. Present calculations can be thus used as a

benchmark and test for the ab-initio studies with 3N forces in heavier mass nuclei.

I have studied as well the $N = 49$ nuclei, where the spectroscopy of ^{79}Zn has been obtained via ^{78}Zn(d,p)^{79}Zn transfer reaction. The SM calculations reproduced well the systematics of positive parity states in $N = 49$ isotones and predicted perfectly the position of the first $5/2^+$ state in ^{79}Zn, which carries a substantial part (SF$\sim$ 0.5) of the single-particle strength [84].

2.3 Region around ^{100}Sn: a challenge for the LSSM

I have contributed to the developments of interactions in the *gds* model space, suited for the studies of mass $A \sim 100$ nuclei. Among others, I have undertaken studies of the core-excited states and high-spin isomers in ^{96}Cd [85], ^{96}Ag [86] and ^{96}Pd [87].

An important achievement was improving the interaction for the description of Gamow-Teller transitions in nuclei towards mass $A = 100$, which permitted, in particular, the interpretation of the *superallowed Gamow-Teller* decay observed in ^{100}Sn in GSI. This unique decay, with a log ft value smaller than all the known superallowed Fermi transitions, was explained due to the large shell gaps in ^{100}Sn and its particular single-particle structure, leading to a one dominant $g_{9/2} - g_{7/2}$ GT transition. The theoretical results were included in the experimental work announcing this discovery in the review Nature [88].

The subject that remains of a special interest for SM studies is the systematics of the reduced transition probabilities in the tin isotopic chain. The experimental situation in this region is ambiguous with $B(E2)$ values varying substantially in different measurements, which are biased by large experimental errors. SM calculations of tin nuclei in the vicinity of ^{100}Sn are extremely complex, as both proton and neutron core excitations should be taken into account. Recently, we have performed SM calculations for ^{104}Sn and its neighbors, as the new value of $B(E2)$ in this nucleus was measured in Coulex in GSI [89]. While the agreement between SM and experiment was found good, a different value was reported in Ref. [90] from RIKEN, which is higher than the current SM prediction. In addition to unclear experimental situation the impossibility of performing full space diagonalizations and getting converged results is also penalizing the optimization of effective interactions for this region. A comparative study of nickel and tin isotopes would help to determine the role of the core excitations on the $B(E2)$ values (some results were presented in Vietri Spring Seminar on Nuclear Physics, 2011) and to understand the modifications of the multipole part of the interactions necessary for a coherent description of the excited states and transition strengths in light tin isotopes.

2.4 Developments of effective interactions in the $r4h-r5i$ model space: Nuclei above ^{132}Sn core

I have as well undertaken the developments of empirically adjusted interactions in the region above ^{132}Sn. The first motivation came with the measurements of isomeric transitions

from the 6^+ states in ^{134,136}Sn and the failure of shell model description of those with the empirical and realistic interactions existing on the market. The results I obtained have been published along with the experimental data in [41] and have been discussed in the PhD thesis of G. Gey (LPSC Grenoble, 2014, currently post-doctoral researcher in Japan), whom I tutored for the shell model and theory part of his work.

In the next subsection I discuss in more detail the problems of pairing in realistic interactions and the description of tin isotopes. I continued further the developments of the effective interaction based on the ^{110}Zr core to study new spectroscopic information on ^{138}Te and ^{140}Xe nuclei in collaboration with the Warsaw experimental group. This subject has been a part of the research project of H. Naidja (post-doc in Strasbourg 2013-2015) [91].

2.4.1 Description of isomeric transitions in $^{134-138}$Sn nuclei

In Ref. [41] I have performed calculations using the realistic 2-body V_{lowk} interaction based on the CD-Bonn potential, adapted to the model space (outside ^{132}Sn core) by perturbation techniques including all diagrams up to second order in the Q-box. The calculations for tin isotopes presented here are performed in the model space containing $0h_{9/2}, 3p, 2f, 0i_{13/2}$ orbitals. The same single-particle energies as in Refs. [92, 93] were adopted.

It appears from the calculations that the realistic 2-body neutron-neutron interaction derived this way provides spectra within a reasonable agreement with experiment but faces difficulties to reproduce in detail the transition strengths. In accordance with the previous results of Refs. [92, 93, 94] the main discrepancy is found in the mid-shell (^{136}Sn), where all previous calculations were off by at least a factor of 2 for the $B(E2, 6^+ \rightarrow 4^+)$ transition. With the interaction described above, this transition is severely underestimated, see Fig. 2.2.

A reduction of the $f_{7/2}$-diagonal and off diagonal pairing interaction by ~ 150keV turned out necessary to obtain a good agreement with data. As one can see from Figures 2.2 and 2.3, it allowed to reproduce in detail the spectra of $^{134-138}$Sn and the known transition rates (0.65 effective charge was used as in Ref. [93], to take into account the missing proton-neutron excitations from the ^{132}Sn core).

The problems in the description of isomeric transitions in semi-magic nuclei in other regions of nuclear chart have been already encountered in SM calculations and postulated due to the seniority mixing effects [95] or the absence of 3N effects that could be approximated via particle-hole core excitations in Ref. [96]. Here we focus on seniority structure of the calculated states. It can be shown [97] that all energy differences of seniority 0 and 2 states in n-particle configuration are identical to those in the 2-particle system and are independent of n. Thus the constant energy of excited states (especially 2^+ but also 4^+ and 6^+) observed in heavy tins is compatible with the dominance of the seniority scheme. However, the experimentally established behavior of the $6^+ \rightarrow 4^+$ transition in the tin chain shows substantial deviation from the pure seniority scheme in the $f_{7/2}$ orbital, see Fig. 2.2. It can be shown [97] that $B(E2)$ values for the seniority conserving transitions, such as isomeric transitions, follow a parabolic behavior reaching a minimum value in the

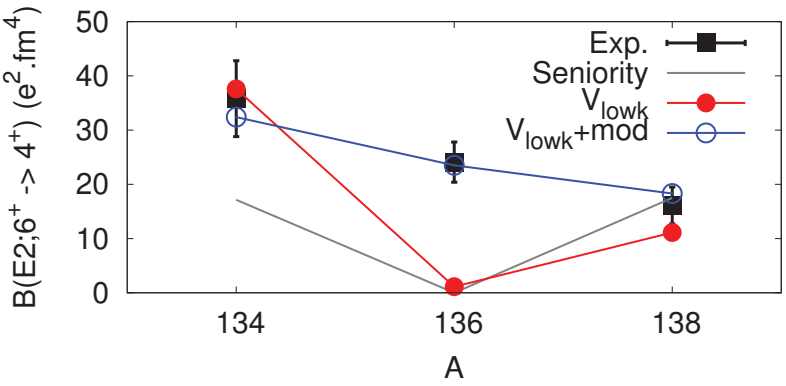

Figure 2.2: Reduced transition probabilities from 6^+ to 4^+ states in the tin chain. In addition to the experimental values (black points) calculations are reported with the realistic V_{lowk} interaction (red), with V_{lowk} interaction with a slight reduction of pairing (blue points) and of the diagonalization in the $f_{7/2}$ shell (grey curve) which corresponds to the pure seniority scheme.

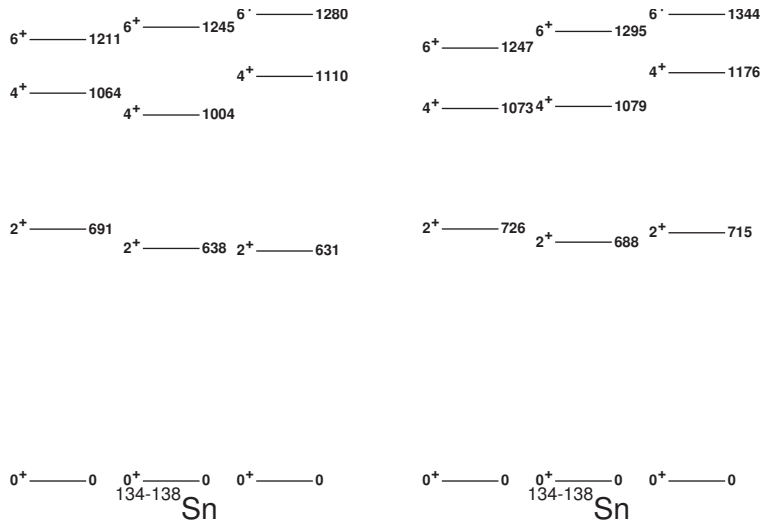

Figure 2.3: Spectra of tin isotopes obtained in shell model with V_{lowk} interaction with a pairing modification (left) in comparison to experiment (right).

Table 2.1: Dominating seniority components of the low lying states in tin isotopes.

J^π	seniority	^{136}Sn	^{138}Sn
0^+	$\nu = 0$	98%	96%
	$\nu = 2$	2%	4%
2^+	$\nu = 2$	93%	87%
	$\nu = 4$	7%	10%
4^+	$\nu = 2$	46%	84%
	$\nu = 4$	54%	12%
6^+	$\nu = 2$	95%	87%
	$\nu = 4$	5%	9%

mid-shell:

$$B(E2; \nu J \rightarrow \nu J - 2) \sim (1 - 2f)^2, \Delta\nu = 0, \tag{2.1}$$

where $f = n/(2j + 1)$ is the fractional filling of shells.

The substantial $B(E2)$ value measured in ^{136}Sn indicates that we do not deal here with a seniority $6^+(\nu = 2) \rightarrow 4^+(\nu = 2)$ transition but that the structure of one or both states should be more mixed. It is interesting to note that the realistic V_{lowk} interaction without any further modification follows well the pure seniority pattern and predicts the 6^+ state to be composed in 96% of seniority $\nu = 2$ and the 4^+ state of 84% of seniority 2, which leads to a nearly disappearing transition between them. The slight pairing modification which brings the results into agreement with experiment leads to a more complex structure of the 4^+, containing now 46 and 55 percent of $\nu = 2$ and $\nu = 4$, respectively. In Table 2.1 I list the seniority components dominating the $0^+ - 6^+$ states in $^{136-138}$Sn in the calculations which reproduce well the transition strengths (V_{lowk}+mod interaction).

Recently, in the work of [98] the authors have shown that a good agreement with experiment can be obtained by a very slight (25keV) reduction of the pairing matrix elements of their realistic interaction obtained in the same model space. Of course, as will be shown in the next Chapter, the strength of the multipole component is sensitive to the cut-off and especially to the number of $\hbar\omega$ excitations in the Q-box function, which explains the difference between empirical pairing corrections applied in Refs. [41, 98] which are not using the same effective interaction as a starting point. There is however no golden rule on how many $\hbar\omega$ excitations should be included and the pairing interaction is known to be badly converging in the many-body perturbation expansion. Another important issue is the choice of the model space, i.e. taking into account (or not) the enlarged model spaces, going beyond one harmonic oscillator shell.

In Fig. 2.4 I show a comparison of excitation energies and the reduced transition probabilities for tin isotopes as discussed above with two effective interactions based on the same N3LO potential and treated in the same way in the perturbation expansion ($2\hbar\omega$

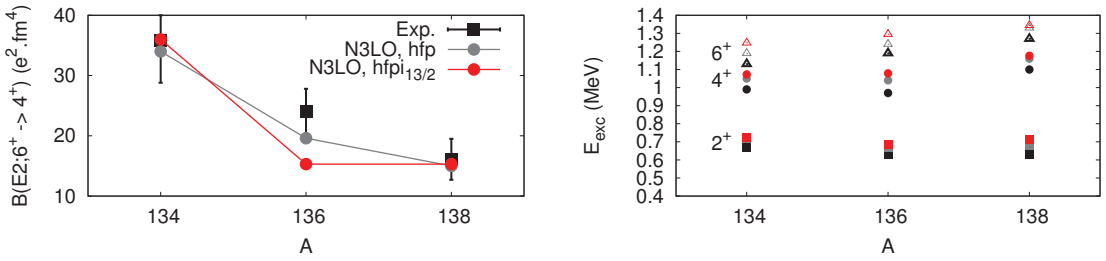

Figure 2.4: Reduced transition probabilities (left) and excitation spectra (right) of tin isotopes depending on the valence space used for the derivation of the effective interaction.

excitations in the Q-box), the only difference being adding or excluding the neutron $i_{13/2}$ orbital in the model space composed of hfp orbits. The renormalization of pairing due to the presence of the $i_{13/2}$ orbit leads to an overall worse agreement with experiment. One should note that the Kuo-Kreciglowa [22] and Lee-Suzuki [23] methods used to obtain the effective Hamiltonian are done within the degenerate perturbation theory, thus are a proper approach for one harmonic oscillator shell. Only recently an extended Kuo-Kreciglowa method for multi-shell spaces have been proposed in Ref. [99], which could be applied in future to derive effective interactions for exotic nuclei that necessitate the presence of orbits from more than one harmonic oscillator shell. The use of the non-perturbative approaches to the effective interactions like those proposed recently in Refs. [27, 28] could be another solution to the problems encountered in the study of tin isotopes above ^{132}Sn.

2.4.2 Collectivity above the ^{132}Sn core

The $N = 86$ isotones that can be described in the shell model as a few particles outside the ^{132}Sn core are analogous cases to $N = 54$ nuclei above ^{78}Ni core studied recently in Ref. [63]. The spectra of ^{133}Sn and ^{133}Sb show that at least the two lowest orbits in the proton and neutron valence spaces are separated by less than 1MeV which looks quite favorable for the development of quadrupole collectivity.

As mentioned, I have also developed interactions based on the ^{110}Zr core, derived from a realistic V_{lowk} interaction based on the N3LO potential. All diagrams through the second order were summed in the Q-box expansion in the many-body perturbation theory. Single particle energies of the ^{110}Zr core from the GEMO model [100] were employed. Further, monopole corrections were applied in order to reproduce the proton and neutron gaps $Z = 50$ and $N = 82$, the spectra of ^{133}Sn and ^{133}Sb as well as low lying levels of $N = 83, 84$ isotones. The $f_{7/2}$ pairing matrix elements were slightly reduced to obtain also a good agreement with data for the heavy tins, as discussed in the previous section.

With the interaction described above, I have performed calculations of selected $N = 86$ isotones within the *gds-hpfi* model space, closing the proton $g_{9/2}$ and $h_{11/2}$ orbitals (no excitations of the ^{132}Sn core) [102]. As shown in Fig. 2.5, the agreement between experiment and theory for the known yrast levels in ^{138}Te and ^{140}Xe is excellent. Selected

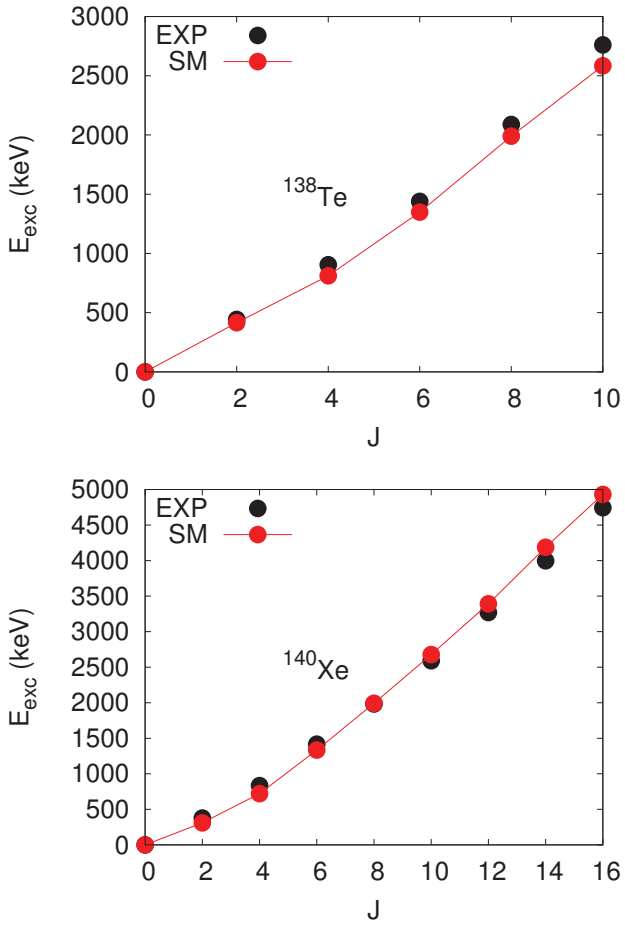

Figure 2.5: Yrast states of ^{138}Te and ^{140}Xe obtained from LSSM diagonalization in comparison to known experimental levels from NNDC [101].

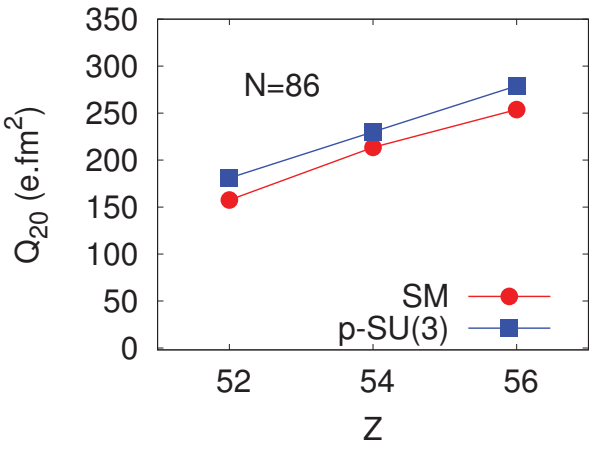

Figure 2.6: Intrinsic quadrupole moments of $N = 86$ isotones from LSSM and pseudo-SU(3) calculations.

quadrupole properties of both nuclei and of the subsequent ^{142}Ba obtained within this framework are presented in Table 2.2. In Fig. 2.6 I show as well the comparison of values of intrinsic quadrupole moments from pseudo-SU(3) and diagonalization shell model. As can be seen, they agree closely for both, the trend and the magnitude of deformation.

Selected quadrupole properties of these nuclei are collected in Table 2.2. ^{138}Te with only 2 protons outside the closed shell, is the least deformed of the $N = 86$ isotones. The quadrupole transitions through the yrast band are of the order of dozens of W.u. and are of collective nature but still small for what one can expect in deformed nuclei in this mass region. Adding a few more protons to the $g_{7/2} - d_{5/2}$ shells should enhance considerably the collectivity leading to strongly deformed shapes and appearance of distinct γ-bands. In ^{140}Xe the deformation is more pronounced: it has quite equal quadrupole moments ($\sim 220e.fm^2$) calculated from spectroscopic moments and $B(E2)$ transitions up to spin 6^+. This allows to associate to the yrast band β deformation parameter of 0.14 by means of the collective model. The transitions throughout this band are of the order of 20-30 W.u. The $B(E2, 3^+ \rightarrow 2_2^+)$ transition value is of 44 W.u. and spectroscopic quadrupole moments of 2_1^+ and 2_2^+ states are of equal values ($61e.fm^2$) but opposite signs, a clear sign of triaxiality. There is also a sequence of $2_2^+, 3^+, 4_2^+, 5^+$ states connected by strong transitions that can be identified as a γ-band.

The $B(E2; 2^+ \rightarrow 0^+)$ transition in ^{142}Ba is predicted stronger than in ^{140}Xe while the $B(E2; 3^+ \rightarrow 2_2^+)$ is less collective. This is in perfect analogy to $N = 54$ isotones where the triaxiality was maximized in ^{86}Ge (4 valence protons) and the axial deformation was larger in ^{88}Se (6 valence protons). To get further insight into the intrinsic shape of these nuclei, I have performed the same analysis as done before in Ref. [63], using SM $E2$ matrix elements and the method of Kumar [103]. In ^{138}Te it leads to intrinsic shape parameters $\beta = 0.11$, $\gamma = 9^o$, in ^{140}Xe $\beta = 0.15$, $\gamma = 15^o$. The values clearly supporting the precedent

Table 2.2: Selected quadrupole properties of $N = 86$ isotones obtained from LSSM diagonalization.

Nucleus	$B(E2; 2^+ \rightarrow 0^+)$	$B(E2; 3^+ \rightarrow 2_2^+)$	$Q_{spec}(3^+)$
^{138}Te	12 W.u.	18 W.u.	-3.5$e.fm^2$
^{140}Xe	24 W.u.	44 W.u.	-2.2$e.fm^2$
^{142}Ba	31 W.u.	37 W.u.	-4.1$e.fm^2$

interpretation.

A joined experimental and theoretical study of spectroscopic properties and deformation in ^{138}Te and ^{140}Xe has been undertaken and the first article on the subject has been just published [104], where possible experimental candidates for the γ-band members have been identified.

Chapter 3

Spin-tensor decomposition of realistic and empirical effective interactions

As discussed previously, effective interactions for the shell model framework are obtained from realistic potentials, which are further softened via V_{lowk} or G-matrix procedure and adapted for the model space via MBPT techniques. For the purpose of SM studies, the TBME obtained first in relative coordinates need to be transformed to the laboratory frame and represented in terms of anti-symmetrized two-body states coupled to a given spin/isospin (JT). This requires a summation that contains the contributions from central, spin-orbit and tensor channels. Once the set of TBME for actual calculations derived, the information of the underlying spin-isospin structures is thus lost, but can be recovered by the use of the so-called spin-tensor decomposition (see e.g. [45, 46]). Spin-tensor analysis of effective interactions appears to be a very useful tool to quantify the role of terms dominating the shell evolution and detect the terms that are modified in the empirical fits, i.e. are not well given by realistic NN interactions. The spin-tensor decomposition can be performed for TBME in a valence space that contains all spin-orbit partners.

The first results of such a decomposition which I have obtained for the $sd-pf$ nuclei have been published in a joined paper with N. Smirnova (CENBG Bordeaux) and collaborators, who carried in parallel a similar analysis [45]. Another part of my work on the subject have been included in the second joined publication [46] where I have performed a systematic spin-tensor analysis of sd, pf and gds nuclei, using both, realistic and empirical interactions adjusted in the Strasbourg group. The major conclusions of the two papers were the following:

- Both central and tensor terms play a crucial role in the creation and evolution of the $N = 20$ and $N = 28$ shell gaps.
- The tensor term is dominant for the evolution of spin-orbit splittings governed by cross-shell proton-neutron centroids.
- The tensor part of the interaction remains nearly untouched in empirical fits, while the central and especially vector parts need to be modified substantially to reproduce

the known monopole trends.

- The $N = 14, 28, 50$ shell gaps between ^{22}O and ^{28}Si, ^{48}Ca and ^{56}Ni, ^{90}Zr and ^{100}Sn, respectively, are not enhanced enough in the realistic NN interactions. The empirical interactions that reproduce the gaps are modified substantially in their central and vector parts. The contribution of the proton-neutron tensor to this gap is of a minor importance.

- As the empirical adjustments in the $T = 1$ channel, which are rendering the monopoles more repulsive, enhance mostly the spin-orbit (vector) and central terms, those should be the most sensitive to the inclusion of 3N forces.

In the following I add several unpublished observations. First, concerning the monopole part, I discuss shortly the analysis of the LNPS fit for the case of the calcium chain. Then I present results of the analysis of the multipole part of various effective Hamiltonians (the monopole-multipole decomposition is done following Refs. [14, 37]).

3.1 Monopole interactions

In a recent work Ref. [105] the author investigates the tensor effects on a mean-field level with the Skyrme force (SLy4) in the creation of magicity of ^{48,52,54}Ca nuclei. First the neutron-neutron tensor effects are analyzed: It is put forward that the neutron-neutron tensor component is responsible for the separation of the $0f_{7/2}$ and $1p_{3/2}$ orbitals with the filling of the former, leading to the shell closure of ^{48}Ca. Next, the same mechanism is suggested to separate the $1p_{3/2}$ and $1p_{1/2}$ orbits leading to the magicity of ^{52}Ca, and finally, in ^{54}Ca, due to a separation between $1p_{1/2}$ and $0f_{5/2}$ states.

The first conclusion of Ref. [105] about the creation of the $N = 28$ gap as a like-particle tensor effect, seems contradictory to the abundant shell model and ab-initio studies, which postulated the creation of this type of gaps (called usually spin-orbit or EI in Refs. [1, 17]) due to the action of three-nucleon forces. One should note, that the tensor effects have always been present in realistic and empirically adjusted two-body interactions used in shell model diagonalizations or recently also in coupled-cluster approaches in this region of nuclei. In particular, the so-called spin-tensor decomposition has been performed previously in Ref. [46] for the calcium isotopes showing that the tensor contribution is usually well given by the two-body realistic interaction and it is not affected by empirical fits, reproducing well the evolution of the structure of a given isotopic chain (see table III and Fig. 3 of Ref.[46]). Here, I perform such a decomposition using the LNPS interaction [5] which is the best up to date empirical interaction for the mass $A = 40 - 60$ nuclei and has been shown to reproduce in great detail the spectroscopy of a large number of known nuclei as well as to predict correctly the onset of deformation around $N = 40$. In Figure 3.1 I show the evolution of the 2^+ energies in the calcium chain obtained with the LNPS interaction. The agreement with experiment is very good in the known region. Note that the accurate 2^+ energy of the ^{54}Ca is a model prediction, as it has not been measured the

Figure 3.1: Evolution of the 2^+ energies along the Ca chain from experiment and shell model calculations with the LNPS interaction.

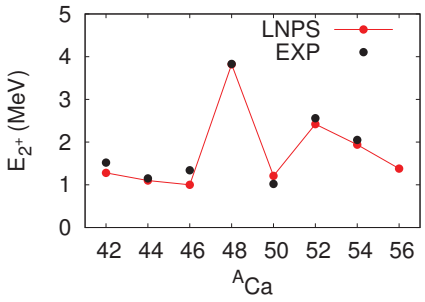

time when the interaction was adjusted to data in the pf-shell (fit by E. Caurier before 2010).

Having found a detailed agreement between calculated and observed 2^+ energies in the calcium chain, one can analyze the underlying shell evolution on the mean-field level. I plot in Fig. 3.2 the so-called effective single-particle energies (ESPE) that represent the variation of the spherical mean-field (in other terms, that correspond to the Hartree-Fock single-particle energies). In addition to the evolution of the neutron ESPE with neutron number obtained with the LNPS interaction, I distinguish their evolution due to the central, vector (spin-orbit) and tensor components (see as well Tab. 3.1). As one can see, the variation of the $0f_{7/2} - 1p_{3/2}$ splitting between $N = 20$ and $N = 28$ is entirely due to the spin-orbit part of the interaction, while due to the central and tensor parts of the force this splitting remains nearly constant with the filling of the neutron $0f_{7/2}$ shell. This result is consistent with our previous finding from Ref. [45] with another empirical interaction KB3, where the major variation of the $N = 28$ gap was also provided by the vector term and a small variation due to the central term, dependent on the choice of the starting single-particle energy of the $0p_{3/2}$ orbital. The changes of $N = 32$ and $N = 34$ gaps are much softer with subsequent neutron fillings and are not dominated by a single component of the nuclear force.

The current shell model analysis, in which the particle-like tensor effects seem to be inexistent in the creation of the $N = 28$ gap does not confirm the results of Ref. [105]. The possible reason for that is the way the parameters of the forces are adjusted to data. While in the shell model the whole TBME are fitted to large sets of data, in the present Skyrme case the multi-step fitting procedure was adopted in which first the spin-orbit strength was adjusted to the spin-orbit splitting in ^{40}Ca and then the tensor force strength have been adjusted to reproduce the spin-orbit splittings in ^{48}Ca and ^{56}Ni. One should however notice that the shell model examination shows in many cases that tensor and vector effects tend to go in opposite directions and counter balance in the creation of the gaps. In particular, this is the case of the gap between $0f_{7/2}$ and $0f_{5/2}$ orbitals while moving from ^{48}Ca to ^{56}Ni,

Figure 3.2: Evolution of neutron effective single-particle energies with neutron number due to the LNPS interaction and its central, vector and tensor parts separately.

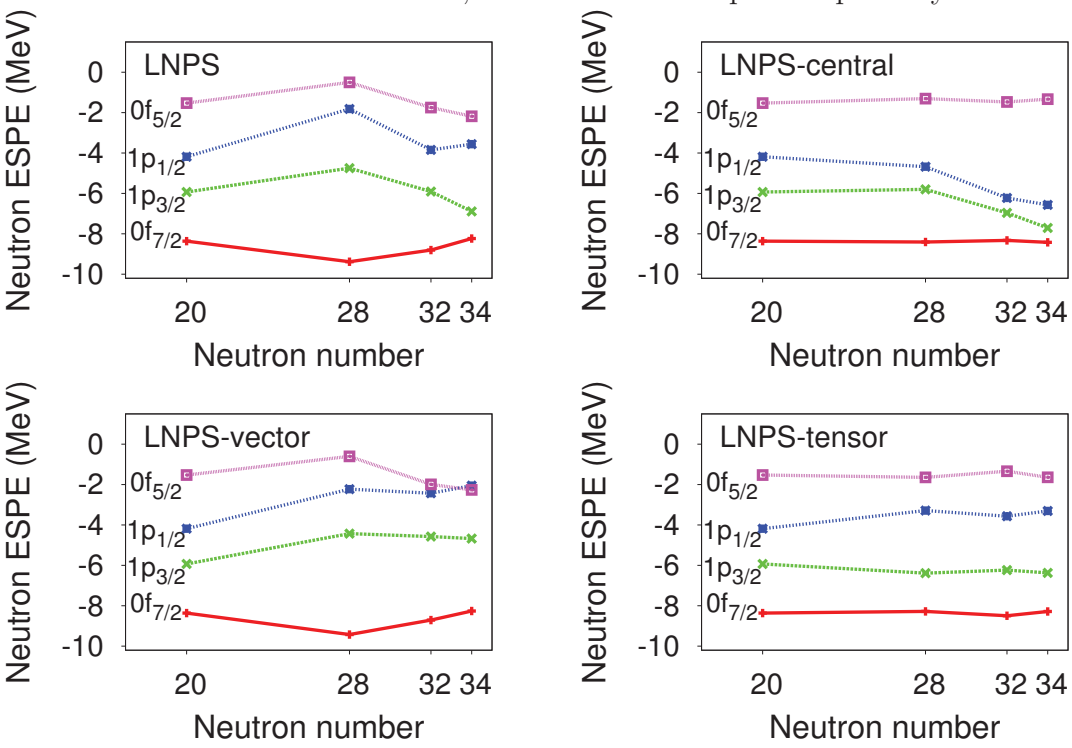

Table 3.1: Changes in the neutron energy gaps (in MeV) with the filling of subsequent neutron orbitals as obtained with the LNPS interaction.

Energy gap	$\Delta\nu(0f_{7/2}-1p_{3/2})$	$\Delta\nu(1p_{3/2}-1p_{1/2})$	$\Delta\nu(0f_{5/2}-1p_{1/2})$
filling orbital	$\nu 0f_{7/2}$ ^{40}Ca$\rightarrow^{48}$Ca	$\nu 1p_{3/2}$ ^{48}Ca$\rightarrow^{52}$Ca	$\nu 1p_{1/2}$ ^{52}Ca$\rightarrow^{54}$Ca
LNPS	2.20	-0.86	-0.72
LNPS-central	0.17	-0.38	0.49
LNPS-vector	2.57	-0.05	-0.65
LNPS-tensor	-0.54	-0.43	-0.56

Table 3.2: Changes in the neutron spin-orbit $0f_{7/2}-0f_{5/2}$ splitting (in MeV) with the filling of subsequent neutron orbitals as obtained with the LNPS interaction.

Energy gap	$\Delta\nu(0f_{7/2}-0f_{5/2})$		
filling orbital	$\nu 0f_{7/2}$ ^{40}Ca$\rightarrow^{48}$Ca	$\nu 1p_{3/2}$ ^{48}Ca$\rightarrow^{52}$Ca	$\nu 1p_{1/2}$ ^{52}Ca$\rightarrow^{54}$Ca
LNPS	2.044	-1.825	-1.004
LNPS-central	0.261	-0.244	0.234
LNPS-vector	1.986	-2.102	-0.725
LNPS-tensor	-0.203	0.520	-0.512

where the vector contribution is $-1/2$ of the tensor one in the empirical KB3 interaction. It is thus possible that the tensor effects from Ref. [105] can be exaggerated as they were adjusted to mock up a joined action of vector and tensor components.

I have also analyzed the evolution of the spin-orbit splittings due to the $T = 1$ part of the force. The size of the gap between the $0f_{7/2}$ and $0f_{5/2}$ orbits is determined mainly by the vector part of the interaction, the central and tensor components being smaller in size and cancelling due to the opposite signs. The evolution of the $1p_{3/2}$-$1p_{1/2}$ splitting looks more complicated, with many terms contributing to the size of the gap, as detailed in Tables 3.1,3.2,3.3.

3.2 Multipole interactions

While there was a lot of interest in the understanding of the monopole drifts and thus spin-tensor analysis of monopole interactions, little attention have been paid to the multipole components. I have realized systematic studies of the multipole content of realistic NN interactions in *p* and *sd* shells, its spin-tensor content and their sensitivity to the cut-off and convergence in the many-body treatment. Further, the interactions fitted to data

Table 3.3: Changes in the neutron spin-orbit $1p_{3/2} - 1p_{1/2}$ splitting (in MeV) with the filling of subsequent neutron orbitals as obtained with the LNPS interaction.

Energy gap	$\Delta\nu(1p_{3/2} - 1p_{1/2})$		
filling orbital	$\nu 0f_{7/2}$ ^{40}Ca$\rightarrow^{48}$Ca	$\nu 1p_{3/2}$ ^{48}Ca$\rightarrow^{52}$Ca	$\nu 1p_{1/2}$ ^{52}Ca$\rightarrow^{54}$Ca
LNPS	1.185	-0.870	1.270
LNPS-central	-0.623	-0.384	0.401
LNPS-vector	0.456	-0.055	0.473
LNPS-tensor	1.354	-0.433	0.398

obtained from the very same realistic interactions have been examined. Here I summarize the major conclusions of this analysis:

- The eigenvalues of the central part of the multipole Hamiltonian are very close to those of the total multipole one. This has been expected from [37], where the coherent terms of the Hamiltonian were identified as the well known central operators (pairing, quadrupole, ...) though never proved in terms of spin-tensor analysis. The results for the *sd*-shell are listed in table 3.4.

- The eigenvalues of tensor and vector components in $JT = 10$ and $\lambda\tau = 10$ are the largest and these are the cases for which the weakest overlaps with the schematic operators have been found in Ref. [14, 37].

- In-medium corrections to NN interactions and empirical fits affect all spin-isospin structures, though the changes are the most considerable in the central part. The first-order tensor and vector effects in the multipole Hamiltonian can be neglected.

- The eigenvalues of the multipole Hamiltonian augment with the number of $\hbar\omega$ excitations used in the Q-box functions in the MBPT treatment. The empirical fits of Hamiltonians converged in number of $\hbar\omega$ excitations in the Q-box tend to reduce the multipole content to a value in between the V_{lowk} and V_{eff}, roughly V_{lowk}/V_{eff}=1.2.

- The convergence of the multipoles of a V_{lowk} potential in terms of the cut-off is shown in Fig. 3.3. The negligible tensor and vector terms are weakly cut-off dependent. The multipole content is most cut-off sensitive in its $JT = 10$ channel.

- The convergence of multipoles in terms of $\hbar\omega$ excitations in the Q-box function calculated to 3rd order is shown in Fig. 3.4. For the lower cut-offs, the multipoles are converged at $10\hbar\omega$, for larger cut-offs more excitations are necessary. The cut-off dependence gets weaker with many-body correlations included for nearly all multipoles, except of the quadrupole $\lambda\tau = 20$ terms.

Table 3.4: Eigenvalues of the leading multipoles in the *sd*-shell (in MeV). Central, spin-orbit and tensor components of the CD-Bonn potential smoothed with the V_{lowk} procedure, 3rd order interaction with folded diagrams (V_{eff}) and the empirical fit based on the latter (V_{emp}) are distinguished. The operator structure corresponding to a given multipole is also listed: P stands here for the pairing operator.

Multipole	Operator type	Interaction	Central	Spin-orbit	Tensor	Total
$JT = 10$	P_{10}	V_{lowk}	-4.78	-0.02	-0.98	-4.93
		V_{eff}	-7.24	-0.62	-2.02	-8.08
		V_{emp}	-5.61	-0.61	-2.03	-6.58
$JT = 01$	P_{01}	V_{lowk}	-4.18	-0.02	-0.24	-4.41
		V_{eff}	-6.37	-0.02	-0.15	-6.38
		V_{emp}	-5.76	-0.13	-0.10	-5.80
$\lambda\tau = 10$	σ	V_{lowk}	-1.38	-0.32	-0.71	-1.53
		V_{eff}	-1.91	-0.19	-0.77	-2.09
		V_{emp}	-1.22	-0.89	-0.43	-1.66
$\lambda\tau = 20$	r^2Y_2	V_{lowk}	-2.85	-0.31	-0.35	-2.86
		V_{eff}	-4.47	-0.69	-0.17	-4.54
		V_{emp}	-3.38	-0.52	-0.16	-3.44
$\lambda\tau = 11$	$\sigma\tau$	V_{lowk}	2.77	0.10	0.24	2.75
		V_{eff}	4.11	0.10	0.28	4.09
		V_{emp}	3.81	0.28	0.31	3.85
$\lambda\tau = 30$	r^3Y_3	V_{lowk}	-0.75	-0.23	-0.48	-0.77
		V_{eff}	-0.99	-0.22	-0.23	-1.10
		V_{emp}	-0.73	-0.23	-0.34	-1.04

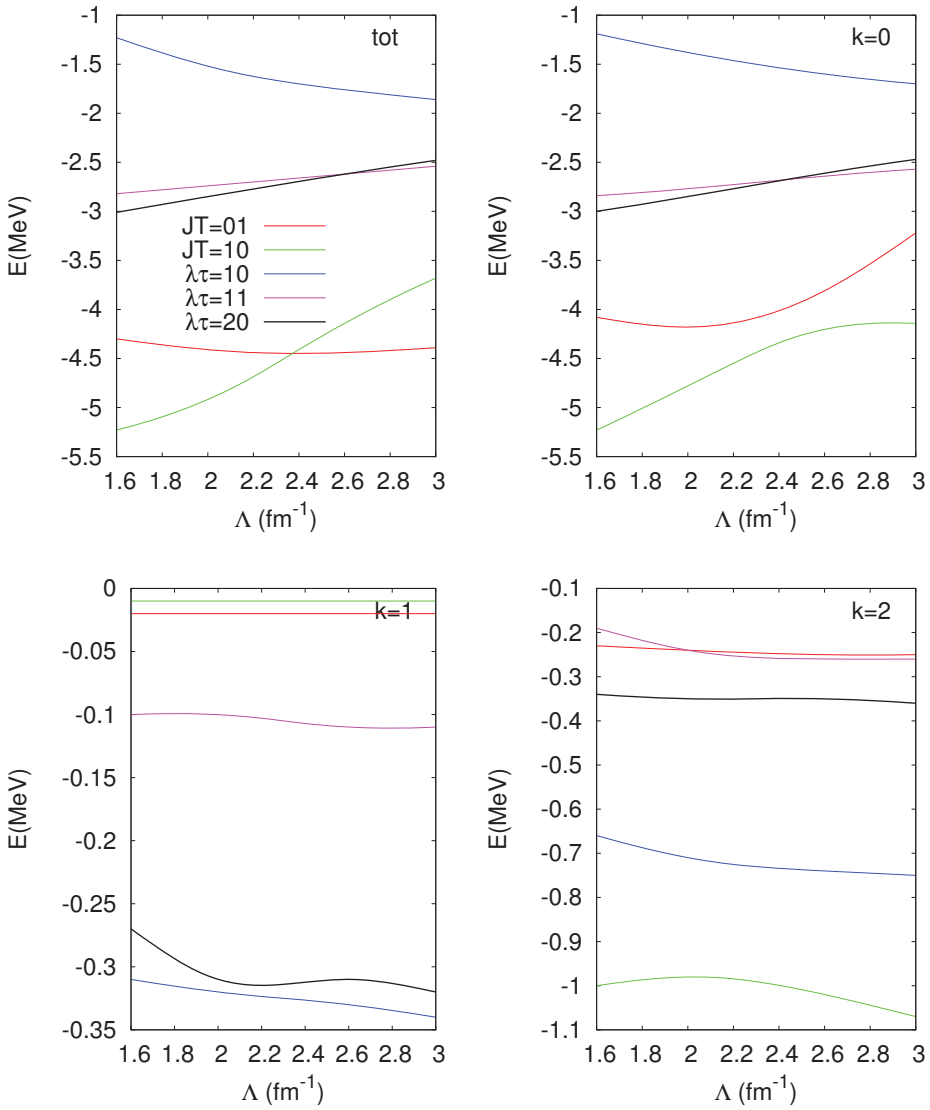

Figure 3.3: Multipole eigenvalues in the V_{lowk} potential and its central, vector and tensor components depending on the cut-off Λ. The value of $\lambda\tau = 11$ is multiplied by -1.

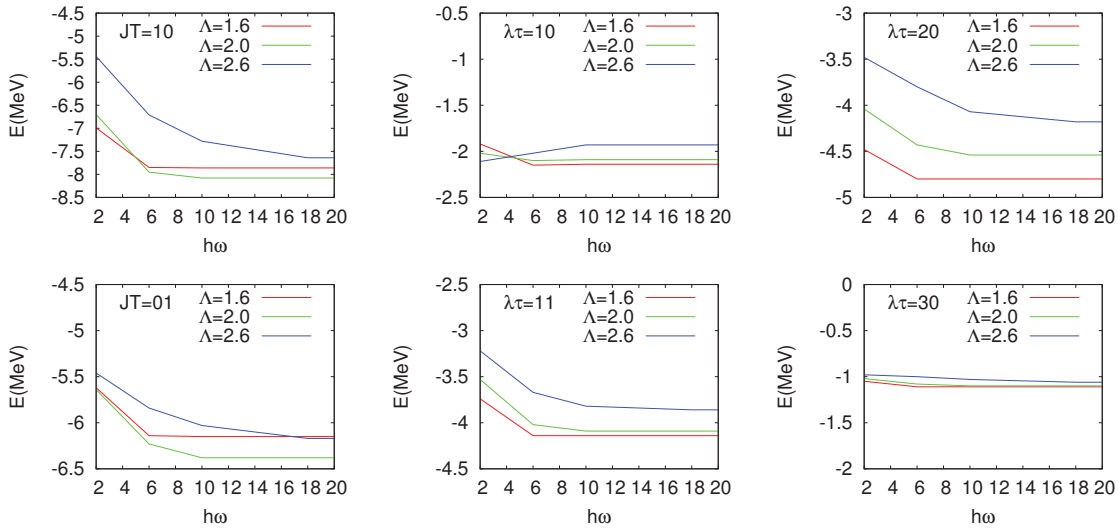

Figure 3.4: Multipole Hamiltonian eigenvalues plotted vs $\hbar\omega$ excitations of 2-body diagrams included in the evaluation of Q-box for different cut-offs of the starting V_{lowk} potential. $\lambda\tau = 11$ value is multiplied by -1.

- The convergence of the calculated multipoles in the perturbation expansion is far from being satisfactory, as shown in Tab. 3.5. A better convergence is obtained in terms of Q-boxes, as noticed previously in Ref. [20, 21]. The behavior of the $JT = 10$ terms is the most unstable.

- Finally, I have tested the influence of the possible errors in the multipole terms on the calculations of many-body observables. The differences in pairing interactions from V_{lowk}, V_{eff} and V_{emp} are major (see Table 3.4) and lead to considerable effects. As an example, the 2^+ of ^{18}O experimentally located at 1.98MeV is given at 1.24MeV by the V_{lowk} and 2.21MeV by V_{eff} and accurately reproduced by the empirical fit at 1.97MeV. Even larger differences are found in ^{38}Ar, where the 2^+ energy of the V_{lowk} is 0.52MeV, 1.62MeV in the V_{eff} and 1.86MeV in the empirical fit (experimental value 2.16MeV). On the contrary, despite the differences in the eigenvalues of the quadrupole component, all the interactions give remarkably similar results, see Table 3.6. This is a result of the very mixed structures in deformed nuclei with wave functions spread over many components. Thus the 20% deviations of the quadrupole content have no much impact on observables, contrary to the pairing-governed cases, where the wave functions are dominated by one type of configuration.

To summarize this part, the analysis of multipole Hamiltonians were performed on different levels. While the multipole content is only slightly modified in the empirical fits, a simultaneous fit of monopole and multipole parts is required to obtain high precision in many-body calculations. It would be instructive to investigate how the 3N forces influence

Table 3.5: Convergence of the eigenvalues (in MeV) of different multipole terms in the order-by-order perturbative expansion. V_{lowk} stands for the first order interaction, CP means the second-order interaction with the core-polarization contribution, 2nd-the second order interaction with all possible contributions (CP and 4p2h and ladder diagrams and folded diagrams), $Q(2)$ is the second order Q-box with folded diagrams and $Q(3) \equiv V_{eff}$ is the 3rd order Q-box interaction with folded diagrams.

Multipole	V_{lowk}	CP	2nd	$\hat{Q}(2)$	3rd	$\hat{Q}(3)$
$JT = 10$	-4.92	-4.48	-8.23	-6.90	-10.05	-8.08
$JT = 01$	-4.41	-6.31	-7.41	-6.29	-7.16	-6.38
$\lambda\tau = 10$	-1.52	-2.11	-1.93	-1.71	-2.37	-2.09
$\lambda\tau = 20$	-2.85	-3.43	-4.58	-3.96	-5.24	-4.54
$\lambda\tau = 11$	2.74	3.15	3.80	3.35	4.68	4.09
$\lambda\tau = 30$	-0.77	-1.00	-1.07	-0.94	-1.02	-1.10

Table 3.6: Quadrupole properties of ^{20}Ne and ^{24}Mg nuclei obtained with different interactions.

Nucleus	Observable	V_{lowk}	V_{eff}	V_{emp}
^{20}Ne	$Q(2^+)$ $(e.fm^2)$	-15.7	-15.9	-15.8
	$B(E2; 2^+ \to 0^+)$ $(e^2.fm^4)$	59.8	59.7	59.3
	$B(E2; 4^+ \to 2^+)$ $(e^2.fm^4)$	72.9	70.9	71.8
^{24}Mg	$Q(2^+)$ $(e.fm^2)$	-18.2	-18.1	-19.2
	$B(E2; 2^+ \to 0^+)(e^2.fm^4)$	92.7	109.8	97.6
	$B(E2; 4^+ \to 2^+)(e^2.fm^4)$	127.7	143.1	133.5

the multipole part and whether they can explain the changes brought by empirical fits. One has also to note, that there is no ideal prescription on how to derive the effective Hamiltonian in the MBPT and apparently, the multipoles converged in terms of $\hbar\omega$ excitations in the Q-box function are too strong and need to be readjusted in the fit. Certain multipole terms, like pairing, are not well converged in the perturbation expansion, either. Thus the non-perturbative resummations, like CC or IM-SRG, could be better tools to provide unambiguous treatment of correlations in the effective interactions for shell model calculations.

Chapter 4

Interest of present LSSM studies for nuclear astrophysics

During my post-doctoral period in GSI/TU Darmstadt, I have participated in developments of empirical effective interactions and shell model codes which have permitted studying the subjects of interest for the astrophysical applications, briefly summarized here in points 4.1 and 4.2. My current interests are focalized on investigating in a systematic way the low energy γ strength functions in different regions of nuclei, trying to pin down the origin and character of the low energy enhancement of radiation observed in several parts of the nuclear chart. Some observations on this subject are given in Sec. 4.3.

4.1 Half-lives of r-process nuclei

The β half-lives of waiting point nuclei have two effects on the r-process dynamics and abundance distributions. They mainly determine the time it takes the mass flow within the r-process to transmute seed nuclei to heavy nuclei in the third peak around $A \sim 200$. Second, in the astrophysical environment the nuclear r-process time scale competes with dynamical time scale of the environment, i.e. the expansion time scale of the ejected matter. If the r-process path and half-lives were known, one could constrain the conditions of the astrophysical environment from the abundance distribution.

Experimentally, only a few of the half-lives of $N = 50, 82$ nuclei are known while no data exist for $N = 126$. While these are usually very neutron rich nuclei, where proton and neutron Fermi surfaces are located in different harmonic oscillator shells, the first-forbidden (FF) transitions can not be omitted in theoretical description of half-lives. Including such transitions in the shell model framework was a part of PhD project of J.J. Cuenca-Garcia (PhD TU Darmstadt 2007-2009) and of a post-doc of Q. Zhi (TU Darmstadt, 2009-2011). In collaboration with E. Caurier and G. Martinez-Pinedo (TU Darmstadt), we have developed the code NATHAN to take into account such transitions. We have included all forbidden operators following Behrens and Bühring treatment [106]. The quenching of the FF operators have been established by the least-square fit to several

half-lives known for $N = 82$ and $N = 126$ nuclei.

Further, systematic calculations of half-lives and β-delayed neutron emission probabilities for waiting point nuclei have been performed [107]. We have found that the inclusion of the FF transitions does not affect much the half-lives of $N = 50, 82$ nuclei but speed up the decays in the $N = 126$ region. Our results for $N = 126$ were shown to be in agreement with other SM calculations with FF transitions of Suzuki et al.[108], in spite of differences in the model space, interaction and chosen quenching. Our conclusions support the earlier observations from the DF3 model of Borzov et al. [109].

In addition to half-lives calculations, the studies of FF transitions are of a great importance for interpretation of nuclear structure studies of the β-decays of very neutron-rich nuclei, studied currently in RIB facilities. A recent measurement from RIKEN has shown, that the SM faces a difficulty to reproduce the β-delayed emission probability in ^{79}Cu, where a factor 2 difference was noted. Calculations for this case could be now performed using the $fpgd$ model space and the updated version of the LNPS interaction, which should be more predictive for the low lying structures of this and the neighboring nuclei. Further studies of β-decay in this region are envisaged and are discussed in the next Chapter.

4.2 Microscopic evaluations of strength functions for capture rates

The Lanczos method, used in SM codes to diagonalize Hamiltonian matrices, can be also used to evaluate the strength functions of any operator, e.g. transition operators such as EM or GT transitions (see [1] for more detail about the method and its applications). Due to the developments of empirical interactions in the fpg model space, we could have investigated two interesting problems:

1. How the microscopically derived strength functions influence the neutron capture rates, when used instead of the usually applied global parameterizations [110]. We have looked into the role of the $M1$ transitions in the iron chain, from ^{54}Fe to ^{69}Fe, simulated the effect of the scissor mode on the neutron capture rates and tested the Brink hypothesis. We have found that the Lorentzian parameterizations overpredict the capture cross sections with respect to those obtained with microscopically determined strength functions. We have found that the scissor mode appearing around neutron threshold can enhance the capture rate by 2 orders of magnitude. Finally, a factor 2 difference has been found between the step-by-step evaluated cross section and that obtained using Brink hypothesis and ground state $M1$ distribution.

   It is however known that the neutron capture rate, in majority of nuclei in question, is determined by the $E1$ contribution. However the parity-changing transitions are difficult to handle in shell model, where due to the basis truncation a proper treatment of spurious center-of-mass excitations becomes impossible. Nonetheless, some attention has been recently devoted to the problem of the role of $E1$ transitions, see Section 4.3.

2. The unblocking of the Gamow-Teller transitions due to nuclear correlations across the $N = 40$ gap and its role for stellar electron capture rates [111]. Large scale SM calculations have been performed for ^{76}Se, where the GT_+ distributions has been measured. Using different valence spaces and interactions, we have achieved a reasonable agreement with experiment. The experimental and calculated GT_+ strengths have been converted to electron capture rates, which supported the argument that the process during the collapse of the core is dominated by electron capture on nuclei.

4.3 Low energy enhancement of γ strength functions and developments of interactions in $1\hbar\omega$ model spaces

Photoneutron cross sections and radiative neutron capture cross sections are fundamental nuclear inputs to stellar model calculations of nucleosynthesis processes. Evaluation of (n,γ) cross sections requires knowledge of statistical nuclear quantities, such as γ-ray strength function (γ-SF) and nuclear level density. The γ-SF below the neutron threshold plays a key role in defining the electromagnetic de-excitation taking place after the neutron capture, which, together with the β-decay, drives the $s-$ and $r-$process nucleosynthesis. Recently, a non-statistical behavior of the radiative strength functions has been observed in several regions of nuclei, e.g. [112, 113, 114], which could have an impact on the related neutron capture rates.

The nuclear shell model is commonly used to calculate nuclear spectra and transitions as well as strength distributions of electromagnetic operators. Recently, a method of obtaining the dipole strength functions from averages of a large number of $M1$ transitions within the shell model has been proposed [113]. It has been demonstrated for mass ~ 90 region that the $M1$ γ-SF are enhanced toward low energy, in agreement with experimental observations. It has been suggested that it happens in nuclei near closed shells where high j proton and neutron orbitals are located near the Fermi surface with magnetic moments adding up coherently. Later calculations in iron nuclei [114] supported such an enhancement mechanism. On the other hand, in Ref. [115] the role of $E1$ transition has been studied in the finite-temperature relativistic quasiparticle random phase approximation and it has been found that a non-negligible enhancement of the $E1$ strength is present in Mo nuclei in a given temperature range. So far, calculations of both $M1$ and $E1$ components of radiative strength function within the same framework have not been achieved.

I have thus developed an effective interaction in the full $1\hbar\omega$ model space: $sd-pf-gds$. The interaction is based on a realistic set of matrix elements from a V_{lowk} [12] based on the CD-Bonn potential [9]. The pf-shell monopoles have been replaced by the monopoles of the latest empirical LNPS interaction [5], which reproduces with a great accuracy the ensemble of nuclei in the pf-shell. Such a procedure allows to find a good agreement for the low lying states of pf-shell nuclei. Other monopole corrections have been applied to the cross-shell interactions in order to fix the known positions of single-particle/hole states

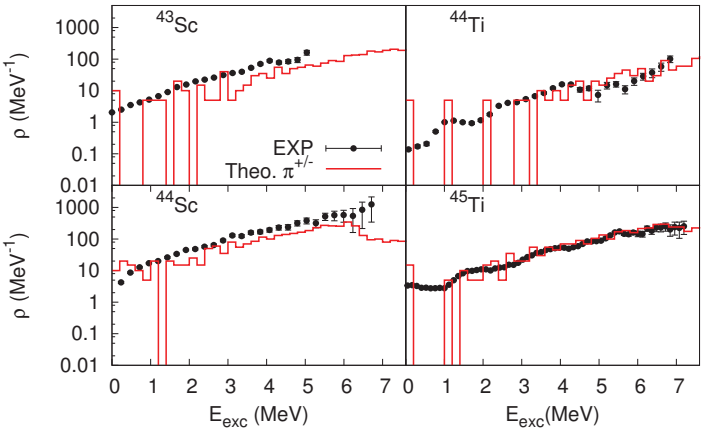

Figure 4.1: Level densities from the present calculations compared to Oslo data [112, 117, 119].

(spectra of ^{39}K, ^{41}Ca) and the position of the lowest opposite parity-states in ^{41,42}Ca, ^{44}Ti and ^{78}Sr nuclei. The calculations have been carried out using the coupled scheme code NATHAN [1], performing full pf-shell diagonalizations for the natural parity states and taking into account the full $1\hbar\omega$ excitations for the opposite parity states. The latter assures an exact factorization of spurious center of mass and physical (i.e. COM at rest) excitations. The shell model Hamiltonian reads:

$$H = \sum_i \epsilon_i c_i^\dagger c_i + \sum_{ijkl} V_{ijkl} c_i^\dagger c_j^\dagger c_l c_k + \beta H_{c.m.}$$

where the COM Hamiltonian with a multiplication coefficient β has been added to push up the COM eigenvalues to the energy range not considered in the calculations.

The results concerning the low energy enhancement in Sc and Ti nuclei are now in preparation for publication, where for the first time the contributions from the electric and magnetic dipole are obtained within the same model. Some of these results are discussed below.

In Fig. 4.1 we show the level densities obtained in present approach in comparison to available data. The theoretical levels have been sorted into 0.2MeV bins. They are compared to experimental data from Oslo group [112, 116, 117, 118, 119]. The total level densities agree fairly well in the region where experimental data is available in Ti isotopes while some states seem to be missing in scandiums. This comes from the fact that in nuclei very close to the $Z, N = 20$ closures, states built from 2p-2h excitations appear at low energy. Those, however, can not be treated at the same level of complexity in present theoretical approach due to the dimensions of the configuration space beyond current computing possibilities.

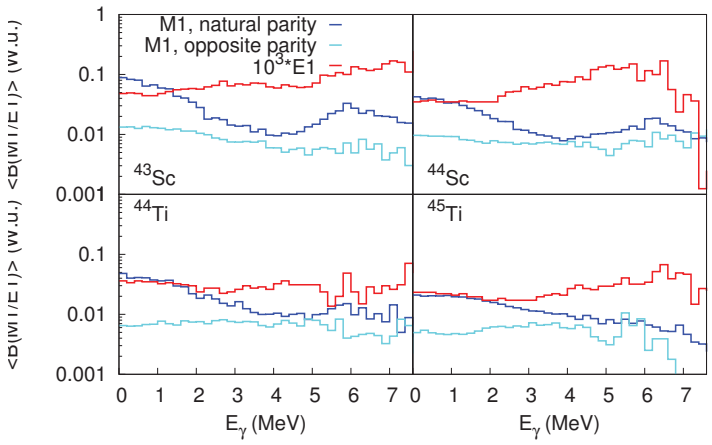

Figure 4.2: Averaged $M1$ and $E1$ transition probabilities for considered nuclei. For $M1$ part the contributions from the natural and non-natural (opposite) parity states are distinguished. Note multiplication factor applied for $E1$'s for the transparency of the Figure.

In Fig. 4.2 we show the averages of the $M1$ reduced transition probabilities per energy bin of 0.2MeV. For the $M1$ part, the averages were deduced for both parities separately. As one can see, the natural parity part of $M1$ is the only that is clearly enhanced at low energy in all cases, though the magnitude of the enhancement is not the same for all nuclei. The natural parity states of considered nuclei contain protons and neutrons in the $f_{7/2}$ orbital, which can be recoupled to generate higher-spin states, leading to many close lying levels connected by $M1$'s involving large $f_{7/2} \rightarrow f_{7/2}$ matrix elements. Such diagonal matrix elements were shown responsible for the lowest part of the $M1$ SF (see Fig. 4 in Ref. [114]). The dependence of the natural parity $M1$ part on excitation energy and spin distribution was discussed in Ref. [114] for the case of ^{56}Fe. I have verified that the results for the natural parity $M1$ part are also quite stable with excitation energy/ number of states considered in the calculations, showing slight modifications of the magnitude of the averaged strength but no change of the trend at low γ energy.

Concerning 1p-1h states, they are formed by lifting proton or neutron particle mostly from the $d_{3/2}$ orbit to the $f_{7/2}$ and have wave functions fragmented over many different configurations. This leads to numerous cancellations and involves many smaller, non-diagonal matrix elements in the magnetic transitions. As a result, the non-natural parity magnetic dipole behaves differently: its average magnitude is much lower and the low energy part much flatter.

The averaged electric dipole requires more caution as its behavior can be biased by the distribution of both parity states. Generally, the computed density of pf states is lower at intermediate energies than that of 1p-1h states in these nuclei, with only a few particles in the pf-shell. Since the same number of states of both parities is calculated, at higher energy

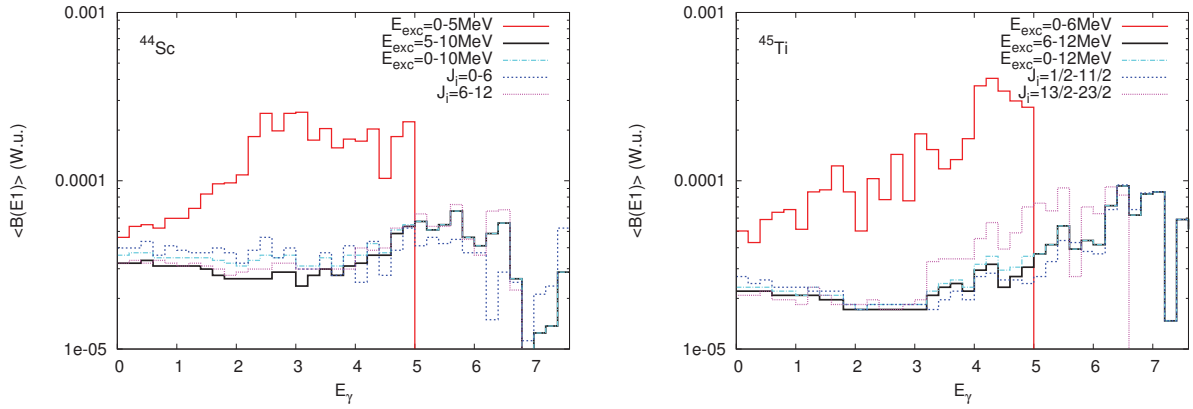

Figure 4.3: Averaged $B(E1)$ values deduced for different ranges of initial spins and excitation energies for ^{44}Sc and ^{45}Ti nuclei.

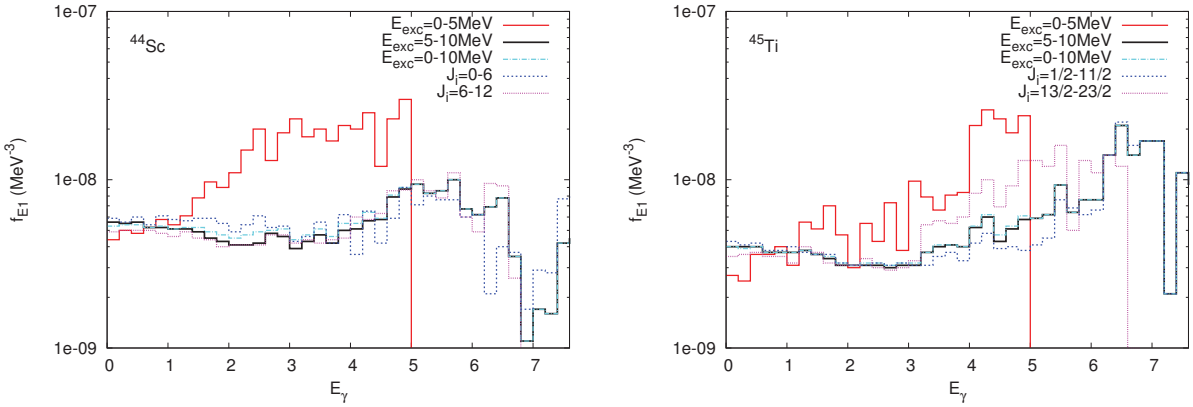

Figure 4.4: γ-SF deduced for different ranges of initial spins and excitation energies for ^{44}Sc and ^{45}Ti nuclei.

natural parity states dominate. Therefore, I have determined for each nucleus separately the excitation energy up to which both parities with different spin values are represented in the present SM calculation and $\langle B(E1)\rangle$ values have been evaluated only up to this energy.

As can be seen in Fig. 4.2, averaged electric dipole has a similar behavior in all cases, quite steady at low energy and increasing slightly towards higher γ-energies. I have further tested its dependence on the energy cut-off and spin distributions in the calculations. The results are shown in Fig. 4.3 for the averaged dipole and in Fig. 4.4 for the SF obtained

using those averages, taking as examples ^{44}Sc and ^{45}Ti. The lowest γ energy behavior is quite independent of the excitation energy and spin range considered in the sense of not showing any upbend towards zero γ energy. There is however a substantial difference in the case of averages and SF deduced for $E_{exc} = 0 - 5$MeV only, which are substantially larger than those including contributions from the higher energy states. On the contrary, there is practically no difference between summation of all states up to 10MeV and in the intervals 5-10MeV: since the level density is growing with excitation energy, the total averages and strength functions are dominated by those of the highest energy states. There is also little difference whether only lower or higher spins are taken into account. The results are strikingly similar for both nuclei in spite of the differences coming from the fact we deal here with odd-odd and even-odd nuclei, the calculated level densities and the number of $E1$ transitions are not the same etc. Most importantly, the shape of the $\langle B(E1)\rangle$ at low energy does not show any clear upbend in neither case and seems more consistent with the statistical behavior. However one needs to note that the zero-γ energy limit is not null in shell model calculations.

In addition to the results discussed above, the calculations for higher pf-shell nuclei are in progress and a detailed analysis of deformation effects, model space limitations, effects of including giant resonances on the radiative strength function is under way (see next Chapter). Also a study of low energy γ-SF in ^{87}Kr, in collaboration with the Oslo experimental group, is currently in progress.

Chapter 5

Perspectives

The present synthesis omits several more subjects I have investigated during last years. The publication list given in Sec. 8 contains a couple of theoretical studies that I have carried out (7, 9, 13) and several other publications with experimentalists that are out of the major axes discussed here (33, 37, 39, 41). I should also mention an undertaken study within the no-core approach aiming in the ab-initio description of purely neutron systems. In collaboration with E. Caurier and R. Lazauskas (IPHC Strasbourg) we have developed tools necessary to tackle this problem with the use of Lee-Suzuki interactions and preliminary calculations have been performed up to mass 12. However it would be more appropriate to use V_{lowk} potentials to this purpose which is one of the subjects that could be undertaken in future.

In addition to further developments of effective interactions and various studies already mentioned in Chapters 2-4, my future research will focus on three topics:

- β-decay studies around ^{78}Ni
  A great part of the joined experimental-theoretical studies of nuclei above ^{78}Ni has been carried out and published in collaboration with W. Urban (UW Warsaw), PI in the research project in which I participate as theory expert (36 months grant DEC-2013/09/B/ST2/03485 of Polish National Science Center). The studies of the nuclei in the region are also a subject of PhD thesis of M. Czerwinski (UW Warsaw, underway). Our collaboration continues for the physics of nuclei in the close vicinity of ^{78}Ni, and in particular, we envisage a program to search for the neutron $g_{7/2}$ orbital in neutron-rich nuclei close to the ^{78}Ni core through the study of β-decays and of the medium-spin states possibly involving this orbital (the current funding scheme can be extended up to 2018).

  The experimental studies of neutron-rich nuclei include their β-decays, which at low energies are dominated by forbidden decays. As described previously, the model spaces and interactions have been developped for the study of spectroscopic properties of nuclei around ^{78}Ni, which could be also used to study their weak-decays. Also the NATHAN code is ready for calculations of first-forbidden operators. In our recent work [120] a number of $\log ft$ have been obtained experimentally, including

several unique first-forbidden transitions. The description of those within the existing framework has been presented for a master project. Further, a PhD thesis will be proposed to continue this work for all first-forbidden operators and other applications. In particular, including the possibility of calculations of first-forbidden decays in ANTOINE code will extend the applicability of our tools to more complex nuclei and to other subjects of interest for nuclear structure and for nuclear astrophysics (e.g. β decay studies above ^{132}Sn, competition of GT and FF decays at $N = 40$ to understand better the evolution of the neutron star crust).

- Statistical properties of nuclei: photoabsorption γ-SF and level densities
  The evaluations of (n, γ) cross sections, necessary e.g. for s- and r-process calculations, are based on very simple (statistical) assumptions for the shape of strength functions, both of magnetic and electric type. It is however expected that the phenomena like the low energy enhancement, pygmy resonance or scissor mode can enhance neutron capture cross sections. Also the limits of applicability of the Brink-Axel hypothesis, assumed in calculations and experimental analyses, are still a subject of a great debate. The shell model is a perfect tool to examine in more detail the shape of the strength functions depending on deformation effects, shell structure, energy range, etc. which could help in providing a more realistic modeling of the strength distribution for astrophysical applications. The systematic calculations of photoabsorption strength functions including both dipole modes (presented in Sec. 4.3) will be thus continued for sd and pf nuclei and extended to higher mass nuclei for the $M1$ part. For this purpose, ANTOINE code needs to be employed with several modifications to circumvent numerical errors related to angular momentum loss in computations with many iterations, necessary to obtain a wealth of low lying states and transitions strengths between them.
  The project will be founded by IN2P3 for three years (2017-2020).

- Nuclear masses and DZ formulae
  An important subject I have undertaken concerns many-body forces in nuclear systems and their modeling, which could lead to the construction of a "generalized monopole" model. This is to say, to establish an universal mechanism of shell evolution which could be extrapolated safely to the unknown, i.e. used in the construction of effective interactions far from the stability, where the paucity of experimental data does not allow to obtain fitted interactions of a good quality. A preliminary study of three-body monopoles was done in collaboration with A. P. Zuker. We have shown that using the mechanism proposed by Zuker in [121] we can describe reasonably the spectroscopy of the p-shell and sd-shell nuclei, adjusting to data only a few parameters, which in addition do not depend much on the initial realistic interaction (unpublished, presented in Zakopane conference 2012). It remains to be verified whether the same mechanism will work satisfactorily in the pf-shell (one expects it will, given the results of [17]) and in the $2\hbar\omega$ model spaces. A related aspect is the inclusion of 3-body monopoles in the Duflo-Zuker mass formula. The DZ10 model,

which is a functional of occupations with only 10 parameters and an associated fortran code of 80 lines, gives an rms deviation of 506keV for 1810 nuclei. Its more elaborated version with 28 parameters (DZ28) fits known nuclei above ^{16}O with the rms of only 375keV. The DZ formula remains however quite obscure in the description of extruder-intruder shell closures. Since the 3N forces are supposed to be at the origin of such closures, as discussed in this dissertation and in Ref. [121], a part of the DZ formula could be replaced by the 3-body monopole term, which could lead us to a formulation as powerful but as well elegant, with a robust physics mechanism ensuring a proper propagation to the unknown mass regions.

Bibliography

[1] E. Caurier, G. Martinez-Pinedo, F. Nowacki, A. Poves, and A. P. Zuker. *Rev. Mod. Phys.*, 77:427–488, 2005.

[2] E. Caurier and F. Nowacki. *Acta Phys. Pol.*, B30:705, 1999.

[3] E. Caurier, A. P. Zuker, A. Poves, and G. Martínez-Pinedo. *Phys. Rev. C*, 50:225–236, 1994.

[4] E. Caurier, G. Martinez-Pinedo, F. Nowacki, A. Poves, J. Retamosa, and A. P. Zuker. *Phys. Rev.*, C59:2033, 1999.

[5] S. M. Lenzi, F. Nowacki, A. Poves, and K. Sieja. Island of inversion around ^{64}cr. *Phys. Rev. C*, 82(5):054301, Nov 2010.

[6] E. Caurier, F. Nowacki, A. Poves, and K. Sieja. *Phys. Rev. C*, 82:064304, Dec 2010.

[7] E. Caurier, P. Navrátil, W. E. Ormand, and J. P. Vary. *Phys. Rev. C*, 64:051301, Oct 2001.

[8] C. Forssen. private communication.

[9] R. Machleidt. High-precision, charge-dependent bonn nucleon-nucleon potential. *Phys. Rev. C*, 63(2):024001, Jan 2001.

[10] R. B. Wiringa, V. G. J. Stoks, and R. Schiavilla. Accurate nucleon-nucleon potential with charge-independence breaking. *Phys. Rev. C*, 51:38–51, Jan 1995.

[11] K.A. Brueckner. *Phys. Rev.*, 97:1353, 1955.

[12] S.K. Bogner, T.T.S. Kuo, and A. Schwenk. *Phys. Rep.*, 386:1, 2003.

[13] S. K. Bogner, R.J. Furnstahl, and A. Schwenk. From low-momentum interactions to nuclear structure. *Prog. Part. Nucl. Phys.*, 65:94–147, 2010.

[14] Marianne Dufour and Andres Zuker. The realistic collective nuclear Hamiltonian. *Phys. Rev.*, C54:1641–1660, 1996.

[15] Achim Schwenk and Andres P. Zuker. Shell-model phenomenology of low-momentum interactions. *Phys. Rev.*, C74:061302, 2006.

[16] A. Cortes and A. P. Zuker. *Phys. Lett.*, B84:25, 1979.

[17] A.P. Zuker. *Phys. Rev. Lett.*, 90:042502, 2003.

[18] P. Navratil, V. G. Gueorguiev, J. P. Vary, W. E. Ormand, and A. Nogga. *Phys. Rev. Lett.*, 99:042501, Jul 2007.

[19] Steven C. Pieper, V. R. Pandharipande, R. B. Wiringa, and J. Carlson. *Phys. Rev. C*, 64:014001, Jun 2001.

[20] M. Hjorth-Jensen, T. Engeland, A. Holt, and E. Osnes. *Phys. Rep.*, 242:37–69, 1994.

[21] M. Hjorth-Jensen, T.T.S. Kuo, and E. Osnes. *Phys. Rep.*, 261:125–270, 1995.

[22] E.M. Kreciglowa and T.T.S. Kuo. *Nucl. Phys.*, A235:171, 1974.

[23] K. Suzuki and S.Y Lee. *Prog. Theo. Phys..*, 64:2091, 1980.

[24] Takaharu Otsuka, Toshio Suzuki, Jason D. Holt, Achim Schwenk, and Yoshinori Akaishi. Three-body forces and the limit of oxygen isotopes. *Phys. Rev. Lett.*, 105(3):032501, Jul 2010.

[25] J. D. Holt, J. Menendez, and A Schwenk. *Eur. Phys. J.*, A49:39, 2013.

[26] J. D. Holt, J. Menéndez, J. Simonis, and A. Schwenk. Three-nucleon forces and spectroscopy of neutron-rich calcium isotopes. *Phys. Rev. C*, 90:024312, Aug 2014.

[27] G. R. Jansen, J. Engel, G. Hagen, P. Navratil, and A. Signoracci. *Phys. Rev. Lett.*, 113:142502, Oct 2014.

[28] S. K. Bogner, H. Hergert, J. D. Holt, A. Schwenk, S. Binder, A. Calci, J. Langhammer, and R. Roth. Nonperturbative shell-model interactions from the in-medium similarity renormalization group. *Phys. Rev. Lett.*, 113:142501, Oct 2014.

[29] L. Coraggio, A. Covello, A. Gargano, N. Itaco, and T. T. S. Kuo. Shell-model study of quadrupole collectivity in light tin isotopes. *Phys. Rev. C*, 91:041301, Apr 2015.

[30] L. Coraggio, A. Covello, A. Gargano, N. Itaco, and T. T. S. Kuo. Shell-model study of the $n = 82$ isotonic chain with a realistic effective hamiltonian. *Phys. Rev. C*, 80:044320, Oct 2009.

[31] L. Coraggio, A. Covello, A. Gargano, and N. Itaco. Realistic shell-model calculations for isotopic chains "north-east" of ^{48}Ca in the (n,z) plane. *Phys. Rev. C*, 89:024319, Feb 2014.

[32] B.A. Brown and B.H. Wildentahl. *Annu. Rev. Nucl. Part. Sci.*, 38:29, 1988.

[33] B. Alex Brown and W. A. Richter. *Phys. Rev. C*, 74:034315, 2006.

[34] M. Honma, T. Otsuka, B. A. Brown, and T. Mizusaki. *Phys. Rev. C*, 69:034335, Mar 2004.

[35] M. Honma, T. Otsuka, T. Mizusaki, and M. Hjorth-Jensen. New effective interaction for f_5pg_9-shell nuclei. *Phys. Rev. C*, 80:064323, Dec 2009.

[36] A. Gniady, E. Caurier, F. Nowacki, and A. Poves. unpublished.

[37] Andres P. Zuker and Marianne Dufour. Separation of the monopole contribution to the nuclear Hamiltonian. 1995.

[38] A. Poves and A.P. Zuker. *Physics Reports*, 70:235, 1981.

[39] F. Nowacki and A. Poves. New effective interaction for $0\hbar\omega$ shell-model calculations in the $sd-pf$ valence space. *Phys. Rev. C*, 79(1):014310, Jan 2009.

[40] K. Sieja, F. Nowacki, K. Langanke, and G. Martinez-Pinedo. Shell model description of zirconium isotopes. *Phys. Rev.*, C79:064310, 2009.

[41] G. S. Simpson, G. Gey, A. Jungclaus, J. Taprogge, S. Nishimura, K. Sieja, et al. *Phys. Rev. Lett.*, 113:132502, Sep 2014.

[42] M. Hjorth-Jensen. http://www.fys.uio.no/ mhjensen/.

[43] A. F. Lisetskiy, B. Alex Brown, M. Horoi, and H. Grawe. *Phys. Rev.*, C70:044314, 2004.

[44] Takaharu Otsuka, Toshiaki Matsuo, and Daisuke Abe. Mean Field with Tensor Force and Shell Structure of Exotic Nuclei. *Phys. Rev. Lett.*, 97:162501, 2006.

[45] N. Smirnova, B. Bally, K. Heyde, F. Nowacki, and K. Sieja. *Phys. Lett.*, B686:109–113, 2010.

[46] N. A. Smirnova, K. Heyde, B. Bally, F. Nowacki, and K. Sieja. *Phys. Rev. C*, 86:034314, Sep 2012.

[47] Takaharu Otsuka, Toshio Suzuki, Michio Honma, Yutaka Utsuno, Naofumi Tsunoda, Koshiroh Tsukiyama, and Morten Hjorth-Jensen. Novel features of nuclear forces and shell evolution in exotic nuclei. *Phys. Rev. Lett.*, 104(1):012501, Jan 2010.

[48] W. Urban, K. Sieja, G. S. Simpson, H. Faust, T. Rzaca-Urban, A. Złomaniec, M. Łukasiewicz, A. G. Smith, J. L. Durell, J. F. Smith, B. J. Varley, F. Nowacki, and I. Ahmad. New isomers and medium-spin structure of the ^{95}Y nucleus. *Phys. Rev. C*, 79:044304, Apr 2009.

[49] T. Rzaca-Urban, K. Sieja, W. Urban, F. Nowacki, J. L. Durell, A. G. Smith, and I. Ahmad. $(h_{11/2}, g_{7/2})_{9^-}$ neutron excitation in ^{92,94,96}Sr. *Phys. Rev. C*, 79:024319, Feb 2009.

[50] W. Urban, K. Sieja, G. S. Simpson, T. Soldner, T. Rzaca-Urban, A. Złomaniec, I. Tsekhanovich, J. A. Dare, A. G. Smith, J. L. Durell, J. F. Smith, R. Orlandi, A. Scherillo, I. Ahmad, J. P. Greene, J. Jolie, and A. Linneman. Isomeric levels in ^{92}rb and the structure of neutron-rich ^{92,94}rb isotopes. *Phys. Rev. C*, 85:014329, Jan 2012.

[51] G. S. Simpson, W. Urban, K. Sieja, J. A. Dare, J. Jolie, A. Linneman, R. Orlandi, A. Scherillo, A. G. Smith, T. Soldner, I. Tsekhanovich, B. J. Varley, A. Złomaniec, J. L. Durell, J. F. Smith, T. Rzaca-Urban, H. Faust, I. Ahmad, and J. P. Greene. Near-yrast, medium-spin, excited states of ^{91}Rb, ^{93}Rb, and ^{95}Rb. *Phys. Rev. C*, 82:024302, Aug 2010.

[52] G. J. Kumbartzki et al. *Phys. Rev. C*, 89:064305, Jun 2014.

[53] T. Rzaca-Urban, M. Czerwiński, W. Urban, A. G. Smith, I. Ahmad, F. Nowacki, and K. Sieja. *Phys. Rev. C*, 88:034302, Sep 2013.

[54] K. Sieja and F. Nowacki. *Phys. Rev.*, C81:061303, 2010.

[55] M. Czerwinski, T. Rzaca-Urban, K. Sieja, H. Sliwinska, W. Urban, A. G. Smith, J. F. Smith, G. S. Simpson, I. Ahmad, J. P. Greene, and T. Materna. *Phys. Rev. C*, 88:044314, Oct 2013.

[56] A. Korgul et al. *Phys. Rev. C*, 88:044330, Oct 2013.

[57] K. Kolos, D. Verney, F. Ibrahim, F. Le Blanc, S. Franchoo, K. Sieja, F. Nowacki, C. Bonnin, M. Cheikh Mhamed, P. V. Cuong, F. Didierjean, G. Duchêne, S. Essabaa, G. Germogli, L. H. Khiem, C. Lau, I. Matea, M. Niikura, B. Roussière, I. Stefan, D. Testov, and J.-C. Thomas. *Phys. Rev. C*, 88:047301, Oct 2013.

[58] P. Baczyk, W. Urban, D. Złotowska, M. Czerwiński, T. Rzaca-Urban, A. Blanc, M. Jentschel, P. Mutti, U. Köster, T. Soldner, G. de France, G. Simpson, and C. A. Ur. *Phys. Rev. C*, 91:047302, Apr 2015.

[59] Z. Vajta et al. to be published.

[60] T. Materna, W. Urban, K. Sieja, U. Köster, H. Faust, M. Czerwiński, T. Rzaca-Urban, C. Bernards, C. Fransen, J. Jolie, J.-M. Regis, T. Thomas, and N. Warr. *Phys. Rev. C*, 92:034305, Sep 2015.

[61] M. Czerwiński, T. Rzaca-Urban, W. Urban, P. Baczyk, K. Sieja, B. M. Nyakó, J. Timár, I. Kuti, T. G. Tornyi, L. Atanasova, A. Blanc, M. Jentschel, P. Mutti, U. Köster, T. Soldner, G. de France, G. S. Simpson, and C. A. Ur. *Phys. Rev. C*, 92:014328, Jul 2015.

[62] M. Czerwiński, T. Rzaca-Urban, W. Urban, P. Baczyk, K. Sieja, J. Timár, B. M. Nyakó, I. Kuti, T. G. Tornyi, L. Atanasova, A. Blanc, M. Jentschel, P. Mutti, U. Köster, T. Soldner, G. de France, G. S. Simpson, and C. A. Ur. Neutron-proton multiplets in the odd-odd nucleus $^{90}_{37}Rb_{53}$. *Phys. Rev. C*, 93:034318, Mar 2016.

[63] K. Sieja, T. R. Rodríguez, K. Kolos, and D. Verney. *Phys. Rev. C*, 88:034327, Sep 2013.

[64] J. Litzinger et al. Transition probabilities in neutron-rich ^{84,86}Se. *Phys. Rev. C*, 92:064322, Dec 2015.

[65] E. Caurier, F. Nowacki, and A. Poves. *Eur. Phys. J.*, A15:145, 2002.

[66] O. Sorlin et al. *Eur. Phys. J.*, A16:55–61, 2003.

[67] A. Gade et al. *Phys. Rev. Lett.*, 112:112503, Mar 2014.

[68] V. Modamio et al. *Phys. Rev. C*, 88:044326, Oct 2013.

[69] J. Ljungvall et al. *Phys. Rev. C*, 81(6):061301, Jun 2010.

[70] E. Fiori et al. *Phys. Rev. C*, 85:034334, Mar 2012.

[71] J. Diriken et al. *Physics Letters B*, 736(0):533 – 538, 2014.

[72] P.-A. Söderström, S. Nishimura, Z. Y. Xu, K. Sieja, V. Werner, P. Doornenbal, G. Lorusso, F. Browne, G. Gey, H. S. Jung, T. Sumikama, J. Taprogge, Zs. Vajta, H. Watanabe, J. Wu, H. Baba, Zs. Dombradi, S. Franchoo, T. Isobe, P. R. John, Y.-K. Kim, I. Kojouharov, N. Kurz, Y. K. Kwon, Z. Li, I. Matea, K. Matsui, G. Martínez-Pinedo, D. Mengoni, P. Morfouace, D. R. Napoli, M. Niikura, H. Nishibata, A. Odahara, K. Ogawa, N. Pietralla, E. Şahin, H. Sakurai, H. Schaffner, D. Sohler, I. G. Stefan, D. Suzuki, R. Taniuchi, A. Yagi, and K. Yoshinaga. Two-hole structure outside ^{78}Ni: Existence of a μs isomer of ^{76}Co and β decay into ^{76}Ni. *Phys. Rev. C*, 92:051305, Nov 2015.

[73] Z. Meisel, S. George, S. Ahn, D. Bazin, B. A. Brown, J. Browne, J. F. Carpino, H. Chung, R. H. Cyburt, A. Estradé, M. Famiano, A. Gade, C. Langer, M. Matoš, W. Mittig, F. Montes, D. J. Morrissey, J. Pereira, H. Schatz, J. Schatz, M. Scott, D. Shapira, K. Sieja, K. Smith, J. Stevens, W. Tan, O. Tarasov, S. Towers, K. Wimmer, J. R. Winkelbauer, J. Yurkon, and R. G. T. Zegers. Time-of-flight mass measurements of neutron-rich chromium isotopes up to $n = 40$ and implications for the accreted neutron star crust. *Phys. Rev. C*, 93:035805, Mar 2016.

[74] A. Dijon et al. *Phys. Rev. C*, 85:031301, Mar 2012.

[75] Yusuke Tsunoda, Takaharu Otsuka, Noritaka Shimizu, Michio Honma, and Yutaka Utsuno. *Phys. Rev. C*, 89:031301, Mar 2014.

[76] E. Rapisarda et al. *Phys. Rev. C*, 84:064323, Dec 2011.

[77] P. Morfouace, S. Franchoo, K. Sieja, I. Matea, L. Nalpas, M. Niikura, A.M. Shez-Benz, I. Stefan, M. Assi. Azaiez, D. Beaumel, S. Boissinot, C. Borcea, R. Borcea, G. Burgunder, L. Cres, N. De Sville, Zs. Dombr, J. Elseviers, B. Fernez-Domuez, A. Gillibert, S. Giron, S. Gr, F. Hammache, O. Kamalou, V. Lapoux, L. Lefebvre, A. Lepailleur, C. Louchart, G. Marquinez-Duran, I. Martel, A. Matta, D. Mengoni, D.R. Napoli, F. Recchia, J.-A. Scarpaci, D. Sohler, O. Sorlin, M. Stanoiu, C. Stodel, J.-C. Thomas, and Zs. Vajta. *Physics Letters B*, 751:306 – 310, 2015.

[78] P. Morfouace, S. Franchoo, K. Sieja, I. Stefan, N. de Séréville, F. Hammache, M. Assié, F. Azaiez, C. Borcea, R. Borcea, L. Grassi, J. Guillot, B. Le Crom, L. Lefebvre, I. Matea, D. Mengoni, D. Napoli, C. Petrone, M. Stanoiu, D. Suzuki, and D. Testov. Single-particle strength in neutron-rich ^{69}Cu from the ^{70}Zn(d,^{3}He)^{69}Cu proton pick-up reaction. *Phys. Rev. C*, 93:064308, Jun 2016.

[79] E. Sahin et al. *Phys. Rev. C*, 91:034302, Mar 2015.

[80] I. Stefanescu et al. *Phys. Rev. Lett.*, 100:112502, 2008.

[81] K. Sieja and F. Nowacki. *Phys. Rev. C*, 85:051301, May 2012.

[82] G. Hagen, M. Hjorth-Jensen, G. R. Jansen, R. Machleidt, and T. Papenbrock. Evolution of shell structure in neutron-rich calcium isotopes. *Phys. Rev. Lett.*, 109:032502, Jul 2012.

[83] G. Hagen, M. Hjorth-Jensen, G. R. Jansen, R. Machleidt, and T. Papenbrock. Continuum effects and three-nucleon forces in neutron-rich oxygen isotopes. *Phys. Rev. Lett.*, 108:242501, Jun 2012.

[84] R. Orlandi et al. *Physics Letters B*, 740:298–302, 2015.

[85] B. S. Nara Singh, Z. Liu, R. Wadsworth, H. Grawe, T. S. Brock, P. Boutachkov, N. Braun, A. Blazhev, M. Górska, S. Pietri, D. Rudolph, C. Domingo-Pardo, S. J. Steer, A. Ataç, L. Bettermann, L. Cáceres, K. Eppinger, T. Engert, T. Faestermann, F. Farinon, F. Finke, K. Geibel, J. Gerl, R. Gernhäuser, N. Goel, A. Gottardo, J. Grębosz, C. Hinke, R. Hoischen, G. Ilie, H. Iwasaki, J. Jolie, A. Kaşkaş, I. Kojouharov, R. Krücken, N. Kurz, E. Merchán, C. Nociforo, J. Nyberg, M. Pfützner, A. Prochazka, Zs. Podolyák, P. H. Regan, P. Reiter, S. Rinta-Antila, C. Scholl, H. Schaffner, P.-A. Söderström, N. Warr, H. Weick, H.-J. Wollersheim, P. J. Woods, F. Nowacki, and K. Sieja. *Phys. Rev. Lett.*, 107:172502, Oct 2011.

[86] P. Boutachkov et al. *Phys. Rev. C*, 84:044311, Oct 2011.

[87] M. Palacz et al. *Phys. Rev. C*, 86:014318, Jul 2012.

[88] C. Hinke, M. Bohmer, P. Boutachkov, T. Faestermann, H. Geissel, J. Gerl, R. Gernhauser, M. Gorska, A. Gottardo, H. Grawe, J. Grebosz, R. Krucken, N. Kurz, Z. Liu, L. Maier, F. Nowacki, S. Pietri, Zs. Podolyak, K. Sieja, K. Steiger, K. Straub, H. Weick, H.-J. Wollersheim, P. Woods, N. Al-Dahan, N. Alkhomashi, A. Atac, A. Blazhev, N. Braun, I. Celikovic, T. Davinson, I. Dillmann, C. Domingo-Pardo, P Doornenbal, G. de France, G. Farrelly, F. Farinon, N. Goel, T. Habermann, R. Hoischen, R. Janik, M. Karny, A. Kaskas, I. Kojouharov, Th. Kroll, Y. Litvinov, S. Myalski, F. Nebel, S. Nishimura, C. Nociforo, J. Nyberg, A. Parikh, A. Prochazka, P. Regan, C. Rigollet, H. Schaffner, C. Scheidenberger, S. Schwertel, P.-A. Soderstrom, S. Steer, A. Stolz, and P. Strmen. *Nature*, 486:341–345, 2012.

[89] G. Guastalla, D. D. DiJulio, M. Górska, J. Cederkäll, P. Boutachkov, P. Golubev, S. Pietri, H. Grawe, F. Nowacki, K. Sieja, A. Algora, F. Ameil, T. Arici, A. Atac, M. A. Bentley, A. Blazhev, D. Bloor, S. Brambilla, N. Braun, F. Camera, Zs. Dombrádi, C. Domingo Pardo, A. Estrade, F. Farinon, J. Gerl, N. Goel, J. Gręgosz, T. Habermann, R. Hoischen, K. Jansson, J. Jolie, A. Jungclaus, I. Kojouharov, R. Knoebel, R. Kumar, J. Kurcewicz, N. Kurz, N. Lalović, E. Merchan, K. Moschner, F. Naqvi, B. S. Nara Singh, J. Nyberg, C. Nociforo, A. Obertelli, M. Pfützner, N. Pietralla, Z. Podolyák, A. Prochazka, D. Ralet, P. Reiter, D. Rudolph, H. Schaffner, F. Schirru, L. Scruton, D. Sohler, T. Swaleh, J. Taprogge, Zs. Vajta, R. Wadsworth, N. Warr, H. Weick, A. Wendt, O. Wieland, J. S. Winfield, and H. J. Wollersheim. Coulomb excitation of ^{104}Sn and the strength of the ^{100}Sn shell closure. *Phys. Rev. Lett.*, 110:172501, Apr 2013.

[90] P. Doornenbal, S. Takeuchi, N. Aoi, M. Matsushita, A. Obertelli, D. Steppenbeck, H. Wang, L. Audirac, H. Baba, P. Bednarczyk, S. Boissinot, M. Ciemala, A. Corsi, T. Furumoto, T. Isobe, A. Jungclaus, V. Lapoux, J. Lee, K. Matsui, T. Motobayashi, D. Nishimura, S. Ota, E. C. Pollacco, H. Sakurai, C. Santamaria, Y. Shiga, D. Sohler, and R. Taniuchi. *Phys. Rev. C*, 90:061302, Dec 2014.

[91] H. Naidja, F. Nowacki, and K. Sieja. *Acta Phys. Polon.*, B46(3):669, 2015.

[92] L. Coraggio, A. Covello, A. Gargano, and N. Itaco. *Phys. Rev. C*, 88:041304, Oct 2013.

[93] M. P. Kartamyshev, T. Engeland, M. Hjorth-Jensen, and E. Osnes. *Phys. Rev. C*, 76:024313, Aug 2007.

[94] S. Sarkar and M. Saha Sarkar. *Phys. Rev. C*, 78:024308, Aug 2008.

[95] H. Grawe et al. *Nucl. Phys.*, A704:211, 2002.

[96] A. Gottardo et al. *Phys. Rev. Lett.*, 109:162502, Oct 2012.

[97] A. de Shalit and I. Talmi. *Nuclear Shell Theory*. Dover Publications, New York, 1963.

[98] Bhoomika Maheshwari, Ashok Kumar Jain, and P. C. Srivastava. *Phys. Rev. C*, 91:024321, Feb 2015.

[99] Naofumi Tsunoda, Kazuo Takayanagi, Morten Hjorth-Jensen, and Takaharu Otsuka. Multi-shell effective interactions. *Phys. Rev. C*, 89:024313, Feb 2014.

[100] J. Duflo and A. P. Zuker. *Phys. Rev. C*, 59(5):R2347–R2350, May 1999.

[101] http://www.nndc.bnl.gov/.

[102] K. Sieja. *Acta Phys. Polonica*, B247:883, 2016.

[103] K. Kumar. *Phys. Rev. Lett.*, 28:249, 1972.

[104] W. Urban, K. Sieja, T. Rzaca-Urban, M. Czerwiński, H. Naïdja, F. Nowacki, A. G. Smith, and I. Ahmad. First evidence of γ collectivity close to the doubly magic core ^{132}Sn. *Phys. Rev. C*, 93:034326, Mar 2016.

[105] Marcella Grasso. *Phys. Rev. C*, 89:034316, Mar 2014.

[106] H. Behrens and W. Bühring. *Nucl. Phys. A*, 162:111, 1971.

[107] Q. Zhi, E. Caurier, J. J. Cuenca-García, K. Langanke, G. Martínez-Pinedo, and K. Sieja. *Phys. Rev. C*, 87:025803, Feb 2013.

[108] Toshio Suzuki, Takashi Yoshida, Toshitaka Kajino, and Takaharu Otsuka. *Phys. Rev. C*, 85:015802, Jan 2012.

[109] I. Borzov. *Nucl. Phys. A*, 777:645, 2006.

[110] H.P. Loens and et al. *Eur. Phys. J.*, 48:34, 2012.

[111] Q. Zhi, K. Langanke, G. Martínez-Pinedo, F. Nowacki, and K. Sieja. The 76se gamow–teller strength distribution and its importance for stellar electron capture rates. *Nuclear Physics A*, 859(1):172 – 184, 2011.

[112] A. C. Larsen and et al. *Phys. Rev. C*, 85:014320, Jan 2012.

[113] R. Schwengner, S. Frauendorf, and A. C. Larsen. *Phys. Rev. Lett.*, 111:232504, Dec 2013.

[114] B. Alex Brown and A. C. Larsen. *Phys. Rev. Lett.*, 113:252502, Dec 2014.

[115] Elena Litvinova and Nikolay Belov. *Phys. Rev. C*, 88:031302, Sep 2013.

[116] A. Bürger and et al. *Phys. Rev. C*, 85:064328, Jun 2012.

[117] A. C. Larsen and et al.. *Phys. Rev. C*, 76:044303, 2007.

[118] N. U. H. Syed and et al. *Phys. Rev. C*, 80:044309, Oct 2009.

[119] http://www.mn.uio.no/fysikk/.

[120] W. Urban and et al. submitted.

[121] Joel Mendoza-Temis, Jorge G. Hirsch, and Andres P. Zuker. *Nuclear Physics A*, 843(14):14 – 36, 2010.

Chapter 6

Résumé en français

Ce document présente la synthèse de mes travaux dans le cadre de modèle en couches à grande échelle que j'ai menés après ma thèse (2007-2016), lors de deux post-doctorats (au GSI en Allemagne et à l'IPHC à Strasbourg), puis en qualité de chargé de recherches CNRS à l'IPHC de Strasbourg, depuis 2012. Mon travail porte sur les développements des interactions effectives empiriques pour les calculs de type modèle en couches et egalement sur les applications aux études spectroscopiques des noyaux éxotiques et les applications d'intérêt en astrophysique nucléaire.

Le modèle en couches à grande échelle est aujourd'hui la méthode la plus précise pour décrire la spectroscopie et les décroissances des noyaux, sans laquelle l'interprétation des experiences est souvent difficile, voire impossible. C'est une méthode variationelle qui permet de trouver les solutions de l'équation de Schrödinger à plusieurs corps, par la diagonalisation du Hamiltonien nucléaire (habituellement à 2 corps) dans la base des états many-body. Elle permet de trouver les états propres avec une précision numérique arbitraire, pour l'état fondamental et les états excités. En pratique, la complexité numérique du problème limite les applications de la méthode aux noyaux légers et de masse moyenne, ou autour des coeurs fermés pour les noyaux plus lourds. Un progrès significatif a été obtenu ces dernières années dans le groupe de Strasbourg. Grâce aux développements des codes NATHAN et ANTOINE par E. Caurier, il est devenu possible de diagonaliser les matrices d'ordre 10^{10} (en schéma m) sur un seul processeur. Les travaux de parallelisation massive de ces codes menés dans le groupe permettront d'étendre les futures applications de l'approche dans plusieurs autres régions de masse.

Un autre problème lié aux calculs de modèle en couches concerne les interactions effectives utilisées. Celles-ci sont basées sur des interactions réalistes nucléon-nucléon qui reproduisent les dephasages dans le vide. Le coeur dur d'une telle interaction est enlevé par l'approche de matrice G ou dans la méthode V_{lowk} qui permet le découplage des modes à basse et haute énergie dans l'espace de momentum. Les interactions sont ensuite adaptées à l'utilisation dans le milieu nucléaire par les méthodes perturbatives. Néanmoins, les interactions à deux corps de ce type ne permettent pas de reproduire les fermetures spin-orbite dans les noyaux ni d'effectuer des calculs de précision souhaitée. Ceci a été démontré, par exemple dans les calculs ab-initio, faute d'absence de force à trois corps. Malgré le progrès des dernières années, des interactions effectives à 3 corps pour les calculs modèle en couches ne sont actuellement pas disponibles. Pour cette raison, une approche empirique a été employée: Les éléments de matrice du Hamiltonien ont été reajustés aux données spectroscopiques, ce qui a permis les applications de grande qualité dans plusieurs régions de masse: autour de ^{78}Ni, dans la région d'îlot d'inversion à $N = 40$, autour de ^{100}Sn et au dessus du coeur du ^{132}Sn.

- Les interactions effectives dans l'espace $r3g - r4h$
  J'ai commencé les développements des interactions effectives avec des corrections empiriques au dessus du coeur de ^{78}Ni dans l'espace de valence $0f_{5/2}, 1p_{3/2}, 1p_{1/2}, 0g_{9/2}$

proton et $1d_{5/2}, 2s_{1/2}, 1d_{3/2}, 0g_{7/2}, 0h_{11/2}$ neutron (nommé $r3g - r4h$). L'interaction a été initialement employée dans la description des fragments des fission (Y, Rb, Sr) et de la structure des noyaux de Zr. Ensuite, nous l'avons utilisée avec succès dans plusieurs études des noyaux exotiques plus proches du ^{78}Ni en collaboration avec plusieurs groupes expérimentaux. Nous avons également étudié les propriétés de déformation des isotones $N = 52, 54$ dans plusieurs approches théoriques (pseudo-SU3, modèle en couches et l'approche au delà de champ moyen) en démontrant la possibilité de collectivité et de triaxialité de ces noyaux: ^{88}Se a été predit le plus déformé prolate et ^{86}Ge le plus triaxial dans cette région de masse.

Récemment, une partie de cette interaction a été réajustée en prenant en compte des nouvelles données dans les noyaux $N = 50$, ce qui a permis une meilleure déscription théorique des systèmes impaires-impaires dans la région. Plusieurs travaux ont déjà été effectués avec cette nouvelle version avec succès.

- Les interactions effectives dans l'espace $fpgd$
  Un autre développement majeur concerne l'interaction effective nommée LNPS (Lenzi-Nowacki-Poves-Sieja) dans l'espace modèle pf pour les protons et $pfg_{9/2}d_{5/2}$ pour les neutrons. Cet espace modèle est le minimal qui permet de décrire la soudaine apparition de collectivité dans les noyaux $N = 40$ quand on s'éloigne du ^{68}Ni. Nous avons réussi une description détaillée des données existantes qui suggèrent qu'un tel phénomene peut se produire et nous avons fourni des prédictions théoriques qui ont stimulé les efforts experimentaux dans cette région. Nous avons expliqué que l'apparition de ce nouveau îlot de collectivité est lié à la structure en couches sous-jacente, analogique à ce qui est connu dans les isotones $N = 8$ et $N = 20$. Nous avons aussi prédit la possibilité de co-existence des formes dans ^{68}Ni.

  Ensuite, j'ai continué les ajustements de l'interaction et les études de l'évolution des couches $Z = 28$ et $N = 50$ vers ^{78}Ni, par les investigations de structure des isotopes de cuivre et des isotones $N = 49, 50$. Entre outre, j'ai démontré une possible réduction du gap proton entre ^{68}Ni et ^{78}Ni et une persistance du gap $N = 50$ et j'ai prédit le caractère doublement magique du ^{78}Ni. Une forte ressemblance de l'évolution des couches entre ^{68}Ni et ^{78}Ni à celle déjà connue dans les noyaux d'oxygène et de calcium a été remarquée. Le gap $N = 50$ peut emerger dû aux effets de la force à 3 corps en analogie avec les systèmes légers ce qui pourra être testé dans le futur par les approches ab-initio.

- Les noyaux au dessus de ^{132}Sn
  J'ai egalement étudié les noyaux au dessus de ^{132}Sn pour lesquels j'ai établi une interaction effective adaptée. Dans un premier temps, j'ai expliqué la systématique des transitions isomériques $6^+ \rightarrow 4^+$ dans les étains lourds (^{132}Sn-^{138}Sn) comme étant dues aux mélanges de seniorité. En analogie avec la région de masse au dessus du

^{78}Ni, j'ai aussi demontré la possibilité de développement de collectivité et de triaxialité dans les isotones $N = 86$, avec le maximum de triaxialité dans ^{140}Xe. Une étude commune avec les expérimentateurs de Varsovie a confirmé l'existence d'une bande γ dans ce noyau.

- Région autour de ^{100}Sn
  Finalement, des études ont été menées dans la région autour du ^{100}Sn. En outre, nous avons expliqué théoriquement la décroissance super-permise Gamow-Teller du ^{100}Sn. Cette décroissance observée au GSI en Allemagne fut plus rapide que toutes les décroissances β connues auparavant. Cela se produit grâce à une structure particulière en couches et des gaps très rigides du ^{100}Sn. L'information complémentaire sur la stabilité des gaps du ^{100}Sn a été obtenue par les études des états isomériques des noyaux de palladium et cadmium crées par les excitations des neutrons à travers le gap $N = 50$.

A part des études de structure des noyaux exotiques qui ont pu être effectuées grâce aux développements des interactions décrites ci-dessus, des études de propriétés de la force nucléaire dans l'évolution des couches ont été réalisées. Nous avons appliqué la décomposition spin-tenseur des interactions réalistes et empiriques pour déterminer le rôle des termes centraux, vecteur et tenseur dans la création des gaps et l'évolution de couches loin de la ligne de stabilité. Nous avons mis en évidence le rôle majeur du terme tenseur dans l'évolution du splitting de partenaires spin-orbite dans les noyaux riches en neutron dans l'interaction proton-neutron. La nécessité du terme vecteur (spin-orbite) dans la création des gaps spin-orbite (14, 28, 50, ...) dûs à la force $T = 1$ a été également quantifiée.

Un autre volet des applications du modèle en couches concerne les aspects d'intérêt astrophysique. Les modèles stellaires et de nucléosynthèse exigent la connaissance du grand nombre des données nucléaires qui, avant tout dans les noyaux riches en neutron, ne peuvent pas être expérimentalement déterminées. Par conséquent, les modèles théoriques sont nécessaires pour fournir les durées de vie β, les masses, les taux de réactions, les barrières de fission etc. Le modèle en couches peut être employé dans les calculs de tels observables. Par exemple, nous avons développé le code NATHAN pour y inclure les calculs des opérateurs de transitions β interdites qui peuvent jouer un rôle important dans la décroissance β des noyaux très riches en neutron. Nous avons donc effectué une étude de durée de vie des noyaux "waiting point" du processus r, mettant en évidence le rôle important des transitions interdites, avant tout dans les isotones $N = 126$.

Un autre problème qui peut être abordé dans l'approche du modèle en couches concerne la description de fonctions de force γ. Dans les calculs des sections efficaces de capture neutronique il est nécessaire de connaître la densité des niveaux nucléaires et la force γ radiative. Des modèles simples sont employés pour approximer la forme des fonctions de

force. Cependant, les mesures ont démontré dans quelques noyaux accessibles à l'expérience que les fonctions de force γ augmentent à basse énergie, ce qui n'est pas pris en compte dans les modèles statistiques. L'origine de ce phénomène n'est pas encore compris. J'ai commencé une étude des transitions $M1$ et, pour la première fois dans ce contexte, des $E1$ dans les noyaux de la couche pf. Les fonctions de force γ obtenus dans ces calculs confirment la possibilité d'augmentation de la force $M1$ à basse énergie, suggérée précédemment par d'autres calculs théoriques, tandis que la forme de la force $E1$ reste plus proche du comportement statistique. Néanmoins, plus d'efforts et une étude plus systématique sont nécessaire pour déterminer au mieux l'évolution de la force à basse énergie.

Le programme futur de ma recherche contient 3 volets:

- Noyaux autour du ^{78}Ni
  Actuellement, en collaboration avec le groupe expérimental de Varsovie, nous menons des études des décroissances β des noyaux au dessus du ^{78}Ni ayant pour but la localisation de l'orbital $g_{7/2}$ dans le coeur du ^{78}Ni. A part des études spectroscopiques, l'investigation des décroissances Gamow-Teller et des décroissances premières interdites est egalement envisagée dans cett région de masse. Un stage de master a été proposé sur ce sujet.

- Fonctions de force γ
  Une étude systématique de force γ à basse énergie est envisagée pour déterminer le changement de cette force avec la forme du noyaux et l'isospin et pour comprendre des conséquences possibles sur la modélisation du processus r. Une étude en collaboration avec d'autres théoriciens impliqués dans ce type des études (Université de Bruxelles, CEA-DAM) est prévue pour atteindre cet objectif. J'ai également entreprise des études diverses en collaboration avec des groupes expérimentaux à Oslo et IThemba. Un financement In2p3 de 3 ans m'a été accordé pour atteindre ces objectifs.

- Formules de masse
  A part des études systématiques de force γ à basse énergie et les investigations de décroissances β autour du ^{78}Ni, le programme de recherche futur inclut un développement de la formule de masse Duflo-Zuker. La formule DZ est un fonctionnel des occupations, basé sur la phénomènologie de modèle en couches. Elle existe en deux variants, avec 10 ou 28 paramètres et est toujours parmi les meilleurs sur le marché. La formule DZ, bien qu'elle soit déjà puissante, contient des termes assez obscures qui modélisent les fermetures des couches. Ils pourraient être remplacés par des formulations mieux fondées, par exemple, par des termes monopolaires à 3 corps qui furent démontrés responsables de la création de fermetures de couches de type spin-orbite. Cette nouvelle formulation pourrait fournir des meilleures prédictions loin de la ligne de stabilité, grâce aux mécanismes robustes de physique qui pourraient être incorporés.

Chapter 7

Selected publications

PHYSICAL REVIEW C **79**, 064310 (2009)

Shell model description of zirconium isotopes

K. Sieja,[1,2] F. Nowacki,[3] K. Langanke,[2,4] and G. Martínez-Pinedo[1]
[1]*GSI-Helmholtzzentrum für Schwerionenforschung mbH., Planckstrasse 1, D-64-220 Darmstadt, Germany*
[2]*Institut für Kernphysik, Technische Universität Darmstadt, D-64289 Darmstadt, Germany*
[3]*Institute Pluridisciplinaire Hubert Curien, 23 rue du Loess, Strasbourg, France*
[4]*Frankfurt Institute for Advanced Studies, D-60438 Frankfurt am Main, Germany*
(Received 20 March 2009; published 10 June 2009)

We calculate the low-lying spectra and several high-spin states of zirconium isotopes ($Z = 40$) with neutron numbers from $N = 50$ to $N = 58$ using a large valence space with the ^{78}Ni inert core, which *a priori* allows one to study the interplay between spherical and deformed configurations, necessary for the description of nuclides in this part of the nuclear chart. The effective interaction is derived by monopole corrections of the realistic G matrix. We reproduce essential nuclear properties, such as subshell closures in ^{96}Zr and ^{98}Zr. The spherical-to-deformed shape transition in ^{100}Zr is addressed as well.

DOI: 10.1103/PhysRevC.79.064310 PACS number(s): 21.60.Cs, 21.10.−k, 27.60.+j

I. INTRODUCTION

The Zr isotopes between $N = 50$ and $N = 62$ undergo a clear and smooth shape transition with increasing neutron number, from the spherical structure of $^{90-98}$Zr to a rotor in ^{102}Zr [1–4]. The lightest stable isotope, ^{90}Zr, lies at the $N = 50$ shell closure. The heaviest stable isotope, ^{96}Zr, is already very close to the region of deformation, but a large gap between the ground state and the first excited 2^+ state of 1751 keV suggests a subshell closure. Another interesting feature is that this nucleus is one of the few that have a 0^+ as their first excited state. Similar spherical structure pertains in ^{98}Zr; however, the excitation energy of the first excited 0^+ level drops dramatically to roughly half the value observed in ^{96}Zr. Spherical-to deformed transition takes place when going from 58 to 60 neutrons, thus when the $\nu g_{7/2}$ orbital is being filled. This abrupt structure change has long been recognized [5] in terms of the strong isoscalar proton-neutron interaction between particles occupying the $g_{9/2}$-$g_{7/2}$ spin-orbit partners. On the edge of this phenomenon are the nuclei with $N = 59$ in which deformed bands have been observed [6,7]. It seems that an important issue for the appearance of the deformation around $A = 100$ and $Z \leqslant 40$ may be the presence of the neutron $g_{9/2}$ extruder: the $9/2^+$ isomers detected in ^{97}Sr, ^{99}Zr, and ^{101}Zr were interpreted as one-neutron hole excitations, and strong ($\beta \sim 0.4$) deformation was deduced for the neutron $9/2^+$ bands (see Ref. [7] and references therein). From the theoretical point of view, understanding the mechanism responsible for the deformation onset in mass 100 is an essential issue for a proper evaluation of the double-β nuclear matrix elements for ^{96}Zr and ^{100}Mo emitters, where the differences in deformation between parent and daughter nuclei may have substantial impact on the calculated values.

Such dramatic shape changes like those in the zirconium chain are a challenge for any theoretical model, thus the shape transitions in the heavy-Zr region have been calculated by many authors (see e.g., Refs. [8–10] and references cited therein). In most cases, the calculations show large prolate deformations in Sr, Mo, and Zr nuclei with $N \geqslant 60$ (a shape transition appears as well in the neighboring Sr and Mo isotopic chains); however, the details of the transitions are predicted differently and are very sensitive to the adopted model and parametrization, e.g., the relativistic mean-field (RMF) theory with the NL1 force reproduces accurately the deformation changes along the chain, which is no longer the case of RMF with the NL-SH force which predicts a deformed ground state already in ^{94}Zr [10]. The Skyrme Hartree-Fock models face similar difficulties, e.g., calculations with the SIII force results in prolate deformed ground states starting in ^{94}Zr [11], while the recent Skyrme-Hartree-Fock-Bogoliubov (HFB14) calculations with the BSk14 parametrization give oblate solutions from ^{94}Zr to ^{98}Zr [12]. The deformation parameters along the chain obtained in the commonly used Finite Range Droplet Model (FRDM) [13] do not match the experimental values either. An accurate reproduction of the experimental $B(E2)$ values in Zr chain, i.e., of the deformation parameters, was found in the framework of the interacting boson model (IBM) in Ref. [14].

In the shell model (SM) framework, the shape transition of Zr isotopes was studied by Federman and Pittel [5] using a modest valence space with a ^{94}Sr core, tractable in SM calculations of that time. In this model, the authors pointed out that in this or other regions of nuclei, the strong isoscalar $T = 0$ part of the proton-neutron interaction may break pairing correlations and hence induce nuclear deformation. However, in Ref. [5] no $B(E2)$ values were calculated, and the deformation was concluded only on the basis of the systematics of the first excited 2^+ states.

Recently, zirconium isotopes have been studied in Ref. [15] using an inert core of ^{88}Sr. The authors managed to provide a G-matrix-based effective interaction of a satisfying quality as far as ^{91}Zr–^{97}Zr were concerned. For ^{98}Zr, however, they failed badly to obtain a reasonable agreement with experimental data in the considered valence space.

In this paper, we perform for the first time a SM study of Zr isotopes in an extended model space ($1f_{5/2}$, $2p_{1/2}$, $2p_{3/2}$, $1g_{9/2}$) for protons and ($2d_{5/2}$, $3s_{1/2}$, $2d_{3/2}$, $1g_{7/2}$, $1h_{11/2}$) for neutrons, dubbed hereafter $\pi(r3-g)$, $\nu(r4-h)$. One should notice that no spurious center-of-mass excitations can occur in this valence space, since $J^\pi T = 1^-0$ excitations

are not possible. However, two other difficulties arises in the present shell model calculations: first, the dimensions of the full configurational space overcome in general the present computational possibilities, and we have to apply and study different truncation schemes. Second, a reliable effective interaction for this valence space has to be established. To solve this problem, we follow here the procedure to correct the monopole part of the effective interaction to ensure a proper evolution of the single-particle fields. The main task consists in constraining the proton-neutron part. For higher numbers of protons, the shell evolution from ^{91}Zr to ^{101}Sn is well known, with the exception of the location of the $\nu h_{11/2}$ orbital beyond $N = 52$, where it is not yet experimentally established. Thus, it is of special interest to investigate theoretically high-spin states that involve excitations to the $h_{11/2}$ orbital, e.g., $[\pi(g_{9/2}) \otimes \nu(g_{7/2}h_{11/2})]$-type of couplings that were detected in several nuclei. Here we refer to isomeric states in Zr isotopes to locate the $h_{11/2}$ centroid and to test the $V_{h_{11/2}\text{-}g_{9/2}}$ proton-neutron part of the effective interaction. In the higher part of the proton shell, the cross-shell interaction is constrained by extending our calculations of low-spin states and electric transitions up to the neutron number $N = 60$ to study the shape change along the chain.

The paper is organized as follows. In the next section we describe briefly the theoretical framework, i.e., the method used to derive the effective interaction and some calculational details. In Sec. III, we show and discuss the results for low-lying states in even and odd zirconium isotopes. Then we discuss the calculations for the known high-spin isomers (III C) and $B(E2)$ transition rates (III D). We also calculate several magnetic properties in ^{92,94}Zr, where the so-called mixed symmetry states were observed (III E). Finally, we address the problem of the rapid shape change that takes place in ^{100}Zr (III F). Concluding remarks are collected in Sec. IV.

II. SHELL MODEL CALCULATIONS

The model space for protons used in the present work was discussed already in Ref. [16]. The effective proton-proton interaction was found by fitting the two-body matrix elements to the available experimental data, namely, for Ni isotopes with $A = 57$–78 and $N = 50$ isotones (^{70}Cu–^{100}Sn). The starting point for the adjusting procedure was a realistic NN interaction based on the Bonn-C potential. Similarly, we have employed the neutron-neutron interaction based on the CD-Bonn potential, previously used in the calculations in the tin region [17], supplemented by a proton-neutron Hamiltonian also obtained from the CD-Bonn. The proton-neutron effective Hamiltonian was corrected in its monopole part to ensure a correct propagation of the single-particle states between ^{79}Ni and ^{91}Zr [$\pi(r3)$–$\nu(r4 - h)$ monopoles] and between ^{91}Zr and ^{101}Sn [$\pi(g_{9/2})$–$\nu(r4 - h)$ monopoles]. For single-particle levels in ^{101}Sn, we used the extrapolations of Ref. [18]. Similarly, monopole corrections were applied to the neutron-neutron interaction to reproduce the basic spectroscopy along the tin chain. We show how the proton shells for $Z = 40$ evolve when filling subsequent neutron orbitals in Fig. 1, where the effective single-particle energies (ESPE) [19] calculated with our interaction are traced. The $N = 51$ ESPE for $Z = 28$–50 are depicted in Fig. 2.

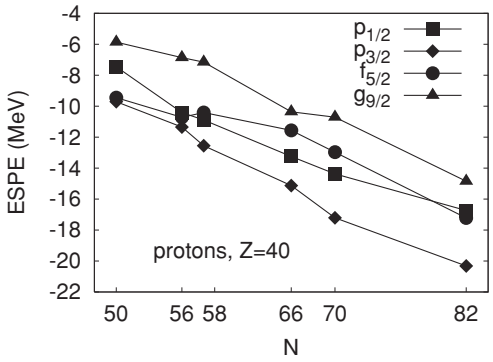

FIG. 1. Proton effective single-particle energies for zirconium isotopes.

The results shown in this work were obtained using the coupled-basis shell-model code NATHAN [20] and the m-scheme code ANTOINE [21]. For ^{90}Zr–^{92}Zr, nontruncated calculations were performed. For larger systems, one needs to use different truncation schemes to reduce the dimensionalities. It is more effective to treat the odd nuclei in the m-scheme and consider particle-hole (p-h) excitations with respect to the $\pi p_{1/2}$ and $\nu d_{5/2}$ shell closures. The even-even nuclei were studied in the coupled scheme with a truncation in seniority. In both cases, we restricted the excitations to the $h_{11/2}$ orbital to maximally 4 particles. The population of this orbital for low-spin states is small (see occupations in Sec. III), thus the additional constraint does not affect the final results considerably. We pursued the calculations up to seniority 8 with NATHAN or up to 8p-8h excitations with ANTOINE. The maximal dimensions considered in this work have been 12×10^9 for the ground state of ^{97}Zr in the m-scheme and 9×10^7 to calculate the 5^- state in ^{98}Zr using the coupled basis. In all studied cases, we reached the convergence of the calculated excitation energies and transition rates. The calculations in which other truncations schemes were used are discussed separately in the text.

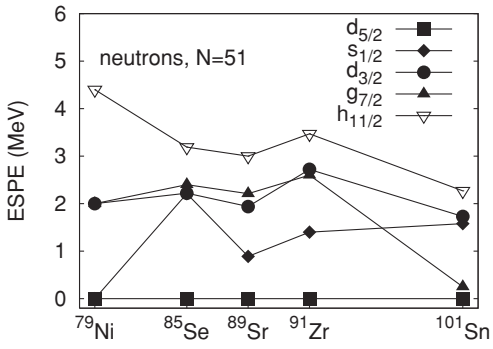

FIG. 2. Evolution of $N = 51$ effective single-particle energies between Ni and Sn.

III. RESULTS

A. Odd isotopes

The results of our calculations for odd zirconium isotopes are presented in Figs. 3–6 in comparison with experimental data [1,22,23]. In addition, the SM results from Ref. [15] calculated with the ^{88}Sr core are shown.

Let us start the discussion with the spectrum of ^{91}Zr, which is well established experimentally and offers clean constraints on the interaction. The only unknown single-particle orbital in ^{91}Zr, which is the neutron $h_{11/2}$, have been estimated to be around 3.5 MeV (it was placed at 3.5 MeV in Ref. [15]), see Sec. III C for further details. The calculated spectrum of ^{91}Zr is shown in Fig. 3. A fair agreement with experiment is also found in ^{93}Zr and ^{95}Zr, as is shown in Figs. 4 and 5. It is worth mentioning that in ^{93}Zr the low-lying state at 950 keV, which has been assigned $1/2^+$ in Ref. [1], is proposed to be rather a $9/2^+$ state in Refs. [22,23]. As was argued in Ref. [15], these states are found to be of seniority $\nu = 3$ nature, three $d_{5/2}$ neutrons being coupled to a $J^\pi = 5/2^+, 7/2^+, 9/2^+$ multiplet below 1 MeV. Indeed, the $9/2^+$ calculated here at 0.917 MeV has a $\nu(d^3_{5/2})$ configuration which supports the $9/2^+$ spin-parity assignment of Refs. [22,23].

The ^{97}Zr nucleus has a pronounced single-particle structure and is fairly reproduced in the present SM calculation, see Fig. 6. We have listed the occupation numbers for its yrast states in Table I. It is seen that the ground state with $J^\pi = 1/2^+$ and the excited $3/2^+, 7/2^+$, and $11/2^-$ states can be considered as one-quasiparticle states built on the closed ^{96}Zr core, while the $5/2^+$ is a one-hole state in the ^{98}Zr core.

Let us discuss in more detail the evolution of $11/2^-$ states in subsequent Zr isotopes. We obtain that the $11/2^-$ level at 2.0 MeV in ^{91}Zr is not a pure single-particle $h_{11/2}$ level,

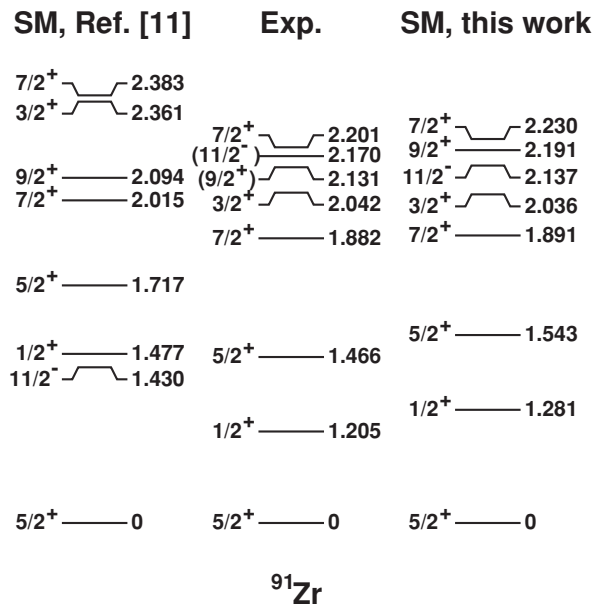

FIG. 3. Experimental low-lying spectra of ^{91}Zr (center) compared with the SM calculations with the ^{78}Ni core and the effective interaction obtained in this work (right) and the SM calculations from Ref. [15] with the ^{88}Sr core (left).

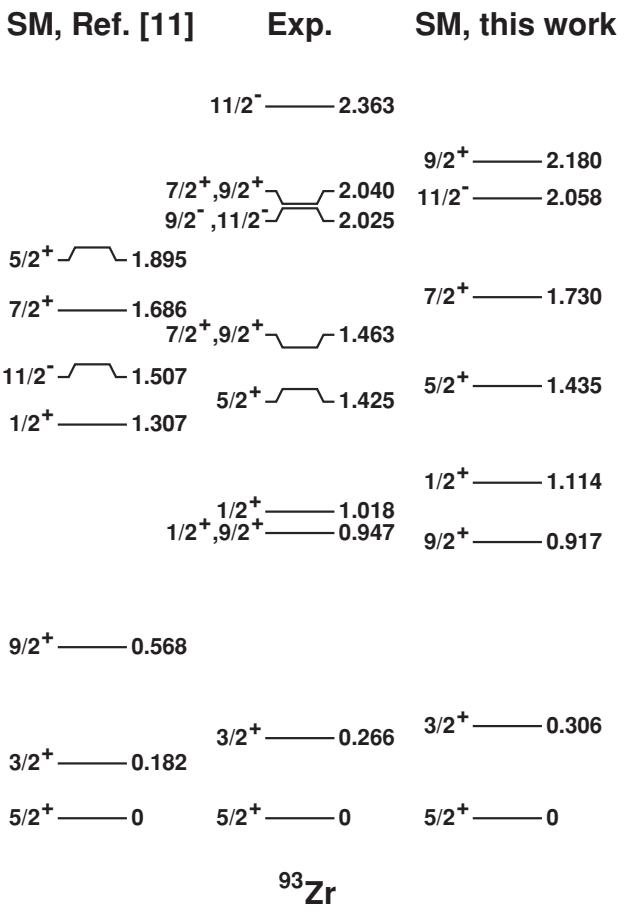

FIG. 4. Same as Fig. 3, but for ^{93}Zr.

but it is calculated to have a dominant $\pi(p^1_{1/2}g^1_{9/2})\nu(d^1_{5/2})$ component (55%). The total number of neutrons in the $h_{11/2}$ orbital is calculated to be only 0.16. The spectroscopic factor for the first $11/2^-$ level was measured to be 0.37–0.53 depending on the reaction mechanism [24], and we obtain in our calculation a value of 0.377. A similar structure is found for $11/2^-$ in ^{93}Zr, where the dominant configuration is the $\pi(p^1_{1/2}g^1_{9/2})\nu(d^3_{5/2})$; and in ^{95}Zr, $\pi(p^1_{1/2}g^1_{9/2})\nu(d^5_{5/2})$. The total occupancies of the $h_{11/2}$ orbital in these nuclei are equal to 0.27 and 0.25, respectively. However, because of the $d_{5/2}$ shell closure in ^{97}Zr, the calculated low-lying $11/2^-$ level acquires a single-particle nature. This result is contradictory to previous SM calculations [15], where the lowest calculated $11/2^-$ states were always predominantly based on the proton $g^1_{9/2}p^1_{1/2}$

TABLE I. Occupation numbers in ^{97}Zr calculated in SM with a ^{78}Ni core.

J^π	$f_{5/2}$	$p_{3/2}$	$p_{1/2}$	$g_{9/2}$	$d_{5/2}$	$s_{1/2}$	$g_{7/2}$	$d_{3/2}$	$h_{11/2}$
$1/2^+$	5.66	3.78	1.84	0.71	5.54	0.96	0.15	0.17	0.16
$3/2^+$	5.67	3.74	1.81	0.76	5.51	0.13	0.16	1.00	0.18
$5/2^+$	5.63	3.82	1.82	0.71	4.73	1.69	0.18	0.19	0.18
$7/2^+$	5.63	3.72	1.79	0.85	5.43	0.16	1.04	0.16	0.18
$11/2^-$	5.71	3.76	1.81	0.69	5.65	0.11	0.10	0.14	0.98

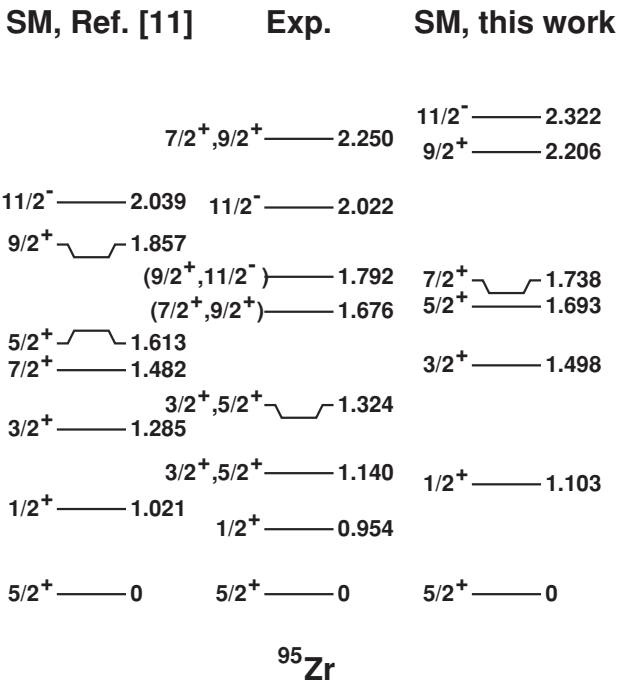

FIG. 5. Same as Fig. 3, but for ^{95}Zr.

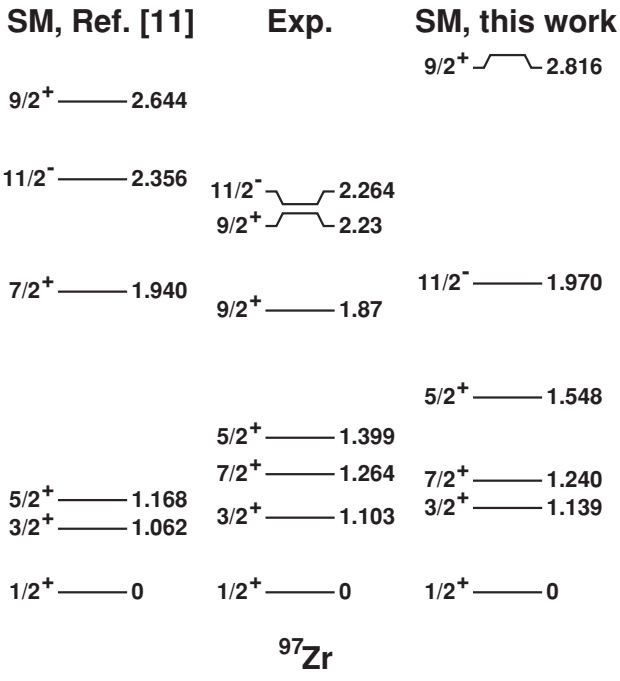

FIG. 6. Same as Fig. 3, but for ^{97}Zr.

configuration. It can be seen from Fig. 1 that our interaction causes an increase of the gap between $p_{1/2}$ and $g_{9/2}$ levels with the filling of the $d_{5/2}$, $s_{1/2}$ orbitals. This explains why the $[\pi(g^1_{9/2}p^1_{1/2})\nu(s^1_{1/2})]_{11/2^-}$ coupling is no longer favored in our calculation for ^{97}Zr. The fact that our SM calculations predict a $11/2^-$ level of a single-particle structure around 2 MeV in ^{97}Zr is, however, in agreement with the experimental $\nu h_{11/2}$ level identification at 2263 keV from Ref. [25]. Future studies of the ^{97}Zr nucleus with the inclusion of the recent data for high-spin states [26] will be done to better determine the evolution of the single-particle $h_{11/2}$ orbital along the chain [27].

B. Even isotopes

The spectra of even zirconium isotopes compared with SM results from Ref. [15] are shown in Figs. 7–11. A nice description of the measured data is found for the yrast bands in all isotopes. Nevertheless, this is no longer the case for the 3^- states which deviate considerably from experimental data beginning with ^{94}Zr. The experimental spectrum of ^{94}Zr is of a vibrational nature, where the 3^- state can be interpreted as the one-octupole phonon. The 3^- very collective states may correspond to a more complex superposition of cross shell excitations out of the valence space of these calculations.

It is important to note that the overall agreement with the measured data is far more satisfying in the present case than the calculations in a reduced valence space with the effective interaction from Ref. [15]. Our calculations indicate the non-negligible importance of the proton orbitals $f_{5/2}$ and $p_{3/2}$, especially when it comes to the reproduction of the energies of the first excited 0^+ states. The occupation numbers of 0^+_1 and 0^+_2 states are given in Table II. Taking as examples ^{94}Zr and ^{96}Zr, one sees that the first excited 0^+ state is predicted at a much too high energy in the calculation of Ref. [15], while it is brought down to the correct energy position in our case.

TABLE II. Calculated occupation numbers in ^{90}Zr–^{98}Zr for the ground and first excited 0^+ states.

N	J^π	$f_{5/2}$	$p_{3/2}$	$p_{1/2}$	$g_{9/2}$	$d_{5/2}$	$s_{1/2}$	$g_{7/2}$	$d_{3/2}$	$h_{11/2}$
50	0^+_1	5.67	3.67	1.27	1.38	–	–	–	–	–
	0^+_2	5.70	3.58	1.0	1.71	–	–	–	–	–
52	0^+_1	5.62	3.56	1.30	1.50	1.62	0.06	0.11	0.09	0.11
	0^+_2	5.67	3.39	1.22	1.69	1.67	0.05	0.09	0.09	0.09
54	0^+_1	5.60	3.59	1.53	1.26	3.31	0.11	0.19	0.16	0.22
	0^+_2	5.61	3.29	1.17	1.91	3.05	0.17	0.23	0.34	0.18
56	0^+_1	5.64	3.68	1.76	0.90	5.26	0.12	0.17	0.16	0.27
	0^+_2	5.43	3.31	1.13	2.11	4.10	0.63	0.45	0.49	0.32
58	0^+_1	5.52	3.76	1.77	0.93	5.37	1.57	0.40	0.33	0.32
	0^+_2	5.41	3.60	1.53	1.44	5.07	0.71	1.26	0.54	0.40

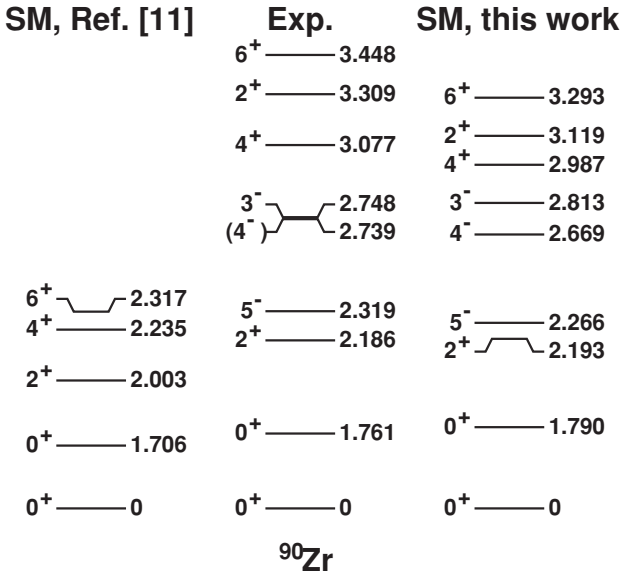

FIG. 7. Experimental low-lying spectra of even-even ^{90}Zr (center) compared with the SM calculations of this work (right) and those from Ref. [15] (left).

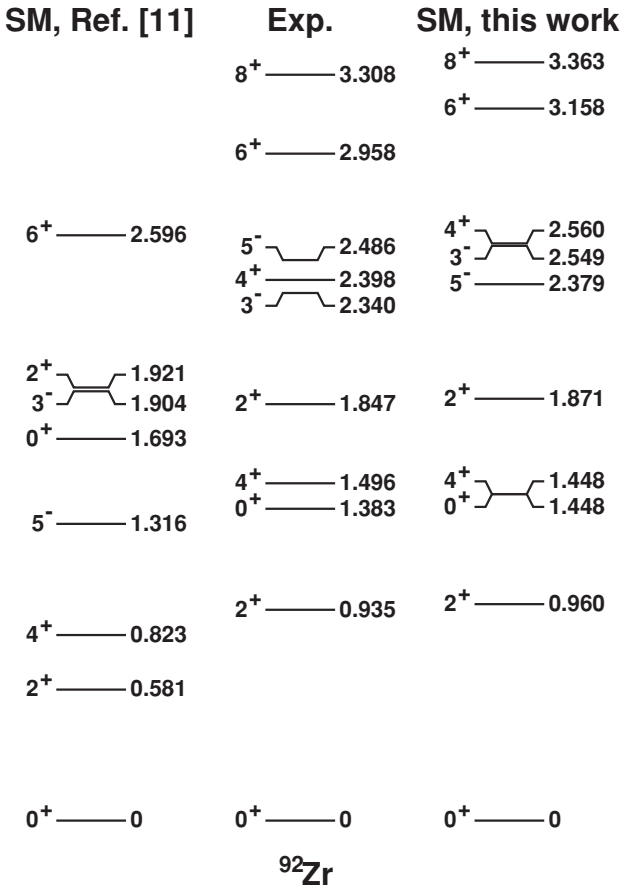

FIG. 8. Same as Fig.7, but for ^{92}Zr.

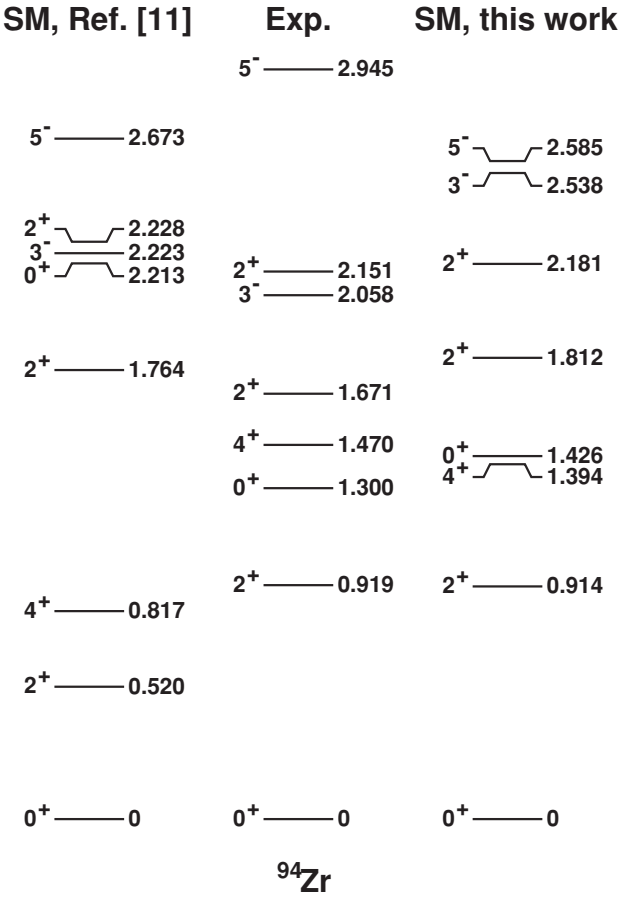

FIG. 9. Same as Fig. 7, but for ^{94}Zr.

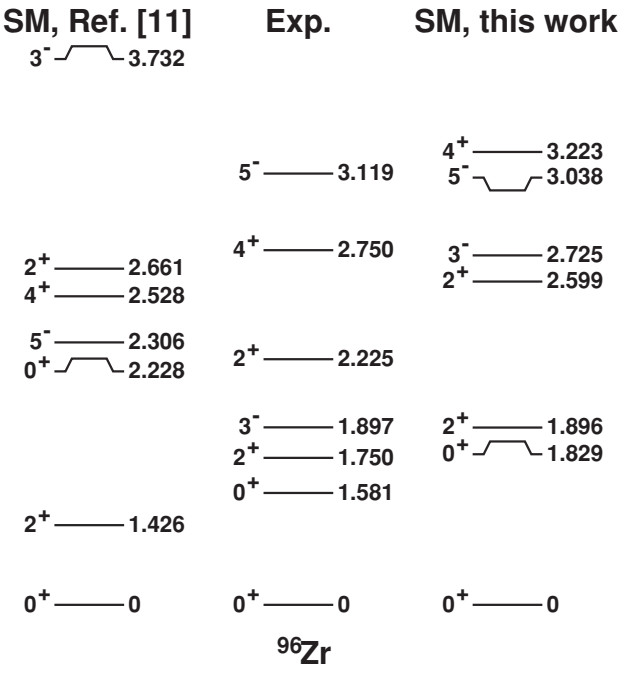

FIG. 10. Same as Fig. 7, but for ^{96}Zr.

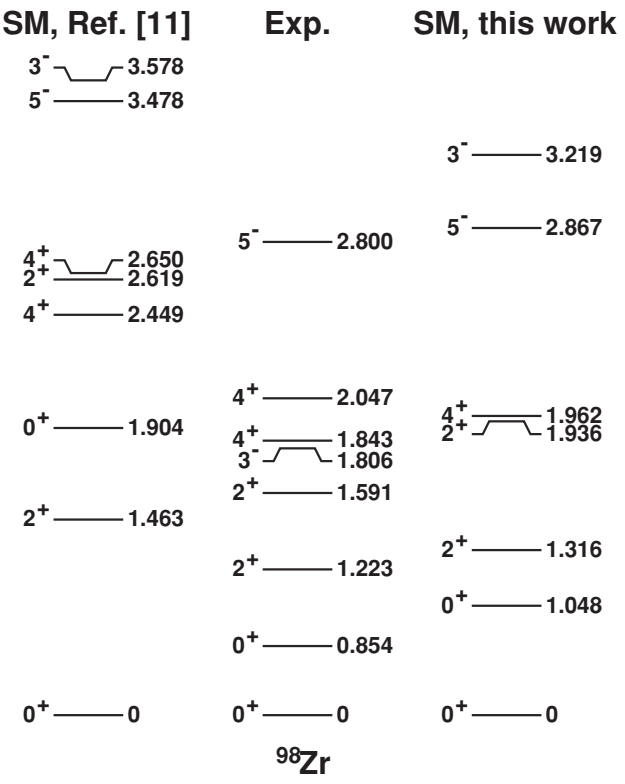

FIG. 11. Same as Fig. 7, but for ^{98}Zr.

In these nuclei, our calculations indicate that first excited 0^+ states correspond to 2p-2h proton excitations from the $p_{1/2}$ and $p_{3/2}$ to the $g_{9/2}$ orbital.

Another feature worth pointing out here is the subshell closure in ^{96}Zr and ^{98}Zr, due to the filling of the $d_{5/2}$ and $s_{1/2}$ orbitals, respectively. Clear signs for such a closure come from experimental data: the spacing between the ground state and the first 2^+ state, almost equal for $N = 52$ and $N = 54$, is doubled for $N = 56$. This effect is accurately reproduced in our calculations, similar to the corresponding spacing in ^{98}Zr (see Fig. 12).

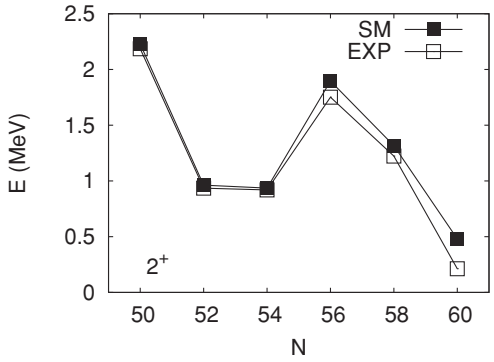

FIG. 12. Systematics of the experimental and theoretical first excited 2^+ states along the zirconium chain.

C. High-spin isomers

To better determine the position of the $\nu h_{11/2}$ level and to check the proton-neutron interaction between the $\nu h_{11/2}$ and the $\pi g_{9/2}$ orbitals, we looked for high-spin isomers observed in zirconium isotopes. The only two known cases, both assigned spin and parity $J^\pi = 17^-$, appear in ^{92}Zr at an energy of 8041 keV [28] and in ^{98}Zr at 6603 keV [29]. States with such a high spin in these nuclei can be generated by fully aligned $[\pi(g_{9/2}^2) \otimes \nu(g_{7/2}^1 h_{11/2}^1)]$ and $[\pi(g_{9/2} f_{5/2}^{-1}) \otimes \nu(h_{11/2}^2)]$ configurations, among which the former is more probable because of the strong attractive proton-neutron interaction between spin-orbit partners, which will lower the energy of such a level substantially. The (possibly) isomeric state in ^{92}Zr is a good testing case because, thanks to the simple neutron structure of this nucleus (2 neutrons in $d_{5/2}$), a full diagonalization can be done in our valence space. We calculate the lowest 17^- state at the energy of 8310 keV, in a good agreement with experiment. As expected, the main component of the wave function (60%) of the state is the fully aligned $[\pi(g_{9/2})^2 \otimes \nu(g_{7/2}^1 h_{11/2}^1)]$ configuration. Turning to ^{98}Zr, the additional six neutrons compared to ^{92}Zr complicate the situation, since only a truncated calculation can be performed, and the final wave function is much more sensitive to the details of the monopole part of the effective interaction. We have done a 8p-8h calculation with respect to the $\nu s_{1/2}, \pi p_{1/2}$ closures, constraining additionally the maximal total occupancies of $g_{9/2}$ and $h_{11/2}$ orbitals to four. This way, we calculate the lowest 17^- state as a 5p-5h excitation at the energy of 6232 keV with the aligned $[\pi(g_{9/2})^2 \otimes \nu(g_{7/2}^1 h_{11/2}^1)]$ component as a dominant part of the wave function. In Table III, we list the total occupation numbers for the calculated 17^- states in ^{92,98}Zr.

D. Electric transition rates

To further test the quality of our SM wave functions, we have calculated several $E2$ electric transitions, which are listed in Table IV. First, we performed the calculations with the standard effective charges, i.e., $e_{\text{eff}}^\nu = 0.5$ and $e_{\text{eff}}^\pi = 1.5$. In this case in ^{90}Zr, where only proton excitations are possible in our valence space, the electric transition is far too small as compared to the experiment. Thus proton excitations from the pf shell to orbits above $\pi g_{9/2}$ and/or neutron excitation from the $\nu g_{9/2}$ orbital to higher shells may be necessary to account for the collectivity observed in ^{90}Zr. This issue can only be clarified by studies performed in a valence space which is even larger than the present one, e.g., with the ^{56}Ni inert core. Such calculations, however, are beyond the present computational possibilities. To account for the missing mixing of configurations, we therefore increased the effective charges to 1.8 for protons and 0.8 for neutrons. In Table IV,

TABLE III. Calculated structure of 17^- states in ^{92}Zr and ^{98}Zr.

Nucleus	$f_{5/2}$	$p_{3/2}$	$p_{1/2}$	$g_{9/2}$	$d_{5/2}$	$s_{1/2}$	$g_{7/2}$	$d_{3/2}$	$h_{11/2}$
^{92}Zr	5.69	3.58	0.43	2.27	0.02	0.0	0.99	0.0	0.97
^{98}Zr	5.37	3.37	1.13	2.11	4.62	0.82	1.05	0.46	1.02

TABLE IV. Experimental $B(E2)$ transition rates in $e^2\,\mathrm{fm}^4$ vs SM results. SMI means calculations with standard effective charges: $e^{\nu}_{\mathrm{eff}} = 0.5$, $e^{\pi}_{\mathrm{eff}} = 1.5$; SMII stands for calculations with enhanced effective charges: $e^{\nu}_{\mathrm{eff}} = 0.8$, $e^{\pi}_{\mathrm{eff}} = 1.8$.

N	Transition	Exp	SMI	SMII
50	$B(E2; 2^+_1 \to 0^+_1)$	122(8)	84	121
52	$B(E2; 2^+_1 \to 0^+_1)$	166(12)	78	151
	$B(E2; 2^+_1 \to 0^+_2)$	71(15)	35	50
	$B(E2; 2^+_2 \to 0^+_1)$	84(10)	72	100
54	$B(E2; 2^+_1 \to 0^+_1)$	132(28)	58	120
	$B(E2; 2^+_1 \to 0^+_2)$	48(2)	24	39
	$B(E2; 2^+_2 \to 0^+_1)$	198(18)	84	140
56	$B(E2; 2^+_1 \to 0^+_1)$	110(44)	57	113
58	$B(E2; 2^+_1 \to 0^+_1)$	>6	40	70
	$B(E2; 2^+_1 \to 0^+_2)$	>1	42	68

we compare the experimental values with calculations with standard effective charges (SMI) and with these slightly enhanced values (SMII). It is seen that in the SMII calculation, we reproduce the transitions rates rather well (note that in Ref. [15] much larger effective charges $e^{\nu}_{\mathrm{eff}} = 1.8$, $e^{\pi}_{\mathrm{eff}} = 1.5$ were needed to obtain agreement with data).

E. Mixed symmetry states

The nuclides ^{92,94}Zr belong to the $N = 52, 54$ isotone chains in which the so-called mixed symmetry (MS) states, which are proton-neutron isovector excitations of vibrational nature, have been observed [30–32]. These states are neither fully symmetric nor fully asymmetric with respect to the proton-neutron degree of freedom. Thus they are of special interest as a sensitive probe of the *pn* part of the residual interaction. The fundamental MS mode in nearly spherical nuclei is a 2^+ excitation with a strong $M1$ transition to the one-phonon 2^+_1 level and typically, a rather weak $E2$ transition to the ground state (see, e.g., Ref. [33] for a review). In this respect, an anomalous behavior for a MS state was observed in ^{94}Zr [31]. The 2^+_2 state at the energy 1667 keV depopulates by a strong $M1$ transition to the first excited 2^+ state, suggesting the evidence of the mixed symmetry in this nucleus. However, an inversion of the $E2$ strengths takes place in ^{94}Zr, i.e., the transition from the second excited (MS) 2^+_2 state to the ground state is considerably larger than the one from the first excited 2^+. Such an inversion has not been explained in the IBM-2 model with the F-spin symmetry, which is often used to describe mixed-symmetry states.

Our $B(E2)$ values, given in Table IV, are in fair agreement with experiment for the $2^+_i \to 0^+$ transitions. In particular, our calculation reproduces the inversion of $B(E2)$ strength, as we also calculate the transition from the second 2^+ state to the ground state larger than from the first 2^+ state. However, the calculated inversion is not as pronounced as experimentally observed. This might be due to the strong sensitivity of the $B(E2)$ values to small changes in the mixing between MS states. We note that in both ^{92}Zr and ^{94}Zr, the calculated structure of the first excited 2^+_1 is the same, i.e., it corresponds predominantly to a neutron excitation (85% in both nuclei).

TABLE V. Experimental $B(M1)$ transition rates in μ^2_N vs SM results.

N	Transition	Exp	SM
52	$B(M1; 2^+_2 \to 2^+_1)$	0.37(4)	0.21
	$B(M1; 2^+_3 \to 2^+_1)$	<0.024	0.06
54	$B(M1; 2^+_2 \to 2^+_1)$	0.33(5)	0.10
	$B(M1; 2^+_3 \to 2^+_1)$	0.06(2)	0.0

The 2^+_2 state has a different structure in both nuclei. We find that in ^{94}Zr, the main configurations in the wave function are $2^+_\nu \otimes 0^+_\pi$ (40%) and $0^+_\nu \otimes 2^+_\pi$ (35%), while in ^{92}Zr the $0^+_\nu \otimes 2^+_\pi$ configuration dominates (51%) over the $2^+_\nu \otimes 0^+_\pi$ (25%). This inversion of proton and neutron components may explain the observed behavior of $E2$ transitions to the ground state.

In Table V, we have listed the calculated $B(M1)$ values for selected transitions. We have used the usual orbital g factors ($g^p_l = 1.0$, $g^n_l = 0.0$) and a "standard" quenching factor 0.75 [34] of the spin g factors. This allows us to reproduce the measured g values, see Table VI, including the sign change between the first and second 2^+ states. The calculated $B(M1)$ transitions are clearly enhanced for the second 2^+ states in agreement with experimental data. In the calculations, the 0^+ states contain 84% in $N = 52$ and 80% in $N = 54$ of seniority $\nu = 0$ configuration. The first excited 2^+ states are dominated by the $\nu = 2$ component (87% and 76%, respectively). The second, mixed symmetry 2^+ states are mainly formed of $\nu = 2, 4$, and 6 components: 60%, 18%, and 20% in ^{92}Zr and 57%, 21%, and 18% in ^{94}Zr. This complexity of wave functions shows that the calculated 2^+ levels are not fully the symmetric and the MS one-phonon 2^+ states.

F. Shape transition

The experimental data in the zirconium chain exhibit a clear and smooth shape transition as a function of neutron number, from a spherical structure of ^{90}Zr to an axially symmetric rotor in ^{102}Zr. While the former can be well described in our calculations in the large model space with configuration mixing, similar calculations for ^{102}Zr exceed the present computational possibilities. The shape transition is accompanied by a lowering of the first excited 0^+ level, which moves from an energy of 1.5 MeV in ^{96}Zr to only 0.2 MeV in ^{100}Zr.

As demonstrated in Figs. 7–11, our SM calculations reproduce very nicely the low-lying spectra of even-even isotopes, including the subshell closures as well as the

TABLE VI. Experimental and theoretical values for g factors in $N = 52, 54$ zirconium nuclei.

N	$g(J^\pi)$	Exp	SM
52	$g(2^+_1)$	$-0.18(2)$	-0.24
	$g(2^+_2)$	$+0.76(50)$	$+0.79$
54	$g(2^+_1)$	$-0.32(2)$	-0.31
	$g(2^+_2)$	$+0.88(27)$	$+0.55$

lowering of the first excited 0^+ from ^{96}Zr (1.8 MeV) to ^{98}Zr (1.0 MeV). In Fig. 12, we compare the experimental and theoretical evolutions of the energy spacing between the ground state and the first 2^+ state in Zr isotopes. For the calculations in ^{100}Zr, however, we were forced to remove the $h_{11/2}$ orbital from the valence space. This restriction should not affect considerably the deformation of the ground state. The convergence of the calculated energies was achieved at 10p-10h level.

Figure 12 shows that the systematics of the 2^+ levels changes rapidly at $N = 60$, where the energy of the calculated 2^+ state is lowered from 1.31 MeV in ^{98}Zr to only 0.48 MeV in ^{100}Zr. This behavior has been already observed in the previous SM calculations of Federman and Pittel [5], however, within a smaller valence space. It seems to confirm the important role of the strong, attractive $g_{9/2}$-$g_{7/2}$ interaction. However, a proof of the intrinsic deformation in the laboratory frame can only be obtained from the $B(E2)$ value, which in experiment grows enormously, from 120 e^2 fm^4 for $N = 56$ to 2220 e^2 fm^4 for $N = 60$. Our SM calculations fail to produce such an enhancement: a value of only 180 e^2 fm^4 is obtained in the present calculation for ^{100}Zr.

To understand this shortcoming, we have performed a set of explanatory studies. SM calculations of rotors in the pf shell and in heavier nuclei [20] show that the Elliott's SU(3) scheme that is applicable to sd nuclei can be there replaced by the approximate quasi-SU(3) [35] and pseudo-SU(3) [36] symmetries. One can use these findings to estimate the value of the quadrupole moment in any valence space. In our valence space, we may assume two pseudo-SU(3) blocks for the lower shells: a pseudo-pf shell [$\nu(d_{5/2}, s_{1/2}, g_{7/2}, d_{3/2})$] and a pseudo-$sd$ shell [$\pi(f_{5/2}, p_{3/2}, p_{1/2})$]. The $g_{9/2}$ and $h_{11/2}$ orbitals themselves do not induce quadrupole deformation. However, adding the proton $d_{5/2}$ orbital, quasi-SU(3) can operate for the upper proton shells. Similarly, to create a quasi-SU(3) block for neutrons, the $f_{7/2}$ orbital can be added to the $h_{11/2}$. One can then estimate the quadrupole moment of ^{100}Zr in such a scheme.

The maximal value from the quadrupole moment is obtained if one considers six proton holes in the pseudo-sd shell and six protons in the quasi-gds shell in addition to six neutrons in the pseudo-pf and four neutrons in the quasi-fph shells. Adopting standard effective charges (1.5 for protons and 0.5 for neutrons), we obtain an $B(E2)$ value of $\sim$3300 e^2 fm^4, which is much larger than the observed one. Removing the quasi-SU(3) block for neutrons, the $B(E2)$ value is reduced to $\sim$2200 e^2 fm^4, which agrees well with experiment. Finally, taking into account only two pseudo-SU(3) blocks, thus the valence space considered in this work, we estimate a $B(E2)$ of only $\sim$700 e^2 fm^4. These results lead to the conclusion that the extension of the present valence space is necessary, but adding the $\pi d_{5/2}$ orbital may be already sufficient to account properly for the observed deformation in ^{100}Zr.

IV. SUMMARY AND PERSPECTIVES

We have performed large-scale shell model calculations for zirconium isotopes in a model space based on a ^{78}Ni core [referred to as the $\nu(r4-h), \pi(r3-g)$ space], with a new effective interaction tailored for this valence space. Our calculations reproduce the low-spin spectroscopic data of $^{90-98}$Zr quite well. After estimating the position of the $h_{11/2}$ centroid in ^{91}Zr at 3.5 MeV, the calculations do reproduce the isomeric states in ^{92,98}Zr, which clearly involve excitations to this intruder orbital. We conclude that the interaction within this valence space can be used for calculations of other high-spin isomeric states in this mass region, which originate from deep proton holes coupled to neutron excitations to the $h_{11/2}$ intruder [37,38]. Such studies, in turn, should help to further constrain the location of the $h_{11/2}$ centroid and to tune the proton-neutron part of the effective interaction. We have probed as well the proton-neutron part of the interaction by calculating magnetic transitions in ^{92,94}Zr, where the mixed-symmetry states, sensitive to the details of the pn interaction, were observed. As a good qualitative description of these $B(M1)$ transition rates was achieved, the present interaction can be further explored in the investigations of MS states in $N = 52$ and $N = 54$ isotones. We have also reproduced qualitatively the $B(E2)$ transition rates; however, theoretical values calculated with standard effective charges $e^{\nu}_{\text{eff}} = 0.5$, $e^{\pi}_{\text{eff}} = 1.5$ are on average 40% smaller than the experimental ones. This defect can be cured by a readjustment of the effective charges: enhanced values $e^{\nu}_{\text{eff}} = 0.8$, $e^{\pi}_{\text{eff}} = 1.8$ allow us to get very good agreement with the data. Finally, we have shown that the deformation of the ^{100}Zr ground state cannot be fully accounted in our adopted valence space, pointing to the need for a suitable enlargement together with an appropriate modification of the effective interactions. Such improvements are needed for a proper accounting of the deformation in $A \sim 100$ nuclei, and in particular for SM studies of the double-β decays of ^{100}Mo.

ACKNOWLEDGMENTS

Discussions with E. Caurier, N. Pietralla, A. Poves, and W. Urban are greatfully acknowledged. This work has been supported by the state of Hesse within the Helmholtz International Center for FAIR (HIC for FAIR), by the DFG under Grant No. SFB 634 and by the Alliance Program of the Helmholtz Association (HA216/EMMI).

[1] http://www.nndc.bnl.gov/.
[2] H. Mach *et al.*, Nucl. Phys. **A523**, 197 (1991).
[3] H. Mach, M. Moszynski, R. L. Gill, G. Molnar, F. K. Wohn, J. A. Winger, and J. C. Hill, Phys. Rev. C **41**, 350 (1990).
[4] H. Mach *et al.*, Phys. Lett. **B230**, 21 (1989).
[5] P. Federman and S. Pittel, Phys. Rev. C **20**, 820 (1979).
[6] W. Urban *et al.*, Eur. Phys. J. A **16**, 11 (2003).
[7] W. Urban *et al.*, Eur. Phys. J. A **22**, 241 (2004).
[8] J. Skalski, S. Mizutori, and W. Nazarewicz, Nucl. Phys. **A617**, 282 (1997).
[9] J. Wood, K. Heyde, W. Nazarewicz, M. Huyse, and P. van Duppen, Phys. Rep. **215**, 101 (1992).

[10] G. Lalazissis and M. Sharma, arXiv:nucl-th/9501003v1.
[11] P. Bonche, H. Flocard, P. Heenen, S. Krieger, and M. Weiss, Nucl. Phys. **A443**, 39 (1985).
[12] S. Goriely, M. Samyn, and J. M. Pearson, Phys. Rev. C **75**, 064312 (2007).
[13] P. Möller, J. Nix, and K. Kratz, At. Data Nucl. Data Tables **66**, 131 (1997).
[14] J. García-Ramos, K. Heyde, R. Fossion, V. Hellemans, and S. De Baerdemacker, arXiv:nucl-th/0410045v2.
[15] A. Holt, T. Engeland, M. Hjorth-Jensen, and E. Osnes, Phys. Rev. C **61**, 064318 (2000).
[16] A. F. Lisetskiy, B. A. Brown, M. Horoi, and H. Grawe, Phys. Rev. C **70**, 044314 (2004).
[17] A. Gniady, E. Caurier, and F. Nowacki (unpublished).
[18] H. Grawe, K. Langanke, and G. Martíinez-Pinedo, Rep. Prog. Phys. **70**, 1525 (2007).
[19] T. Otsuka, M. Honma, T. Mizusaki, N. Shimizu, and Y. Utsuno, Prog. Part. Nucl. Phys. **47**, 319 (2001).
[20] E. Caurier, G. Martinez-Pinedo, F. Nowacki, A. Poves, and A. P. Zuker, Rev. Mod. Phys. **77**, 427 (2005).
[21] E. Caurier and F. Nowacki, Acta Phys. Pol. B **30**, 705 (1999).
[22] N. Fotiades *et al.*, Phys. Rev. C **65**, 044303 (2002).
[23] D. Pantelica *et al.*, Phys. Rev. C **72**, 024304 (2005).
[24] S. T. Thornton, D. E. Gustafson, J. L. C. Ford, K. S. Toth, and D. C. Hensley, Phys. Rev. C **13**, 1502 (1976).
[25] G. Lhersonneau *et al.*, Phys. Rev. C **54**, 1117 (1996).
[26] M. Matejska-Minda, B. Fornal, R. Broda, W. Królas, K. Mazurek, T. Pawłat, J. Wrzesiski, M. Carpenter, R. Janssens, and S. Zhu, Acta Phys. Pol. B **40**, 633 (2009).
[27] K. Sieja *et al.* (in preparation).
[28] G. Korschinek, M. Fenzl, H. Hick, A. Kreiner, W. Kutschera, E. Nolte, and H. Morinaga, Proceedings of the International Conference on Nuclear Structure, Tokyo, 1977.
[29] G. Simpson *et al.*, Phys. Rev. C **74**, 064308 (2006).
[30] C. Fransen *et al.*, Phys. Rev. C **71**, 054304 (2005).
[31] E. Elhami, J. N. Orce, S. Mukhopadhyay, S. N. Choudry, M. Scheck, M. T. McEllistrem, and S. W. Yates, Phys. Rev. C **75**, 011301(R) (2007).
[32] V. Werner *et al.*, Phys. Rev. C **78**, 031301(R) (2008).
[33] N. Pietralla, P. von Brentano, and A. Lisetskiy, Prog. Part. Nucl. Phys. **60**, 225 (2008).
[34] P. von Neumann-Cosel, A. Poves, J. Retamosa, and A. Richter, Phys. Lett. **B443**, 1 (1998).
[35] G. Martínez-Pinedo, A. P. Zuker, A. Poves, and E. Caurier, Phys. Rev. C **55**, 187 (1997).
[36] A. Arima, M. Harvey, and K. Shimuzi, Phys. Lett. **B30**, 517 (1969).
[37] T. Rzaca-Urban, K. Sieja, W. Urban, F. Nowacki, J. L. Durell, A. G. Smith, and I. Ahmad, Phys. Rev. C **79**, 024319 (2009).
[38] W. Urban *et al.*, Phys. Rev. C **79**, 044304 (2009).

Laboratory versus intrinsic description of nonaxial nuclei above doubly magic ^{78}Ni

K. Sieja,[1] T. R. Rodríguez,[2] K. Kolos,[3,4] and D. Verney[3]
[1]*Université de Strasbourg, IPHC, CNRS, UMR7178, 67037 Strasbourg, France*
[2]*Institut für Kernphysik, Technische Universität Darmstadt, Schlossgartenstr. 2, D-64289 Darmstadt, Germany*
[3]*Institut de Physique Nucléaire, CNRS/IN2P3 and Université Paris Sud, Orsay, France*
[4]*University of Tennessee, Knoxville, Tennessee 37996, USA*
(Received 2 August 2013; revised manuscript received 28 August 2013; published 30 September 2013)

We study the development of collectivity in neutron rich nuclei in the close vicinity of ^{78}Ni. We report on the large scale shell model calculations in the $N = 52$–54 even-even nuclei with $Z = 30$–36. We predict maximum of triaxiality in ^{86}Ge and explain this phenomenon on the basis of a pseudo-SU(3) symmetry interpretation. For the cases where signs for nonaxial shapes appear, we perform the triaxial Gogny calculations with particle number and angular momentum projections. The comparison of results obtained in the laboratory and intrinsic frames provides a comprehensive and complete picture of nuclear deformation in this region.

DOI: 10.1103/PhysRevC.88.034327 PACS number(s): 21.60.Cs, 21.60.Jz, 23.20.Lv, 21.10.−k

I. INTRODUCTION

The study of collective behavior of deformed nuclei is a classical problem in nuclear physics. Mean-field descriptions in the intrinsic frame are perfectly suited for such studies, as they take advantage of the spontaneous breaking of rotational symmetry. The price to pay for the gain in the physical insight is the loss of angular momentum as a good quantum number. On the contrary, in the nuclear shell model defined in the laboratory frame, angular momentum is conserved but the physical insight associated with the existence of the intrinsic state is lost. However, in the cases of well-deformed nuclei, such as ^{24}Mg or ^{48}Cr, the collective properties in shell model can be traced back to the validity of the Eliott's SU(3) symmetry, for which the relationship between the intrinsic and laboratory frame descriptions is well understood.

The region of neutron-rich nuclei above the $N = 50$ shell closure appears particularly interesting for the study of the quadrupole properties. From the shell model point of view, the nuclei above ^{78}Ni can be described in a model space comprising neutron ($2d_{5/2}$, $3s_{1/2}$, $2d_{3/2}$, $1g_{7/2}$, $1h_{11/2}$) and proton ($1f_{5/2}$, $2p_{3/2}$, $2p_{1/2}$, $1g_{9/2}$) orbitals. These two sets of orbits contain those connected by a strong quadrupole interaction and can form the pseudo-SU(3) blocks. Approaching the SU(3) limit would require a degeneracy or a close proximity of the orbitals of interest. From the shell model extrapolations it appears that at least the $2d_{5/2}$ and $3s_{1/2}$ are degenerate in ^{78}Ni [1] and that proton $1f_{5/2}$ and $2p_{3/2}$ orbits cross around $Z = 28$ with the filling of the $g_{9/2}$ neutron orbital [2]. Thus, while ^{78}Ni itself is predicted to be closed shell nucleus in the shell model picture [3], as soon as few protons and neutrons are added the deformation can set up quickly. Mean-field, Hartree-Fock-Bogoliubov (HFB) calculations with Gogny forces [4], revealed a possibility of shape mixing in this region and indicate a non-negligible role of the nonaxial degrees of freedom in ground states of these nuclei. Nevertheless, beyond-mean field calculations are needed to provide spectroscopic information to be compared with the experimental data and with other theoretical approaches. In particular, the recently developed full triaxial angular momentum restoration and shape mixing with Skyrme [5], relativistic mean-field [6], and Gogny [7] energy density functionals are the perfect tools to study these collective phenomena all over the nuclear chart.

The experimental studies in the region around ^{78}Ni has been also intense in the recent years. While it is still difficult to study the structure of ^{78}Ni itself at currently existing facilities, the knowledge of the light $N = 50$–54 even-even isotones has been extended down to $Z = 30$ for $N = 50$ [8], $Z = 32$ for $N = 52$ [9,10], and $Z = 34$ for $N = 54$ [11]. In particular, the first possible signs of deformation at $N = 52$ have been reported in Ref. [9], where the excited levels of ^{84}Ge have been observed. The comparison with five-dimensional collective Hamiltonian (5DCH) calculations [12] pointed to a certain softness of this nucleus. The detailed spectroscopy of ^{80}Ge clearly reveals the existence of γ-soft collective structures at $N = 48$ [13]. The question that arises now is to understand wether this behavior is maintained after the $N = 50$ shell closure, in the natural valence space above the ^{78}Ni core, and why. Recently, the first observation of excited levels of ^{87}Se ($N = 53$) has been achieved [14]. The adjacent shell model interpretation in such a valence space has suggested the increased collectivity of this nucleus to be responsible for the observed level ordering.

In this work we perform a shell model study of even-even $N = 52$–54 isotopes with $Z = 30$–36 and we focus on the quadrupole properties of these nuclei as seen in the laboratory system. We interpret our results using the limits of the Eliott's SU(3) symmetry in its pseudo-SU(3) variant. In the selected cases, where signs of deformation and triaxiality are present in the shell model framework, we also perform symmetry conserved configuration mixing (SCCM)-Gogny calculations. Our work is organized as follows. First we discuss details of the shell model calculations in Sec. II A and we analyze the limits of the quadrupole deformation of considered systems in a pseudo-SU(3) symmetry model in Sec. II B. We outline the SCCM-Gogny approach with particle number and angular momentum projections in Sec. II C. In Sec. III we gather the quadrupole properties obtained in microscopic shell model

calculations for the ensemble of considered nuclei and then we discuss in more detail selected cases, in comparison with the results of the SCCM-Gogny approach. Finally, we collect our main conclusions in Sec. IV.

II. THEORETICAL FRAMEWORK

A. Shell model: Valence space and interaction

The shell model calculations presented in this work has been achieved in a model space $\pi(1f_{5/2}, 2p_{3/2}, 2p_{1/2}, 1g_{9/2})$ and $\nu(2d_{5/2}, 3s_{1/2}, 2d_{3/2}, 1g_{7/2}, 1h_{11/2})$ outside the ^{78}Ni core, which we name $\pi r3g - \nu r4h$ (following notation of Ref. [15]). The effective interaction used in this model space has been established and described in Ref. [1]. It contains a fit from Ref. [16] in its proton-proton part, the neutron-neutron interaction called GCN5082 [17–19] and the proton-neutron realistic G-matrix constrained in its monopole part to reproduce the shell evolution between ^{91}Zr and ^{101}Sn. It has been originally conceived to study the zirconium isotopes but it appeared also quite successful for the description of low lying and isomeric states in lighter Z nuclei [20–23]. Recently it has been applied to the study of the yrast excitations in $N = 52$ nuclei from $Z = 30$ to $Z = 44$ and in particular, to the evolution of the $4^+ - 6^+$ splitting in these systems. The latter appeared to be reproduced in a great detail in the present shell model approach, confirming its validity also in the closer vicinity of ^{78}Ni [24]. Also a study of $N = 53$ isotones has been achieved within the same framework [14], where shell model has been successful in interpreting the low energy levels systematics and in particular, the descending trend of the $3/2^+$ state between ^{93}Zr and ^{87}Se. A development of deformation in the proton midshell has been suggested to cause the observed ordering of levels in ^{87}Se.

In this work we consider even-even systems having two to six protons and two to four neutrons in the valence space, i.e., the $N = 52, 54$ isotones with $Z = 30$–36. The m-scheme dimensions for these nuclei do not exceed 2×10^8. Full space diagonalizations of such systems using the m-scheme shell model code ANTOINE [25] are not computationally intense at all and can be performed on a laptop.

In the calculations of quadrupole moments and transition rates, we have used an enhanced polarization charge of $0.7e$, as suggested previously in Ref. [1] for this model space. This allows us, in particular, to account for the missing proton excitations from the $f_{7/2}$ orbital to the rest of the shell, crucial in nuclei around $Z = 28$, $N = 50$ [2], and thus to match better the measured $B(E2; 2^+ \to 0^+)$ values of $N = 50$ nuclei: ^{80}Zn and ^{86}Kr. The enhanced neutron polarization charge can account for the missing excitations from the $g_{9/2}$ orbital.

To provide some more insight on the intrinsic shape associated to the calculated shell model states, the $E2$ matrix elements were analyzed following the same method which is applied in multiple Coulomb excitation formalism. For this purpose we use the model independent n-body quadrupole moments introduced in Ref. [26] in a similar way as was already done in Ref. [13]. For the sake of clarity we shall remind here the expressions for the two-body and three-body quadrupole moments of a given state $s \equiv (s, I_s, \Pi_s)$ (as calculated here from shell model results):

$$p_s^{(2)} = (2I_s + 1)^{-1} \sum_r M_{sr}^2 = \frac{5(I_s + 1)(2I_s + 3)}{16\pi I_s(2I_s - 1)} Q_{\text{spec}}^2(s) + \sum_{r \neq s} B(E2; s \to r), \tag{1}$$

where M_{sr} are the reduced $E2$ matrix elements,

$$p_s^{(3)} = -\sqrt{5}(2I_s + 1)^{-1}(-1)^{2I_s} \times \sum_{rt} \begin{Bmatrix} 2 & 2 & 2 \\ I_s & I_r & I_t \end{Bmatrix} M_{sr} M_{rt} M_{ts}, \tag{2}$$

where r and t are the intermediate (shell model here) states connected by $E2$ transitions to the state s considered and M_{ij} are the $E2$ reduced matrix elements between states s, r, and t. These are completely general and model independent measures of the the intrinsic axial deformation and asymmetry, being related to parameters of an equivalent ellipsoid having the same $p_s^{(2)}$ and $p_s^{(3)}$ moments by:

(i) for the intrinsic quadrupole moment $Q_{\text{int}}(s)$ (from which the axial deformation parameter $\beta(s)$ is extracted):

$$Q_{\text{int}}(s) = \sqrt{\frac{16\pi}{5} p_s^{(2)}}, \tag{3}$$

(ii) for the asymmetry angle $\gamma(s)$:

$$\cos 3\gamma(s) = -\sqrt{7/2}\, p_s^{(3)} \left(p_s^{(2)}\right)^{-3/2}. \tag{4}$$

B. Pseudo SU(3) model analysis of quadrupole moments

The quadrupole properties of nuclei contained in the valence space $\pi r3g$-$\nu r4h$ can be anticipated by looking into the limits of the pure pseudo-SU(3) symmetry first proposed by Arima [27] and applied, e.g., in Refs. [1,15,18]. In this work we investigate the nuclei for which the essential features should be described within the $pf_{5/2}$ orbits on the proton side and $dg_{7/2}s_{1/2}$ on the neutron side, thus we can consider having pseudo-SU(3) blocks for protons (pseudo-sd) and for neutrons (pseudo-pf). The quadrupole properties of the Nilsson-like orbitals of a pseudo-SU(3) in a shell with principal quantum number $n + 1$ are the same as those of the SU(3) orbits with principal quantum number n, for which the intrinsic quadrupole moment is given by [15]:

$$q_0(n, \chi, k) = -(2n - 3\chi)b^2, \tag{5}$$

where χ can take integer values between 0 and n, $k = \pm(\frac{1}{2}, \ldots, \frac{1}{2} + \chi)$, and b is the harmonic oscillator length parameter. The total intrinsic quadrupole moment Q_0 is obtained as a sum of all the contributions from the valence particles with corresponding effective charges. In this scheme the energy is proportional to Q_0^2 thus the orbits are filled starting from $\chi = 0$ or $\chi = n$ in a way which maximizes the absolute value of the intrinsic quadrupole moment.

Let us start with two or four neutrons occupying the pseudo-pf orbits. Two neutrons maximize the quadrupole deformation when they occupy the lowest $\chi = 0$ orbital with $k = 1/2$ and

$k = -1/2$, leading to the total $K = \sum k = 0$. Four neutrons can be distributed in several degenerate configurations:

$$(\chi = 0, k = \pm 1/2)^2 (\chi = 1, k = \pm 1/2)^2,$$
$$(\chi = 0, k = \pm 1/2)^2 (\chi = 1, k = \pm 3/2)^2,$$
$$(\chi = 0, k = \pm 1/2)^2 (\chi = 1, k = \pm 1/2)^1 (\chi = 1, k = \pm 3/2)^1,$$

which means a possibility of $K = 0$ and $K = 2$. Even a small mixing of $K = 0$ and $K = 2$ would lead to triaxiality: such a mixing is impossible in a pure pseudo-SU(3) limit but may appear in realistic shell model calculations.

Moving to the proton side, we need to consider two, four, six, or eight valence protons in the pseudo-sd block, which will correspond to Zn, Ge, Se, and Kr nuclei in our model space. The two valence protons of Zn maximize the quadrupole moment when they occupy both the lowest $\chi = 0$ orbital (total $K = 0$). The situation of Ge becomes more complex as the four valence protons can adopt several degenerate configurations:

$$(\chi = 0, k = \pm 1/2)^2 (\chi = 1, k = \pm 1/2)^2,$$
$$(\chi = 0, k = \pm 1/2)^2 (\chi = 1, k = \pm 3/2)^2,$$
$$(\chi = 0, k = \pm 1/2)^2 (\chi = 1, k = \pm 1/2)^1 (\chi = 1, k = \pm 3/2)^1,$$

leading to possible $K = 0$ and $K = 2$. The same analysis in Se (six particles) gives a possibility of two degenerate cases with $K = 0$ having the same Q_0 values, but with opposite signs:

$$(\chi = 0, k = \pm 1/2)^2 (\chi = 1, k = \pm 1/2)^2 (\chi = 1, k = \pm 3/2)^2,$$
$$(\chi = 2, k = \pm 1/2)^2 (\chi = 2, k = \pm 3/2)^2 (\chi = 2, k = \pm 5/2)^2.$$

Similarly, eight particles (Kr) can be redistributed in several degenerate configurations, again with $K = 0, 2$.

The values of total intrinsic quadrupole moments and corresponding $B(E2)$ values obtained in the pseudo-SU(3) limit [using Eq. (10)] are summarized in Table I. The polarization charge of $0.7e$ is used in the pseudo-SU(3) model to make comparisons with SM calculations straightforward.

The major conclusions from the pseudo-SU(3) model analysis are the following: The degenerate configurations with $K = 0$ and $K = 2$ can be obtained for four and eight protons and for four neutrons in the valence space. Thus one may expect some triaxiality in realistic calculations and in experiment, reaching its maximum in ^{86}Ge. The largest axial deformation is predicted for six protons and four neutrons in the valence space (^{88}Se).

TABLE I. Predictions of the pseudo-SU(3) symmetry limit for the values of intrinsic quadrupole moments (in $e$fm^2) and $B(E2; 2^+ \to 0^+)$ transition values (in e^2fm^4) in the studied nuclei.

Nucleus	Q_0	$B(E2; 2^+ \to 0^+)$	Nucleus	Q_0	$B(E2; 2^+ \to 0^+)$
^{82}Zn	114	258	^{84}Zn	135	362
^{84}Ge	131	342	^{86}Ge	151	454
^{86}Se	148	436	^{88}Se	168	561
^{88}Kr	117	272	^{90}Kr	137	373

TABLE II. Properties of the yrast band of $N = 52$ isotones [energies in MeV, quadrupole moments in $e$fm^2, $B(E2)$ in e^2fm^4]. The calculations are done in the $\pi r3g$-$\nu r4h$ model space with $1.7e$ and $0.7e$ effective charges for protons and neutrons, respectively.

Z	J	E^*	$B(E2; J \to J-2)$	$Q_{\rm spec}$	Q_0 from $B(E2)$	Q_0 from $Q_{\rm spec}$	β
30	2^+	0.88	169	−14	92	48	
	4^+	1.50	127	−24	67	66	
	6^+	3.17	182	−40	77	100	
32	2^+	0.75	371	−27	136	93	
	4^+	1.56	364	−37	113	101	
	6^+	3.03	455	−27	120	67	
34	2^+	0.70	436	−37	148	129	0.19
	4^+	1.41	439	−46.5	124	128	0.17
	6^+	2.76	607	−55	139	136	0.19
36	2^+	0.88	329	6.5	129	23	
	4^+	1.66	207	−31	85	86	
	6^+	3.24	95	14	55	35	

C. Details of symmetry conserving configuration mixing–Gogny calculations

In this section we describe briefly the beyond mean-field method used in this work. In this approach, we use the generator coordinate method (GCM) to define the many-body wave functions [28]. Hence, we consider linear combinations of states with different intrinsic quadrupole deformations, axial and triaxial [5,7]:

$$|JM; NZ; \sigma\rangle = \sum_{\beta,\gamma,K} f^{J;NZ;\sigma}_{\beta,\gamma,K} |JMK; NZ; \beta\gamma\rangle, \qquad (6)$$

where N, Z, J, M, K are the number of neutrons and protons, the total angular momentum and the angular momentum component on the z axes of the laboratory and fixed frames, respectively. The quadrupole deformation is parametrized by the (β, γ) coordinates and the states $|JMK; NZ; \beta\gamma\rangle$ are found by performing particle number and angular momentum

TABLE III. Properties of the yrast band of $N = 54$ isotones [energies in MeV, quadrupole moments in $e$fm^2, $B(E2)$ in e^2fm^4].

Z	J	E^*	$B(E2; J \to J-2)$	$Q_{\rm spec}$	Q_0 from $B(E2)$	Q_0 from $Q_{\rm spec}$	β
30	2^+	0.80	193	−26	98	91	
	4^+	1.50	93	3.5	57	10	
	6^+	2.83	139	−52	67	131	
32	2^+	0.65	465	−40	153	140	0.21
	4^+	1.75	628	−40	149	110	0.19
	6^+	3.26	659	−33	145	82	0.17
34	2^+	0.67	568	−48	169	168	0.23
	4^+	1.94	714	−54	158	148	0.21
	6^+	3.58	466	−55	122	137	0.18
36	2^+	0.80	386	−24	139	84	
	4^+	1.75	201	20	84	55	
	6^+	3.15	447	48	119	121	

TABLE IV. Excited bands of selected $N = 52$ isotones [energies in MeV, quadrupole moments in $e$fm^2, $B(E2)$ in e^2fm^4].

Z	J	E^*	$B(E2; J \to J-1)$	$Q_{\rm spec}$
30	2_2^+	1.86		0.7
	3^+	2.46	23	− 20
	4_2^+	2.43	10	− 32
	5^+	3.11	40	− 19
32	2_2^+	1.54		26
	3^+	2.12	639	− 4
	4_2^+	2.31	366	− 22
	5^+	2.96	200	− 28
34	2_2^+	1.64		5
	3^+	2.25	523	− 10
	4_2^+	2.71	27	− 38
	5^+	3.50	118	− 30
36	2_2^+	1.72		− 5
	3^+	2.52	214	− 10
	4_2^+	2.28	11	55
	5^+	3.17	108	− 9

projection of HFB wave functions $|\Phi(\beta,\gamma)\rangle$:

$$|JMK;NZ;\beta\gamma\rangle = P^J_{MK} P^N P^Z |\Phi(\beta,\gamma)\rangle. \quad (7)$$

Here, P^J_{MK}, P^N, and P^Z are the operators that project onto good angular momentum and number of particles, respectively [28]. The HFB wave functions are found by minimizing the particle number projected HFB energy (PN-VAP method [29]) using constraints on the quadrupole degrees of freedom to produce a set of states with the desired deformation. In this work we use for each nucleus a mesh of 72 states with deformations ranges as follows: ($\beta \in [0.0, 0.8]$, $\gamma \in [0^\circ, 60^\circ]$). In addition, the HFB wave functions preserve time-reversal and spatial parity symmetries (only positive parity states can be described) and are expanded in a spherical harmonic oscillator basis including nine major oscillator shells. Finally, the minimization of the energy computed with the GCM states given in Eq. (6) is equivalent to solving the Hill-Wheeler-Griffin (HWG) equations:

$$\sum_{\beta_2',\gamma',K'} \left(\mathcal{H}^{J;NZ}_{\beta,\gamma,K;\beta_2',\gamma',K'} - E^{J;NZ;\sigma}\mathcal{N}^{J;NZ}_{\beta,\gamma,K;\beta_2',\gamma',K'}\right) f^{J;NZ;\sigma}_{\beta_2',\gamma',K'} = 0, \quad (8)$$

where $\mathcal{H}^{J;NZ}_{\beta,\gamma,K;\beta_2',\gamma',K'}$ and $\mathcal{N}^{J;NZ}_{\beta,\gamma,K;\beta_2',\gamma',K'}$ are the energy and norm overlap kernels, respectively. From the solution of the HWG equations we obtain directly the energy spectrum $E^{J;NZ;\sigma}$ ($\sigma = 1, 2, 3, \ldots$) and the coefficients needed to compute expectation values and electromagnetic transitions among the different states. The number of integration points both in gauge and Euler angles for particle number and angular momentum projection, the size of the harmonic oscillator basis, as well as the number of mesh points in the triaxial plane are chosen to ensure the convergence in the expectation values, transition rates and collective wave functions computed in this work. Further details about the performance of the method can be found in Ref. [7]. The main differences with the 5DCH method [12] are: i) exact GCM calculations without gaussian overlap approximation (GOA) are performed, ii) exact symmetry restoration (particle number and angular momentum) is accomplished, iii) the set of intrinsic HFB wave functions is found in the PN-VAP method instead of using a plain HFB. The computations within SCCM approach are time consuming and take approximately twenty days for each nucleus on a cluster with 150 CPUs. Therefore, this method has been used only in the analysis of ^{86}Ge and ^{88}Se, where the role played by the triaxial degree of freedom is expected to be most relevant.

TABLE V. Excited bands of selected $N = 54$ isotones [energies in MeV, quadrupole moments in $e$fm^2, $B(E2)$ in e^2fm^4].

Z	J	E^*	$B(E2; J \to J-1)$	$Q_{\rm spec}$
30	2_2^+	1.43		21
	3^+	1.94	132	− 1
	4_2^+	1.93	0.5	− 20
	5^+	2.81	1.4	− 8
32	2_2^+	1.39		39
	3^+	1.79	747	− 0.7
	4_2^+	2.34	214	3.5
	5^+	2.91	77	− 28
34	2_2^+	2.03		39
	3^+	2.41	583	− 6
	4_2^+	2.53	26	39
	5^+	3.31	234	− 25
36	2_2^+	1.35		27
	3^+	1.87	540	1.0
	4_2^+	2.25	44	14
	5^+	3.0	5	11

III. RESULTS

A. Deformation properties of $N = 52$–54 isotones in the laboratory picture

We start the discussion with the results obtained in the shell model framework. In Tables II and III we collect the properties of the investigated systems which characterize quadrupole properties of the yrast bands: energies, $B(E2)$ values, and spectroscopic quadrupole moments $Q_{\rm spec}$. We derive the intrinsic quadrupole moments Q_0 from the spectroscopic ones using the well known relations:

$$Q_0 = \frac{(J+1)(2J+3)}{3K^2 - J(J+1)} Q_{\rm spec}(J), \quad K \neq 1 \quad (9)$$

and

$$B(E2; J \to J-2) = \frac{5}{16\pi} e^2 \frac{(J+1)(J+2)}{(2J+3)(2J+5)} Q_0^2, \quad (10)$$

for $K \neq 1/2, 1$.

Let us also remind, that a γ band ($K = 2$), apart of a characteristic level sequence, has $Q(2^+_\gamma) = -Q(2^+_y)$ and $Q(3^+) \sim 0$. In the Davidov-Filipov model [30] the amount of the triaxiality is derived from the ratio:

$$\frac{B(E2; 2^+_\gamma \to 2^+_y)}{B(E2; 2^+_\gamma \to 0^+_y)}, \quad (11)$$

TABLE VI. Intrinsic shape parameters of the shell model states.

(Yrast)	State	Q_0	β	γ (deg.)	Q_0(SU3)	$Q_0^{\rm rot}$	$\beta^{\rm rot}$
^{86}Ge	$0^+_{\rm g.s.}$	165	0.238	12	151	–	–
	2^+_1	161	0.232	8		153/140	0.21
	4^+_1	152	0.218	12		149/110	0.19
	6^+_1	118	0.172	10		145/82	0.17
^{88}Se	$0^+_{\rm g.s.}$	174	0.250	9	168	–	–
	2^+_1	169	0.243	12		169/168	0.23
	4^+_1	159	0.229	15		158/148	021
	6^+_1	118	0.173	14		122/137	0.18
(Excited)	State	Q_0	β	γ (deg.)			
^{86}Ge	2^+_2	152	0.219	28			
	3^+_1	148	0.213	32			
	4^+_2	116	0.169	41			
	5^+_1	105	0.154	33			
^{88}Se	2^+_2	152	0.219	35			
	3^+_1	143	0.207	36			
	4^+_2	114	0.166	40			
	5^+_1	100	0.146	36			

where y subscript denotes the yrast states. In Tables IV and V we collect the quantities characterizing the excited bands in several nuclei.

As can be seen, the yrast bands of $N = 52$ zinc, germanium and krypton miss the characteristic features of deformed bands: The inequality of quadrupole moments derived from spectroscopic moments and from transition values assuming $K = 0$, as well as the visible variation of the derived quantities with spin, do not allow us to associate the intrinsic deformation parameter to this band. This situation gets different in selenium, where the features of ground state deformation are present. The results are compatible with a deformed intrinsic state with nearly constant quadrupole moment $Q_0 \sim 130\, e\text{fm}^2$, corresponding to $\beta \sim 0.19$ for ^{86}Se. The SM results confirm the analytic pseudo-SU(3) model predictions that the maximum of deformation is obtained with six protons in the model space, thus in ^{86}Se for $N = 52$. Also qualitative agreement between the pseudo-SU(3) and realistic SM quadrupole moments is reasonable.

From Table III one has clear evidence for sizable deformation of Ge and Se at $N = 54$. The full calculation of the intrinsic shape parameters using the n-body quadrupole operators was done for the yrast $0^+_{\rm g.s.}, 2^+_1, 4^+_1, 6^+_1$ sequence and for the excited band $2^+_2, 3^+_1, 4^+_2, 5^+_1$. The results are summarized in Table VI and compared to the pseudo-SU(3) predictions and results from the simpler axial rotor analysis of Table III. These two bands, with their main $E2$ connections, are also displayed in Fig. 1(a) and 1(b).

Concerning the yrast sequence, a very nice agreement is found for the results obtained with the three different methods. This means that the collectivity originates mainly from the global rotation of the shape, with the triaxial degree of freedom playing only a marginal role. But this collective axial feature stops already at 6^+ both in ^{86}Ge and ^{88}Se, showing that the axial collectivity is not yet fully established and that those nuclei mark the beginning of full shell collectivity or the end of a transitional region. All three methods consistently depict ^{88}Se as more collective than ^{86}Ge which is expected, as ^{88}Se is closer to the proton mid shell. The ground state axial deformation parameter β in particular is stronger in ^{88}Se than in ^{86}Ge. The second part of Table VI contains the results for the nonyrast sequence built on top of the 2^+_2 state. The asymmetry angles of all states considered are close to 30°, this band is clearly characteristic of a triaxial structure and the comparison with the SU(3) or axial rotor limit cannot help. Nor can the comparison with the Davidov and Filipov model as the calculation of the higher order n-body quadrupole moments rather reveals γ instability than

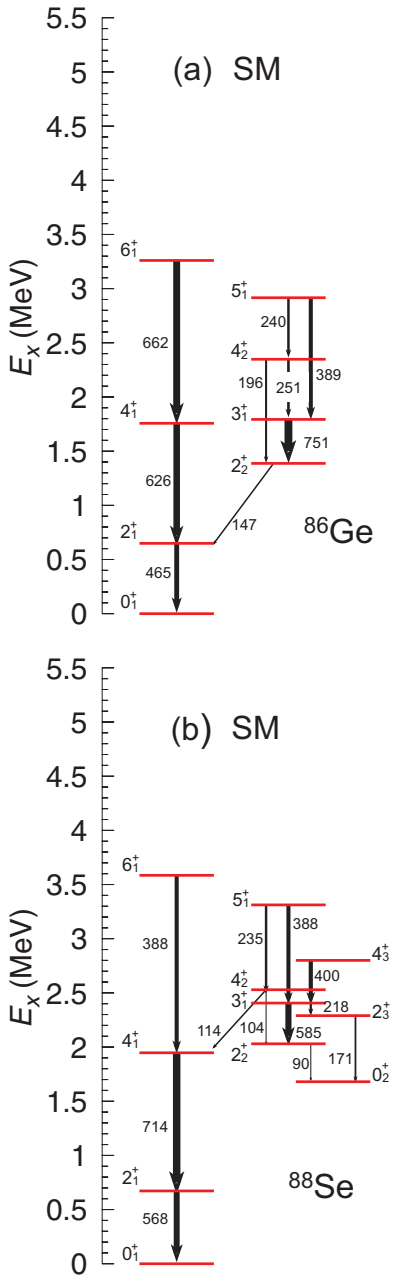

FIG. 1. (Color online) Excitation energies (in keV) and highest reduced transition rates $B(E2)$ (in $e^2\text{fm}^4$) for (a) ^{86}Ge and (b) ^{88}Se, calculated in the shell model framework.

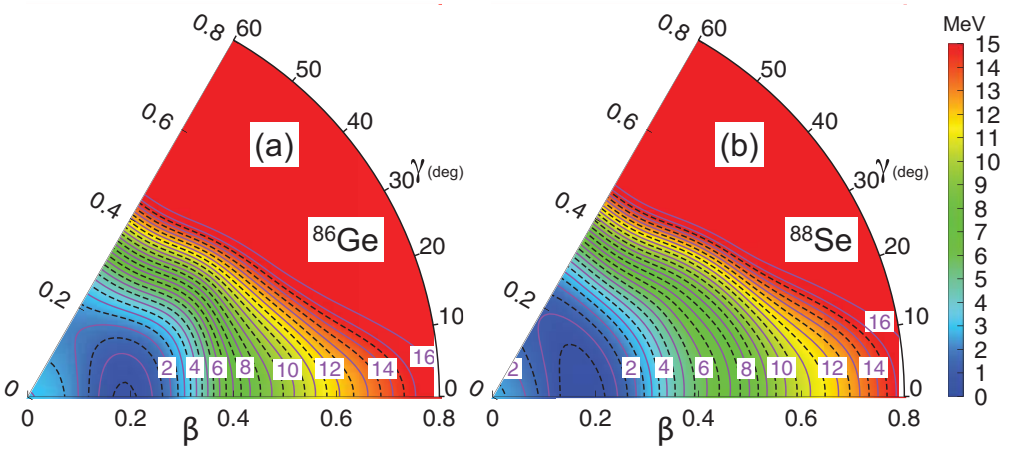

FIG. 2. (Color online) Potential energy surfaces in the particle number variation after projection (PN-VAP) approach along the (β, γ) plane for (a) ^{86}Ge and (b) ^{88}Se nuclei calculated with the Gogny D1S interaction.

permanently triaxially deformed, rotating shape. The axial parameters of the states forming this sequence are practically the same between the two nuclei, the difference comes from the asymmetry angle, higher in the case of ^{88}Se than in ^{86}Ge. One can consider that the triaxiality revealed by this band is maximum in ^{86}Ge while ^{88}Se is already leaning towards oblateness. A fact which, rather unexpectedly, is consistent with the SCCM results as will be shown in the following paragraph.

B. Intrinsic description of triaxial deformation

We now analyze the results obtained with the SCCM method described in Sec. II C for ^{86}Ge and ^{88}Se ($N = 54$) nuclei. To have an insight into the role of the intrinsic deformation in these isotopes we represent in Fig. 2 the potential energy surfaces (PES) along the triaxial (β, γ) plane in the PN-VAP approach. Here we observe that both nuclei have rather similar PES, with absolute minima at axial prolate deformations $\beta \sim 0.15$–0.20 and a quite flat region between $\beta \in [0.0, 0.3]$, $\gamma \in [0°, 60°]$. In addition, ^{88}Se shows a slightly more pronounced γ softness than ^{86}Ge, where the prolate minimum is better defined. This kind of soft potentials suggests that configuration mixing effects can play a key role in understanding the spectra for these nuclei. Hence, we now describe the results obtained by performing shape mixing calculations with particle number and angular momentum restored states. In Fig. 3 we represent the excitation energies and reduced transition probabilities $B(E2)$ for ^{86}Ge [Fig. 3(a)] and ^{88}Se [Fig. 3(b)]. The states are sorted by connecting the different levels with the ones with the larger values of the $B(E2)$. On the one hand, we obtain for both nuclei ground state (g.s.) bands with the sequence of angular momentum $0_1^+, 2_1^+, 4_1^+, 6_1^+$, which in principle indicates the presence of rotational bands. The mean value of the intrinsic third component of the angular momentum is mainly $K = 0$ for all the states belonging to these bands as we show in Table VII and VIII. The $r_{42} = E(4_1^+)/E(2_1^+)$ ratios ($r_{42} = 2.7$ and 2.6 for ^{86}Ge and ^{88}Se, respectively) for these states do not support the existence of

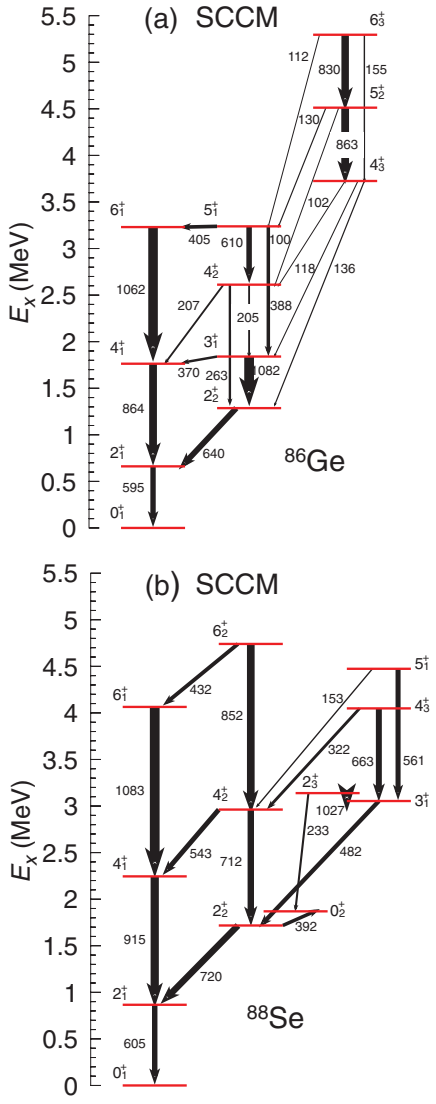

FIG. 3. (Color online) Excitation energies (in MeV) and highest reduced transition probabilities $B(E2)$ (in e^2fm^4) for (a) ^{86}Ge and (b) ^{88}Se calculated with the Gogny D1S interaction.

TABLE VII. Excitation energies (in MeV), spectroscopic quadrupole moments (in $e\text{fm}^2$) and distribution of the intrinsic quantum number K of the states for g.s., first, and second excited bands in ^{86}Ge.

	0_1^+	2_1^+	4_1^+	6_1^+	2_2^+	3_1^+	4_2^+	4_3^+	5_2^+
$E(J_\sigma^+)$	0.000	0.661	1.763	3.230	1.286	1.840	2.612	3.725	4.512
$Q_{\text{spec}}(J_\sigma^+)$	0.000	− 26.691	− 19.165	− 17.057	27.182	0.000	− 57.542	77.500	30.497
$K = 0$	1.000	0.858	0.695	0.561	0.222	0.000	0.261	0.166	0.000
$\|K\| = 2$	0.000	0.142	0.289	0.401	0.778	1.000	0.563	0.149	0.189
$\|K\| = 4$	0.000	0.000	0.016	0.036	0.000	0.000	0.176	0.685	0.811

well-deformed axial rotational bands in these cases. However, the ratios of $4^+/2^+$ energies, strongly dependent on the pairing interaction in nuclei, are hardly indicative for the rotational structures in lighter, even well deformed nuclei. For example, the experimental $E(4^+)/E(2^+)$ value in ^{20}Ne is 2.6, in ^{24}Mg 3.01 and 2.47 in ^{48}Cr, which is also far from the rotational limit value of 3.3. In Fig. 5 we thus represent the ratio of the spectroscopic quadrupole moments $Q_{\text{spec}}(J)/Q_{2^+}$. The 2^+ states vary for each band, and for the ground state bands we see a distinctive deviation from the rotational limit. The main difference between the two isotones is however found in the first and second excited bands. For ^{86}Ge we obtain a $2_2^+, 3_1^+, 4_2^+, 5_1^+$ band (predominantly $K = 2$) strongly connected to the g.s. band and another one with the sequence $4_3^+, 5_2^+, 6_3^+$ (mostly $K = 4$) with smaller $B(E2)$ values both towards the g.s. and first excited bands. On the other hand, ^{88}Se presents a much more mixed band structure as we see in Fig. 3(b). In this case, we find the state 2_2^+ at a slightly lower excitation energy than the 0_2^+ and with a large $B(E2)$ between them. These two states together with $4_2^+, 6_2^+$ develop a $K = 0$ band strongly connected to the g.s. band. In addition, we have also a predominantly $K = 2$ band $(3_1^+, 2_3^+, 4_3^+, 5_1^+)$ with a small admixture of $K = 0$ components that is also connected to the first excited band.

To shed light on the shape structure of these states we represent in Fig. 4 the collective wave functions for the band-head states described above. The rest of the states belonging to the same band have a similar distribution. The maxima in the probabilities are found at $(\beta \sim 0.2, \gamma = 0°)$, $(\beta \sim 0.25, \gamma = 15°)$, and $(\beta \sim 0.25, \gamma = 18°)$ for ^{86}Ge and at $(\beta \sim 0.2, \gamma = 0°)$, $(\beta \sim 0.25, \gamma = 60°)$, and $(\beta \sim 0.2, \gamma = 28°)$ for ^{88}Se. We observe that in most of the states represented in Fig. 4 the probability is distributed in a range of deformations ($\beta \in [0.10, 0, 35]$, $\gamma \in [0°, 60°]$) showing that the triaxial degree of freedom plays an important role, specially for the states in the first and second exited bands. Finally, we notice that the ground state of ^{88}Se is slightly more spherical than the g.s. of ^{86}Ge, consistently having a larger $E(2_1^+)$ (see Fig. 3).

C. Comparison of SM and SCCM calculations for ^{86}Ge and ^{88}Se

The comparison of calculated spectra and transition rates in shell model and beyond mean-field frameworks is done based on results shown in Figs. 1(a) and 3(a) for ^{86}Ge and Figs. 1(b) and 3(b) for ^{88}Se. The comparison of deformation properties in both models is shown in Fig. 5, where the ratios of spectroscopic moments are plotted and compared to those of the rotational limit.

For ^{86}Ge, an excellent agreement between the two models is found for predicted excitation energies. They agree in the two calculations within several keV for the yrast band and within 300 keV for the first excited band. Both models are as well consistent in their description of the relative magnitudes of the intraband transitions. However, shell model predicts two rather disconnected bands: the $B(E2)$ values between the first excited and the ground state band are severely quenched with respect to intraband transitions, except of the $2_2^+ \to 2_1^+$ one, which is the only plotted in the Fig. 1(a). In the SCCM calculations the out-band transitions are closer in magnitude to the intraband ones.

One should note that the absolute magnitude of transition rates is overall much stronger in the SCCM calculations than in the shell model. It appears that SCCM overshoots the transition rate in the neighboring $N = 50$ ^{86}Kr nucleus, where the experimental data is available: 336 $e^2\text{fm}^4$ is calculated against the experimental value of 244(20) $e^2\text{fm}^4$. Nonetheless, the trends of excitation energies and transition rates along the Kr chain in the known region are correctly reproduced in SCCM calculations. Shell model $B(E2)$ values for $N = 50$ are much closer to experimental ones: we obtain 121 $e^2\text{fm}^4$ for ^{80}Zn and 262 $e^2\text{fm}^4$ for ^{86}Kr, while the experimental values are 146(18) $e^2\text{fm}^4$ and 244(20) $e^2\text{fm}^4$, respectively. The good

TABLE VIII. Same as Table VII but in ^{88}Se.

	0_1^+	2_1^+	4_1^+	6_1^+	0_2^+	2_2^+	4_2^+	2_3^+	3_1^+
$E(J_\sigma^+)$	0.000	0.866	2.245	4.740	1.869	1.717	2.962	3.139	3.054
$Q_{\text{spec}}(J_\sigma^+)$	0.000	− 22.730	− 19.789	− 0.261	0.000	25.374	9.750	− 36.351	0.000
$K = 0$	1.000	0.941	0.888	0.771	1.000	0.728	0.853	0.393	0.000
$\|K\| = 2$	0.000	0.059	0.099	0.200	0.000	0.272	0.090	0.607	1.000
$\|K\| = 4$	0.000	0.000	0.013	0.026	0.000	0.000	0.057	0.000	0.000

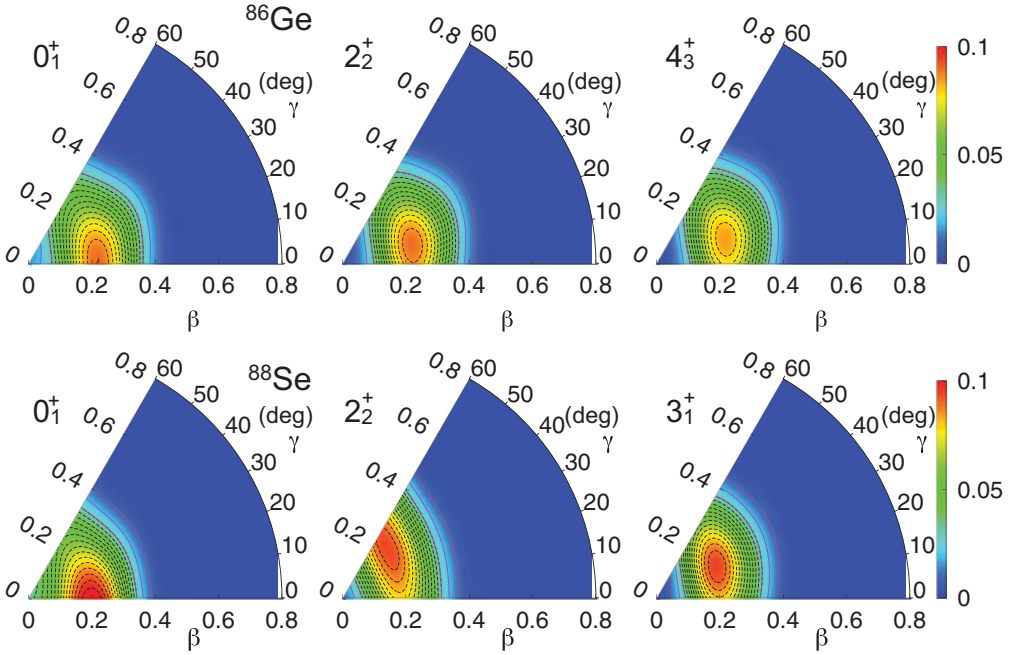

FIG. 4. (Color online) Collective wave functions for the band-head states of Fig. 3 in the (β, γ) plane. Upper and lower panels correspond to ^{86}Ge and ^{88}Se.

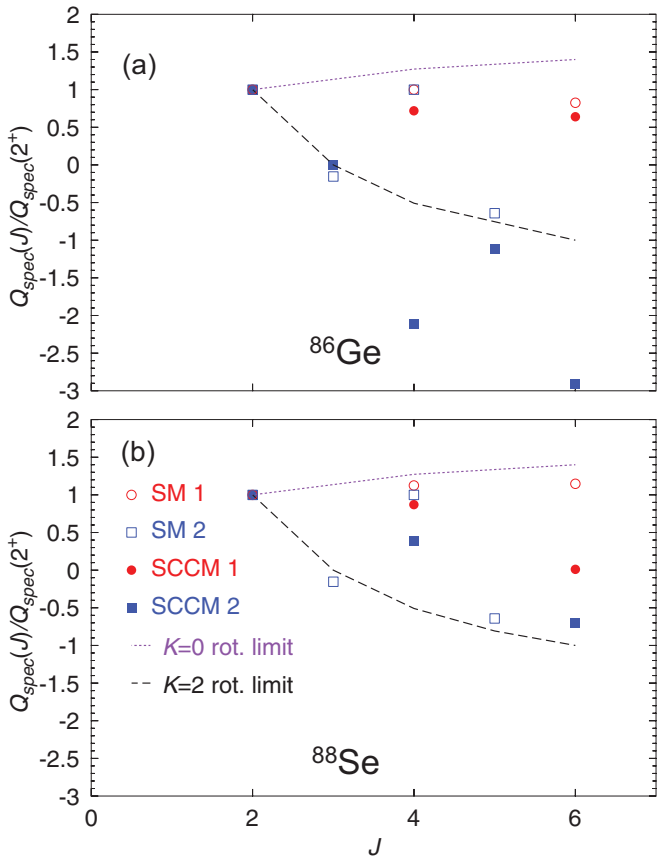

FIG. 5. (Color online) Spectroscopic quadrupole moments normalized to the value $Q_{\rm spec}(2_1^+)$ (g.s. band, bullets) and $Q_{\rm spec}(2_2^+)$ (first excited band, boxes) for (a) ^{86}Ge and (b) ^{88}Se. In lines, the rotor limit for $K = 0$ (dotted) and $K = 2$ (dashed) are given.

agreement is however expected since the effective charges in SM have been chosen so to reproduce the transition rates in the neighboring Zr isotones [1].

In spite of considerable differences in the absolute magnitude of $B(E2)$ values, it is conspicuous that both models predict the largest $B(E2)$ value between the first 3^+ and the second excited 2^+ states in ^{86}Ge. The level sequence and transition rates obtained in both models suggest that ^{86}Ge can be non-axially deformed. Other characteristic features common to triaxial nuclei appear in both calculations for ^{86}Ge: the $Q_{\rm spec}$ values of the first 2^+ and the second 2^+ have the same value but the opposite sign and $Q_{\rm spec}(3^+) \sim 0$ (see Tables III, V, VII).

In ^{88}Se, shell model predicts more deformed structure with a lower lying 2^+ state than SCCM, though the difference is of only 200 keV. A possible experimental candidate for 2^+ state is located at 886 keV according to Ref. [31], SMMC appears thus to be closer to the measurement. However, recently a different value (651 keV) of 2^+ energy in ^{88}Se has been reported [32], which agrees perfectly with the shell model prediction and points to a stronger deformation of this nucleus than obtained in the SCCM model. The remaining yrast levels and the excited bands are located much higher in energy in SMMC calculations than in SM. Both models predict a much more complicated band structure in this nucleus. As previously, transition rates between the yrast and excited bands are relatively small in shell model, while SCCM calculations predict considerable transitions between them.

The major difference in the two models concerns the degree of deformation of both nuclei. While the SCCM calculation find ^{88}Se more spherical than ^{86}Ge, the shell model predicts a larger spectroscopic moment in Se than in Ge, which follows

the pseudo-SU(3) scheme. It can be clearly seen in Fig. 5 that shell model results follow more closely the rotational limit for the ground state and excited bands in both ^{86}Ge and ^{88}Se than the SCCM ones. Interestingly, SCCM supports shell model findings that the triaxiality is more important in ^{86}Ge and ^{88}Se and both models predict much a lower $B(E2; 3^+ \rightarrow 2_2^+)$ value in ^{88}Se. In addition, both models also agree that the $K = 2$ bands do not continue to the second excited 4^+ state in ^{86}Ge and ^{88}Se nuclei.

IV. CONCLUSIONS

We have analyzed the quadrupole properties of neutron rich nuclei, just above the $N = 50$ shell closure. We have employed the algebraic pseudo-SU(3) model, shell model framework with empirically adjusted interactions in a $\pi r3g - \nu r4h$ model space outside the ^{78}Ni core and finally, the particle and angular momentum symmetry conserving beyond-mean field calculations with Gogny forces. The pseudo-SU(3) and shell model results appear to be in a good qualitative and quantitative agreement. Both models predict the signs of deformation in Se and Ge nuclei with four neutrons above the $N = 50$ shell closure. The beyond mean-field calculations agree well with the shell model ones in their predictions of energy levels and band structures of ^{86}Ge. The models used in this work consistently indicate that a maximum of triaxiality can appear in ^{86}Ge, where a low lying 3^+ level connected by a strong transition to the 2_2^+ should be observed. However, some discrepancies are found in the two approaches for ^{88}Se, where shell model calculation envisage stronger deformation effects than SCCM calculations. Further theoretical efforts are required to understand their origin. It is now a challenge for future experiments to verify the degree of collectivity around the $N = 50$ shell closure and wether the triaxiality can indeed develop in the nuclei just above the magic ^{78}Ni.

ACKNOWLEDGMENTS

T.R.R. acknowledges support from BMBF-Verbundforschungsprojekt no. 06DA7047I and Helmholtz International Center for FAIR program. K.S. and T.R.R. acknowledge the support from the French-German IN2P3-GSI 10-63 collaboration agreement.

[1] K. Sieja, F. Nowacki, K. Langanke, and G. Martinez-Pinedo, Phys. Rev. C **79**, 064310 (2009).
[2] K. Sieja and F. Nowacki, Phys. Rev. C **81**, 061303(R) (2010).
[3] K. Sieja and F. Nowacki, Phys. Rev. C **85**, 051301(R) (2012).
[4] http://www-phynu.cea.fr/.
[5] M. Bender and P.-H. Heenen, Phys. Rev. C **78**, 024309 (2008).
[6] J. M. Yao, H. Mei, H. Chen, J. Meng, P. Ring, and D. Vretenar, Phys. Rev. C **83**, 014308 (2011).
[7] T. R. Rodríguez and J. L. Egido, Phys. Rev. C **81**, 064323 (2010).
[8] J. Van de Walle *et al.*, Phys. Rev. C **79**, 014309 (2009).
[9] M. Lebois, D. Verney, F. Ibrahim, S. Essabaa, F. Azaiez, M. C. Mhamed, E. Cottereau, P. V. Cuong, M. Ferraton, K. Flanagan *et al.*, Phys. Rev. C **80**, 044308 (2009).
[10] J. A. Winger *et al.*, Phys. Rev. C **81**, 044303 (2010).
[11] E. F. Jones, P. M. Gore, J. H. Hamilton, A. V. Ramayya, J. K. Hwang, A. P. deLima, S. J. Zhu, C. J. Beyer, Y. X. Luo, W. C. Ma *et al.*, Phys. Rev. C **73**, 017301 (2006).
[12] J. P. Delaroche, M. Girod, J. Libert, H. Goutte, S. Hilaire, S. Péru, N. Pillet, and G. F. Bertsch, Phys. Rev. C **81**, 014303 (2010).
[13] D. Verney, B. Tastet, K. Kolos, F. Le Blanc, F. Ibrahim, M. Cheikh Mhamed, E. Cottereau, P. V. Cuong, F. Didierjean, G. Duchêne *et al.*, Phys. Rev. C **87**, 054307 (2013).
[14] T. Rząca-Urban *et al.*, Phys. Rev. C **88**, 034302 (2013).
[15] E. Caurier, G. Martinez-Pinedo, F. Nowacki, A. Poves, and A. P. Zuker, Rev. Mod. Phys. **77**, 427 (2005).
[16] A. F. Lisetskiy, B. A. Brown, M. Horoi, and H. Grawe, Phys. Rev. C **70**, 044314 (2004).
[17] A. Gniady, E. Caurier, F. Nowacki, and A. Poves (unpublished).
[18] E. Caurier, F. Nowacki, A. Poves, and K. Sieja, Phys. Rev. C **82**, 064304 (2010).
[19] K. Sieja, G. Martinez-Pinedo, L. Coquard, and N. Pietralla, Phys. Rev. C **80**, 054311 (2009).
[20] W. Urban *et al.*, Phys. Rev. C **79**, 044304 (2009).
[21] T. Rzaca-Urban, K. Sieja, W. Urban, F. Nowacki, J. L. Durell, A. G. Smith, and I. Ahmad, Phys. Rev. C **79**, 024319 (2009).
[22] W. Urban, K. Sieja, G. S. Simpson, T. Soldner, T. Rzaca-Urban, A. Złomaniec, I. Tsekhanovich, J. A. Dare, A. G. Smith, J. L. Durell *et al.*, Phys. Rev. C **85**, 014329 (2012).
[23] G. S. Simpson, W. Urban, K. Sieja, J. A. Dare, J. Jolie, A. Linneman, R. Orlandi, A. Scherillo, A. G. Smith, T. Soldner *et al.*, Phys. Rev. C **82**, 024302 (2010).
[24] M. Czerwinski *et al.*, Phys. Rev. C (to be published).
[25] E. Caurier and F. Nowacki, Acta Phys. Pol. B **30**, 705 (1999).
[26] K. Kumar, Phys. Rev. Lett. **28**, 249 (1972).
[27] A. Arima, M. Harvey, and K. Shimizu, Phys. Lett. B **30**, 517 (1969).
[28] P. Ring and P. Schuck, *The Nuclear Many-Body Problem* (Springer-Verlag, Berlin, 1980).
[29] M. Anguiano, J. Egido, and L. Robledo, Phys. Lett. B **545**, 62 (2002).
[30] A. Davydov and G. Filippov, Nucl. Phys. **8**, 237 (1958).
[31] http://www.nndc.bnl.gov/.
[32] J. Pereira, presented at the April Meeting of the American Physical Society, Denver, Colorado, US, April 2013.

PHYSICAL REVIEW C **82**, 054301 (2010)

Island of inversion around ^{64}Cr

S. M. Lenzi,[1] F. Nowacki,[2] A. Poves,[3] and K. Sieja[2,*]

[1]*Dipartimento di Fisica dell'Università and INFN, Sezione di Padova, I-35131 Padova, Italy*

[2]*IPHC, IN2P3-CNRS et Université de Strasbourg, F-67037 Strasbourg, France*

[3]*Departamento de Física Teórica e IFT-UAM/CSIC, Universidad Autónoma de Madrid, E-28049 Madrid, Spain*

(Received 10 September 2010; published 2 November 2010)

We study the development of collectivity in the neutron-rich nuclei around $N = 40$, where the experimental and theoretical evidence suggest a rapid shape change from the spherical to the rotational regime, in analogy to what happens at the *island of inversion* surrounding ^{31}Na. Theoretical calculations are performed within the interacting shell-model framework in a large valence space, based on a ^{48}Ca core, which encompasses the full pf shell for the protons and the $0f_{5/2}$, $1p_{3/2}$, $1p_{1/2}$, $0g_{9/2}$, and $1d_{5/2}$ orbits for the neutrons. The effective interaction is based on a G matrix obtained from a realistic nucleon-nucleon potential whose monopole part is corrected empirically to produce effective single-particle energies compatible with the experimental data. We find a good agreement between the theoretical results and the available experimental data. We predict the onset of deformation at different neutron numbers for the various isotopic chains. The maximum collectivity occurs in the chromium isotopes where the large deformation regime already starts at $N = 38$. The shell evolution responsible for the observed shape changes is discussed in detail, in parallel to the situation in the $N = 20$ region.

DOI: 10.1103/PhysRevC.82.054301 PACS number(s): 21.60.Cs, 21.10.Re, 21.30.Fe, 27.50.+e

I. INTRODUCTION

In the last decades, more and more experimental evidence has been accumulated establishing the breaking of the shell closures known at the stability valley when approaching the drip lines, mainly at the very neutron-rich side. The first example of an unexpected disappearance of a shell closure ($N = 8$) was found in ^{11}Be, whose ground state is an intruder $1/2^+$ located 320 keV below the "natural" $0\hbar\omega$ $1/2^-$ state [1]. However, the true relevance of this finding was not recognized till many years later, and even now it is shadowed by the fame of its more neutron-rich isobar ^{11}Li. In the *sd* shell, the expected $N = 20$ semimagic neutron-rich nuclei turned out to be actually well deformed [2,3]. The presence of deformed ground states in the nuclei around ^{32}Mg and the breaking of the $N = 20$ shell closure in this region has been extensively studied experimentally and theoretically (see Refs. [4–6] for shell-model reviews). The aim of these studies is to map the limits of the so-called *island of inversion*, that is, the region of nuclei where the strong quadrupole correlations overcome the spherical mean-field gaps, favoring energetically the deformed intruders, which often become ground states. Indeed, another basic aim is to understand microscopically the dynamics responsible for these shape transitions.

The question of the persistence of the $N = 40$ harmonic oscillator closure in neutron-rich nuclei comes in naturally in this context. The high-lying 2^+ state observed in ^{68}Ni and its low $B(E2; 2^+ \rightarrow 0^+)$ value are the result of the relatively large energy gap separating the pf and $0g_{9/2}$ orbitals [7]. However, this gap gets reduced (or even disappears) when protons are removed from ^{68}Ni: The nucleus ^{66}Fe, with only two protons less, shows a sudden change in nuclear structure with an increased collectivity manifested via its very low-lying 2^+ state. Along the iron chain, indications for a collective behavior come from the systematics of the 2^+ states [8] as well as from the recent measurement of the $B(E2)$ values in ^{64,66}Fe [9,10]. The evolution of the $B(E2)$ values in iron isotopes points to a sudden increase of collectivity when approaching $N = 40$. Only very recently has the first measurement of the excited levels in ^{64}Cr been reported [11]. This is the nucleus where the theoretical calculations predicted the lowest-lying 2^+ level in the region [12–14]. The measured 2^+ state energy agrees within 100 keV with those theoretical predictions. The sudden shape change at $N = 40$ challenges the theoretical models, which have to account for a particularly rapid shell evolution responsible for these effects. Recent beyond mean-field Hartree-Fock-Bogoliubov (HFB) + Generator Coordinate Method (GCM) calculations with the Gogny force, reported in Ref. [15], show an increase of collectivity toward the proton drip line. The spherical neutron single-particle energies obtained in the HFB approach reveal almost no variation of the $N = 40$ gap with the proton number between $Z = 20$ and $Z = 28$. As a consequence, only a moderate collectivity in the iron and chromium chains is found, without visible structure changes between them. The collectivity at $N = 40$ has previously been a subject of many shell-model studies using different valence spaces and interactions [11–14,16]. In particular, it was shown that the shell-model calculations using the $0f_{5/2}$, $1p_{3/2}$, $1p_{1/2}$, and $0g_{9/2}$ neutron orbits (the fpg valence space) and realistic interactions [13] can reproduce rather well the level schemes of ^{62,64}Fe, but fail to do so for the 2^+ state of ^{66}Fe [16]. To reproduce the large quadrupole collectivity in this mass region, the inclusion of the neutron $1d_{5/2}$ orbital is needed, as was first surmised in Ref. [12] and confirmed recently in Ref. [9]. This can be explained in terms of the quasi-SU3 approximate symmetry: In this framework, the deformation is generated by the interplay between the quadrupole force and the central field in the subspace consisting of the lowest $\Delta j = 2$ orbitals of a major shell [17].

*kamila.sieja@iphc.cnrs.fr

In this work we discuss in detail how the sudden onset of collectivity can be interpreted in terms of shell-model calculations in large model spaces and we look for the similarities in the deformation-driving mechanisms at $N = 20$ and $N = 40$ when approaching the neutron drip line. We present novel calculations for the $N = 40$ region, in a model space including the pf shell for protons and the $0f_{5/2}$, $1p_{3/2}$, $1p_{1/2}$, $0g_{9/2}$, and $1d_{5/2}$ orbits for neutrons. We discuss first our model space and interaction as well as the computational details in Sec. II. The shape evolution along the $N = 40$ line is studied in Sec. III. Next, we illustrate the development of deformation along the isotopic chains of iron and chromium in Sec. IV and we discuss the structure of the nickel isotopes. Conclusions are given in Sec. V.

II. THE VALENCE SPACE

The physics of the $N = 40$ nuclei has been discussed in the recent past both experimentally and theoretically [5,8,9,11–16]. In ^{68}Ni, the $N = 40$ harmonic oscillator shell closure is somewhat weakened, however, whereas some of its properties seem consistent with a superfluid behavior, others may point to a double magic character. Below ^{68}Ni, the iron and chromium isotopic chains are characterized by an open proton shell that favors the development of quadrupole correlations. Such a situation also occurs for the $N = 20$ nuclei in the so-called *island of inversion* around ^{32}Mg [18]: The protons occupy the $N = 2$ harmonic oscillator shell and the neutrons may lie either in the $N = 2$ harmonic oscillator shell (normal filling) or in the $1p_{3/2}$ and $0f_{7/2}$ orbitals from the $N = 3$ major shell (intruder configurations). The latter orbits form a quasi-SU3 block [19], which enhances the quadrupole correlations. Extended shell-model calculations by the Tokyo group, with the SDPF-M effective interaction [18], predict the dominance of different types of configurations (0p0h, 1p1h, 2p2h) for the ground states of the nuclei with $18 \leqslant N \leqslant 22$ and $10 \leqslant Z \leqslant 14$ delineating the contours of the island of inversion.

To assess if such a scenario can develop around ^{68}Ni, we adopt here a model space based on a ^{48}Ca core which comprises the pf shell for protons and the $1p_{3/2}$, $1p_{1/2}$, $0f_{5/2}$, $0g_{9/2}$, and $1d_{5/2}$ orbits for neutrons. The degrees of freedom that can be encompassed in this valence space are very similar to the ones present in the study recalled previously [18] and the same kinds of phenomena can therefore be described. The advantage of this valence space is that it contains all the physical degrees of freedom important for the description of the low-lying properties of these nuclei, it is computationally tractable (see precisions hereafter), and it is almost free of center-of-mass spuriousity since its main components, the $0f_{7/2} \rightarrow 0g_{9/2}$ excitations, are excluded from the space.

The interaction proposed in this work, denoted hereafter LNPS, is a hybrid one, based on several sets of realistic two-body matrix elements (TBME). Its main building blocks are as follows:

(i) The last evolution of the Kuo-Brown interaction (KB3gr) for the pf shell [20].
(ii) The renormalized G matrix of Ref. [21] with the monopole corrections introduced in Ref. [22], for the remaining matrix elements involving the $1p_{3/2}$, $1p_{1/2}$, $0f_{5/2}$, and $0g_{9/2}$ neutron orbits.
(iii) The G matrix based on the Kahana-Lee-Scott potential [23] for the matrix elements involving the $1d_{5/2}$ orbit. This potential was successfully employed in the definition of the recent SDPF-U shell-model interaction [24] for the description of neutron-rich sd-pf nuclei.

In addition, another set of experimental constraints has been taken into account for the final tuning of the monopole Hamiltonian.

(i) The $Z = 28$ proton gap around ^{78}Ni is inferred from recent experimental data in ^{80}Zn and fixed so as to reproduce the measured $B(E2)$. A standard polarization charge of $0.5e$ was used in all the calculations presented in this work.
(ii) The size of the $N = 50$ neutron gap in ^{78}Ni was estimated to be $\sim$5 MeV. The evolution of the neutron gap with the neutron number is rather independent of the proton number. On the contrary, the systematics [25] show that the $0g_{9/2}$–$1d_{5/2}$ gap in Zr isotopes increases by 3 MeV when the neutron $0g_{9/2}$ orbital is filled. We assume a similar behavior for the Ni chain. With this assumption, the observed 5^+, 6^+ states in ^{82}Ge, which are supposed to be 1p-1h excitations across the $N = 50$ gap, are correctly reproduced [26].

Finally, to compensate for the absence in our space of the third member of the quasi-SU3 sequence, the $2s_{1/2}$ neutron orbit, we increased the quadrupole-quadrupole interaction of the neutron $0g_{9/2}$ and $1d_{5/2}$ orbits by 20%. Such a balance between the monopole and correlation effects allows us to describe the observed shape evolution in the $Z = 20$–28, $N = 36$–42 mass region.

The effective single-particle energies (ESPE) of the LNPS interaction are shown in Fig. 1 for the neutron orbits at $N = 40$, between ^{60}Ca and ^{72}Ge. For comparison, we show in the same figure the neutron ESPE at $N = 20$ between ^{28}O and ^{36}S, calculated with the SDPF-U interaction [24]. The similarities are striking. In the $N = 20$ case, a reduction of the neutron $0d_{3/2}$-$0f_{7/2}$ gap takes place when protons are removed from the proton $0d_{5/2}$ orbital. This feature, accompanied by the proximity of the quadrupole partner neutron orbitals $0f_{7/2}$ and $1p_{3/2}$, is responsible for the formation of the *island of inversion* at $N = 20$. At $N = 40$ one observes the same behavior, but for the neutron $0f_{5/2}$-$0g_{9/2}$ gap when going down from ^{68}Ni and the closeness of the quadrupole partners $0g_{9/2}$-$1d_{5/2}$.

The analogy in the shell evolution between $N = 20$ and $N = 40$ suggests therefore the possibility of another *island of inversion* below ^{68}Ni.

As mentioned already, the deformation driving role of the neutron $1d_{5/2}$ orbital below ^{68}Ni was already discussed in the shell-model calculations of Ref. [12]. However, due to the computational limitations at that time, the calculations were performed with a closed neutron $1p_{3/2}$ orbit, therefore using ^{52}Ca as a core. This is no longer an issue here: The present calculations were carried out including up to 14 particle-14 hole excitations across the $Z = 28$ and $N = 40$ gaps, when it appeared necessary to assure the convergence of the calculated

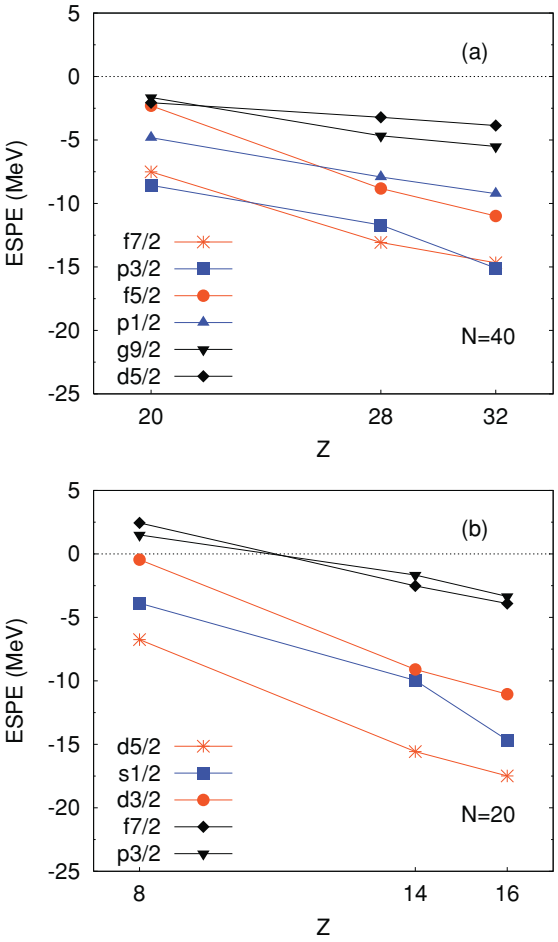

FIG. 1. (Color online) Neutron effective single-particle energies obtained with (a) the LNPS interaction at $N = 40$ and (b) with the SDPF-U interaction at $N = 20$.

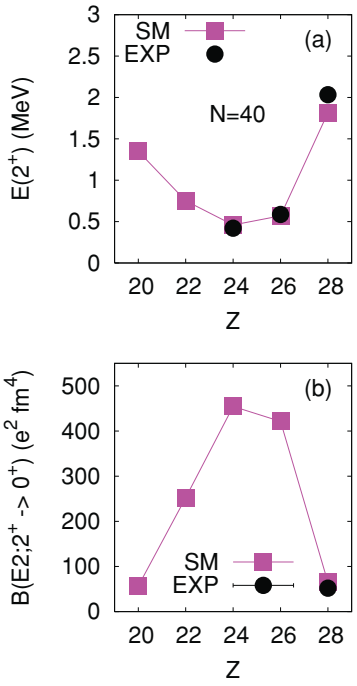

FIG. 2. (Color online) Evolution of the nuclear structure along the $N = 40$ isotonic chain: (a) theoretical 2^+ excitation energies and (b) $B(E2; 2^+ \rightarrow 0^+)$ values, compared to the available experimental data.

electromagnetic properties. The largest dimensions of the matrices treated here reach 10^{10} in the case of ^{64}Fe. All the calculations of this work were performed using the *m*-scheme shell-model code ANTOINE [27].

III. THE PROPERTIES OF THE $N = 40$ ISOTONES FOR $Z \leqslant 28$ AND THE NEW REGION OF DEFORMATION

The change of structure in even-even $N = 40$ isotones from ^{68}Ni down to ^{60}Ca is illustrated in Fig. 2. In Fig. 2(a) the evolution of the excitation energy of the 2^+ state is plotted while Fig. 2(b) shows the corresponding evolution of the $E2$ transition rates. The available experimental data are satisfactorily reproduced in all cases. Our theoretical approach predicts the maximal deformation at the middle of the proton shell (i.e., in ^{64}Cr) where the calculated 2^+ energy is the lowest and the value of $B(E2; 2^+ \rightarrow 0^+)$ is the largest.

In Table I we list the extra occupancies of the two neutron intruder orbitals $0g_{9/2}$ and $1d_{5/2}$ relative to the normal filling. The occupation of the $0g_{9/2}$ orbit in ^{68}Ni is close to 1, which corresponds to ≈50% of the calculated wave function having a $J = 0$ pair excited across $N = 40$ gap. The wave function is, however, difficult to interpret because, in spite of its very large content of excited pairs, the doubly magic component is still substantial. This is probably the reason why ^{68}Ni shows at the same time an increase of the 2^+ excitation energy typical for doubly magic nuclei, and no sign of shell closure in the neutron separation energy.

The occupation of both neutron intruder orbits grows rapidly when protons are removed due to the reduction of the neutron $N = 40$ gap shown in Fig. 1. The ratio of the $0g_{9/2}$ to $1d_{5/2}$ occupations also evolves from Ni to Ca, partly as an effect of the level crossing taking place around ^{62}Ti, but mostly due to the quasi-SU3 structure of the intruder states. The very important role of the $1d_{5/2}$ neutron orbit in the buildup of collectivity in this region sheds doubts about the results of Ref. [14], which do not include this orbit. This is even more so when one examines the very unrealistic ESPE that they enforce into their schematic interaction to get results close to the experimental data.

TABLE I. Occupation of the neutron intruder orbitals and percentage of particle-hole excitations across the $N = 40$ gap in the ground states of the $N = 40$ isotones. The last column contains the correlation energies evaluated for these states.

Nucleus	$\nu g_{9/2}$	$\nu d_{5/2}$	0p0h	2p2h	4p4h	6p6h	E_{corr}
^{68}Ni	0.98	0.10	55.5	35.5	8.5	0.5	−9.03
^{66}Fe	3.17	0.46	1	19	72	8	−23.96
^{64}Cr	3.41	0.76	0	9	73	18	−24.83
^{62}Ti	3.17	1.09	1	14	63	22	−19.62
^{60}Ca	2.55	1.52	1	18	59	22	−12.09

In Table I we list as well the percentages of neutron n-particle n-hole excitations in the ground-state wave functions. The 4p-4h components are dominant in Fe, Cr, Ti, and Ca, however, 2p-2h and 6p-6h contributions are sizable. The complexity of the wave functions constitutes the main difference between the $N = 40$ and $N = 20$ regions. In the latter, nearly pure 2p-2h components have been shown to dominate the 0^+ ground states [18].

It should be also pointed out that this evolution of the neutron filling and of the particle-hole structure does not mean that the nuclei will become more and more deformed with decreasing Z; the ground-state deformation properties result from the total balance between the monopole and the correlation energies (mainly of a proton-neutron character). In Table I, we also list these correlation energies extracted from the multipole Hamiltonian along the $N = 40$ line. Indeed, the correlation energy, reflecting the deformation, increases from Ni to Cr, where it reaches its maximum, and then diminishes toward Ca. The transition between Ni and Cr is not gradual: The removal of two protons already provokes an abrupt change from spherical to a strongly deformed prolate shape.

IV. THE EVOLUTION OF THE DEFORMATION ALONG THE ISOTOPIC CHAINS

The isotope chains provide a very illustrative picture of the evolution of deformation in this region. In Fig. 3 we show the results obtained for the iron chain. In Fig. 3(a) the excitation energies of the 2^+ states are compared to the available experimental data. In Fig. 3(b) we show the ratio of the excitation energies $E(4^+)/E(2^+)$ and $E(6^+)/E(4^+)$, which make it possible to recognize whether a nuclear spectrum is close to that of the rigid rotor or not. Remember that the perfect rotational limit will require $E(4^+)/E(2^+) = 3.33$ and $E(6^+)/E(4^+) = 2.1$. Figure 3(c) depicts the theoretical and experimental $B(E2)$ transition probabilities along the yrast bands. The measured $B(E2; 2^+ \to 0^+)$ values from Ref. [9] are plotted with dots and from Ref. [10] with crosses. Finally, the intrinsic quadrupole moments derived from the calculated spectroscopic ones are shown in Fig. 3(d). To establish a connection between the laboratory and the intrinsic frames we use the relations

$$Q_{\text{int}} = \frac{(J+1)(2J+3)}{3K^2 - J(J+1)} Q_{\text{spec}}(J), \quad K \neq 1, \tag{1}$$

and

$$B(E2, J \to J-2) = \tfrac{5}{16} e^2 |\langle JK20|J-2, K\rangle|^2 Q_{\text{int}}^2, \tag{2}$$

for $K \neq \frac{1}{2}, 1$.

The same properties are plotted in Fig. 4 for the chromium chain. An excellent agreement with the experiment is found for all excitation energies.

The known $B(E2)$ transition rates are well reproduced within the error bars as well. Comparing the results for both isotopic chains it can be seen that the onset of deformation occurs at a different neutron number. In the chromium chain the intrinsic quadrupole moment stays constant along the yrast band already at $N = 38$. This is one of the fingerprints of a good rotor behavior. The iron isotopes undergo the transition at $N = 40$. We also verified that the intrinsic quadrupole moments obtained from the spectroscopic ones [Eq. (1)] are nearly equal to those obtained from the transition probabilities according to Eq. (2) in ^{62,64,66}Cr and ^{66,68}Fe. We obtain a

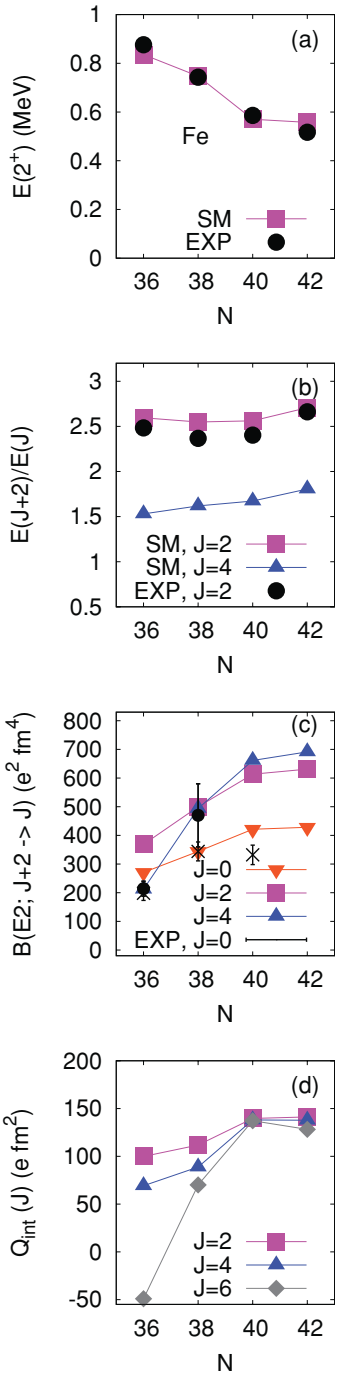

FIG. 3. (Color online) Theoretical results along the iron isotopic chain in comparison with the available experimental data: the excitation energies of the 2^+ states are shown in panel (a), in panel (b) we present the ratio of energies of $E(J+2)/E(J)$, the $B(E2)$ transition rates are plotted in panel (c), and the calculated intrinsic quadrupole moments in panel (d). Two experimental sets of the $B(E2)$ values are shown: from Ref. [9] (black dots) and from Ref. [10] (crosses).

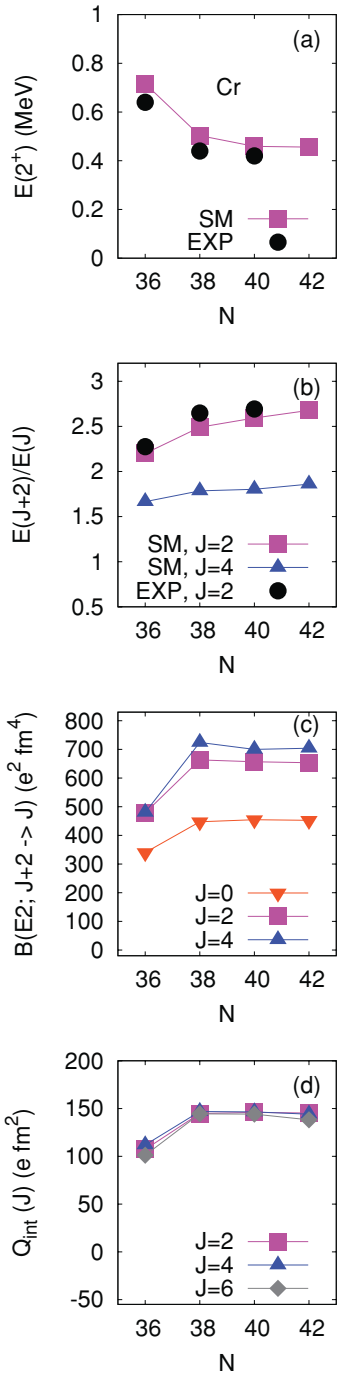

FIG. 4. (Color online) The same as in Fig. 3, but for the chromium isotopes.

value of $Q_{\rm int} \sim 150e$ fm^2 in ^{62,64,66}Cr, which corresponds to $\beta \sim 0.35$. The deformation of ^{66,68}Fe is slightly lower, with $Q_{\rm int} = 145e$ fm^2 ($\beta \sim 0.3$). In the lighter Fe and Cr nuclei, the discrepancies between the calculated quadrupole moments and those obtained in the rotational scheme from the $B(E2)$'s are much larger.

Let us further discuss the structure of the calculated states. In Table II we show the occupancies of the neutron intruder orbitals in the ground states of the chromium and iron chains. In the case of the $0g_{9/2}$ orbit the extra occupancy is reported

TABLE II. Extra occupations of neutron $0g_{9/2}$ and $1d_{5/2}$ orbitals in the ground states of the chromium and iron chains.

Nucleus	N	$\nu 0g_{9/2}$	$\nu 1d_{5/2}$
^{62}Fe	36	0.95	0.12
^{64}Fe	38	2.0	0.27
^{66}Fe	40	3.22	0.51
^{68}Fe	42	2.30	0.62
^{60}Cr	36	1.55	0.31
^{62}Cr	38	2.77	0.66
^{64}Cr	40	3.41	0.76
^{66}Cr	42	2.28	0.90

(i.e., the difference between the value obtained in the configuration mixing calculation and the one that corresponds to the normal filling). The neutron intruder occupations increase with N in both isotopic chains, however, the absolute occupancies are larger in the chromium chain. As mentioned already for the $N = 40$ nuclei, the strong deformation in the Cr chain is not only due to the increased population of the $0g_{9/2}$-$1d_{5/2}$ doublet, but to the strong proton-neutron correlations which tend to be maximal when four protons are active in the pf shell as well.

In Fig. 5 we also show the evolution of the collectivity in the nickel chain: in Fig. 5(a) the theoretical energies of the first excited 2^+ states are compared with experimental ones, while in Fig. 5(b) we show the calculated transition rates in comparison to the available data. The agreement in the calculated energies is very good for all nickels. Concerning transition rates, the model reproduces well the systematics with the minimum in ^{68}Ni and the rapid increase of collectivity in ^{70}Ni. However, the calculated value is closer to the lower tip of

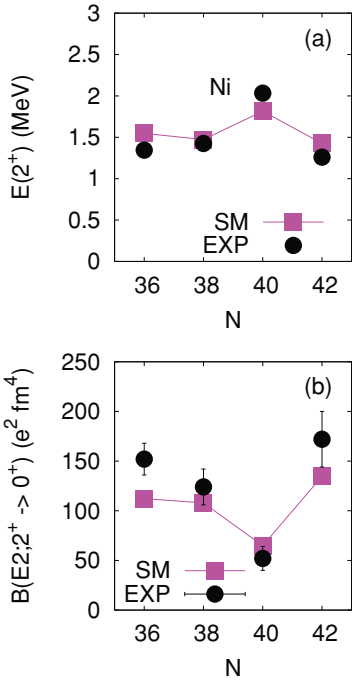

FIG. 5. (Color online) Theoretical versus experimental energies and transition rates of the nickel isotopes in the vicinity of $N = 40$.

the error bar. The transition rate in ^{64}Ni is underestimated. In this case we know that a better agreement with the experiment can be obtained in a full pf-shell calculation as the neutron excitations from the $0f_{7/2}$ orbital are here more important than those through the $N = 50$ gap and, as expected, the occupation of the $1d_{5/2}$ orbit remains close to zero in the calculations.

Finally, let us note the recent work on ^{68}Ni [28], where the excited 0^+ states were investigated and a candidate for a proton 2p-2h intruder was proposed at an excitation energy of 2.2 MeV. We calculated the excited 0^+ states in our model space and we obtained the first excited 0^+_2 state at an energy of 1.2 MeV and the second one 0^+_3 at an energy of 2.4 MeV, in good agreement with the experiment. The too low excitation energy of the first state can be a result of the delicate mixing between the 0^+_1 ground state and the excited 0^+_2 state. These two states are characterized by similar proton occupancies with leading 0p-0h (neutron) configuration for the 0^+_1 ground state and 2p-2h (neutron) configurations for the 0^+_2. For the 0^+_3 state, located at 2.4 MeV, the striking feature is that the dominant proton configuration has exactly two $0f_{7/2}$ protons less than the ground state, (i.e., a pure 2p-2h proton configuration). The total quadrupole sum rules for these states amount to 904, 1162, and 2025 e^2 fm^4 for the ground state, the 0^+_2, and the 0^+_3 states, respectively. This shows, in particular, that the 0^+_3 state carries moderate deformation despite its proton intruder nature.

Deformed, low-lying proton intruder states were also observed in cobalt isotopes around $N = 40$ [29,30] and the LNPS interaction was employed to interpret their structure. These results will be discussed in a forthcoming publication [31].

V. CONCLUSION

The aim of this work was to study the rapid onset of collectivity below ^{68}Ni, suggested by the experimental evidence, which is a great challenge for any theoretical model. Here we presented shell-model calculations in a large valence space including the pf shell for protons and the $0f_{5/2}$, $1p_{3/2}$, $1p_{1/2}$, $0g_{9/2}$, and $1d_{5/2}$ orbitals for neutrons. The effective interaction for this model space was built up using sets of realistic TBME as a starting point and applying monopole corrections thereafter. The progress in algorithms and computer power have made it possible to achieve the largest shell-model diagonalizations in this region of nuclei up to date.

The present calculations were performed in Ni, Cr, Fe, Ti, and Ca isotopes around $N = 40$. We found a satisfactory agreement between the theoretical results and the available data for both excitation energies and transition rates. In particular, it has been possible to describe correctly the rapid onset of collectivity below ^{68}Ni without any collapse of the spherical gaps.

It was also shown that the onset of deformation develops at $N = 40$ in the iron chain and at $N = 38$ in chromium isotopes. The maximum deformation is predicted for the chromiums that exhibit features typical of rotational nuclei. The continuous advances in the experimental side, with particular regard to the transition probability measurements, will be a stringent test for these theoretical predictions.

The calculated wave functions of the deformed ground states were shown to contain large amounts of many-particle-many-hole configurations, with around four neutrons occupying intruder orbitals $0g_{9/2}$, $1d_{5/2}$. We also related the observed shape change with the underlying evolution of the spherical mean field, which bears many similarities to the one at the $N = 20$ *island of inversion*.

ACKNOWLEDGMENTS

This work is partly supported by a grant of the Spanish Ministry of Science and Innovation MICINN (FPA2009-13377), by the IN2P3(France)-CICyT(Spain) collaboration agreements, by the Spanish Consolider-Ingenio 2010 Program CPAN (CSD2007-00042), and by the Comunidad de Madrid (Spain), Project No. HEPHACOS S2009/ESP-1473.

[1] D. E. Alburger, C. Chasman, K. W. Jones, J. W. Olness, and R. A. Ristinen, Phys. Rev. **136**, B916 (1964).
[2] C. Thibault, R. Klapisch, C. Rigaud, A. M. Poskanzer, R. Prieels, L. Lessard, and W. Reisdorf, Phys. Rev. C **12**, 644 (1975).
[3] C. Detraz, M. Langevin, D. Guillemaud, M. Epherre, G. Audi, C. Thibault, and F. Touchard, Nucl. Phys. A **394**, 378 (1983).
[4] E. Caurier, G. Martinez-Pinedo, F. Nowacki, A. Poves, and A. P. Zuker, Rev. Mod. Phys. **77**, 427 (2005).
[5] B. Brown, Prog. Part. Nucl. Phys. **47**, 517 (2001).
[6] T. Otsuka, M. Honma, T. Mizusaki, N. Shimizu, and Y. Utsuno, Prog. Part. Nucl. Phys. **47**, 319 (2001).
[7] O. Sorlin *et al.*, Phys. Rev. Lett. **88**, 092501 (2002).
[8] M. Hannawald *et al.* (ISOLDE Collaboration), Phys. Rev. Lett. **82**, 1391 (1999).
[9] J. Ljungvall *et al.*, Phys. Rev. C **81**, 061301 (2010).
[10] W. Rother *et al.*, arXiv:1006.5297.
[11] A. Gade *et al.*, Phys. Rev. C **81**, 051304 (2010).
[12] E. Caurier, F. Nowacki, and A. Poves, Eur. Phys. J. A **15**, 145 (2002).
[13] O. Sorlin *et al.*, Eur. Phys. J. A **16**, 55 (2003).
[14] K. Kaneko, Y. Sun, M. Hasegawa, and T. Mizusaki, Phys. Rev. C **78**, 064312 (2008).
[15] L. Gaudefroy *et al.*, Phys. Rev. C **80**, 064313 (2009).
[16] S. Lunardi *et al.*, Phys. Rev. C **76**, 034303 (2007).
[17] A. P. Zuker, J. Retamosa, A. Poves, and E. Caurier, Phys. Rev. C **52**, R1741 (1995).
[18] Y. Utsuno, T. Otsuka, T. Mizusaki, and M. Honma, Phys. Rev. C **60**, 054315 (1999).
[19] A. P. Zuker, J. Retamosa, A. Poves, and E. Caurier, Phys. Rev. C **52**, R1741 (1995).
[20] E. Caurier (private communication).
[21] M. Hjorth-Jensen, T. Kuo, and E. Osnes, Phys. Rep. **261**, 125 (1995).
[22] F. Nowacki, Ph.D. thesis, IReS Strasbourg, 1996.

[23] S. Kahana, H. C. Lee, and C. K. Scott, Phys. Rev. **180**, 956 (1969).
[24] F. Nowacki and A. Poves, Phys. Rev. C **79**, 014310 (2009).
[25] J. Duflo and A. P. Zuker, Phys. Rev. C **59**, R2347 (1999).
[26] T. Rzkaca-Urban, W. Urban, J. L. Durell, A. G. Smith, and I. Ahmad, Phys. Rev. C **76**, 027302 (2007).
[27] E. Caurier and F. Nowacki, Acta Phys. Pol. B **30**, 705 (1999).
[28] D. Pauwels, J. L. Wood, K. Heyde, M. Huyse, R. Julin, and P. Van Duppen, Phys. Rev. C **82**, 027304 (2010).
[29] D. Pauwels *et al.*, Phys. Rev. C **78**, 041307 (2008).
[30] D. Pauwels *et al.*, Phys. Rev. C **79**, 044309 (2009).
[31] F. Recchia *et al.* (unpublished).

PHYSICAL REVIEW C **81**, 061303(R) (2010)

Shell quenching in ^{78}Ni: A hint from the structure of neutron-rich copper isotopes

K. Sieja and F. Nowacki
Institute Pluridisciplinaire Hubert Curien, 23 rue du Loess, F-67037 Strasbourg Cedex 2, France
(Received 28 May 2010; published 30 June 2010)

Recent progress in experimental techniques allows us to study very exotic systems like neutron-rich nuclei in the vicinity of ^{78}Ni. The spectroscopy of this region can nowadays be studied theoretically in the large scale shell model calculations. In this work, we perform a shell model study of odd copper nuclei with $N = 40$–50, in a large valence space with the ^{48}Ca core, using a realistic interaction derived from the CD-Bonn potential. We present the crucial importance of the proton core excitations for the description of spectra and magnetic moments, which are for the first time correctly reproduced in theoretical calculations. Shell evolution from ^{68}Ni to ^{78}Ni is discussed in detail. A weakening of the $Z = 28$ gap when approaching the $N = 50$ shell closure, suggested by the experimental evidence, is confirmed in the calculations.

DOI: 10.1103/PhysRevC.81.061303 PACS number(s): 21.60.Cs, 21.10.Ky

The region of nuclei toward the ^{78}Ni is nowadays one of the most extensively studied in both experiment and theory. The doubly closed ^{78}Ni, with an unusual proton to neutron ratio, lies between two regions: of the light nuclei, where experimental evidence for changing magic numbers far from stability is well established [1], and of heavy ones, where no quenching of the known spin-orbit shell closures has been so far observed. The weakening of the $Z = 28$ gap when approaching the $N = 50$ shell closure has been suggested, e.gfor example, by Otsuka in Ref. [2] due to the proton-neutron part of the nuclear force, which has an opposite action on protons in the $f_{7/2}$ and $f_{5/2}$ orbitals while filling the neutron $g_{9/2}$ shell. Previous shell model (SM) calculations [3,4] have also revealed the possibility of a weakening of this shell closure.

A related subject of a great experimental interest is the so-called monopole migration in the copper isotopes and the competition of single-particle and collective modes at low excitation energies [5–7]. A decade ago a sudden drop of the $5/2^-$ level in ^{73,71}Cu was observed [8], giving a hint that this state may become the ground state of ^{75}Cu. Such a scenario may be expected concerning a strong attractive monopole interaction between protons and neutrons occupying the $f_{5/2}$ and $g_{9/2}$ orbitals, respectively. The recent measurements of magnetic moments in the copper chain [7] established experimentally the inversion of $5/2^-$ and $3/2^-$ levels in ^{75}Cu. In the same work, the authors pointed out that, however in the available shell model calculations this inversion is present between ^{73}Cu and ^{79}Cu [9–11], it is not followed by a rapid lowering of the first excited $1/2^-$ level observed in experiment. Therefore, *some important physics mechanism is either omitted or underestimated in the recently developed shell model interactions*.

In this work we show that the $Z = 28$ proton gap is eroded in neutron-rich nuclei, thus the physics part which is missing in all previous shell model calculations is not related to the interaction itself, but rather to the lack of proton core excitations excluded in valence spaces based on the ^{56}Ni core used up to now in SM calculations in this region of nuclei. The SM calculations presented here for the copper isotopic chain are performed in the valence space containing all orbitals necessary for the description of the nuclear structure in this region, that is, $f_{7/2}$, $f_{5/2}$, $p_{3/2}$, $p_{1/2}$ for protons and $f_{5/2}$, $p_{3/2}$, $p_{1/2}$, $g_{9/2}$ for neutrons. Such a valence space allows for simultaneous proton excitations from the $f_{7/2}$ orbital to the rest of the pf shell and neutron excitations across the $N = 40$ harmonic oscillator shell closure. At the same time, the spurious center of mass excitations are excluded as the $J^\pi = 1^-$ couplings are not possible within this set of single-particle orbits. This type of a model space has been previously used in the shell model study of Coulomb excitation in ^{68}Ni [12]. An effective interaction derived from a realistic nucleon-nucleon CD-Bonn potential, corrected empirically in its monopole part to reproduce a large set of nuclear data, has been employed. This work continues the development of the interaction but with a special emphasis on the properties of neutron-rich nuclei between $N = 40$ and $N = 50$ shell closures. We present in detail the results for odd copper isotopes: spectra, magnetic moments, composition of the wave functions, from which we draw conclusions on the underlying shell structure in the vicinity of the doubly magic ^{78}Ni. The calculations are performed using the ANTOINE shell model code [13]. Exact diagonalization in the model space has been achieved for nuclei with $N = 42$–50; for ^{69}Cu truncated calculation allowing 8p-8h excitations across $Z = 28$ and $N = 40$ gaps is presented. Maximal dimensions of the matrices treated here reach 7×10^8.

Let us start the discussion with the shell evolution as obtained in the SM calculations, which is crucial for understanding of the observed nuclear structure in this region. The proton effective single-particle energies (ESPE) evolving with filling of subsequent neutron orbitals are traced in Fig. 1. Two experimental constraints have been taken into account in the monopole corrections of the interaction that lead to the ESPE shown in this figure: the sizes of the gaps at $N = 40$ and at $N = 50$. While the size of the proton gap in ^{68}Ni is well established (5.8 MeV from binding energy differences), the corresponding gap in ^{78}Ni can be now inferred indirectly from the recently measured $B(E2; 2^+ \rightarrow 0^+)$ transition rate in ^{80}Zn [14]. Because ^{80}Zn has a closed neutron shell ($N = 50$) and two protons above the $Z = 28$ shell closure, one expects its first excited 2^+ state to be of a predominantly proton character. We obtain in our calculations with a standard polarization

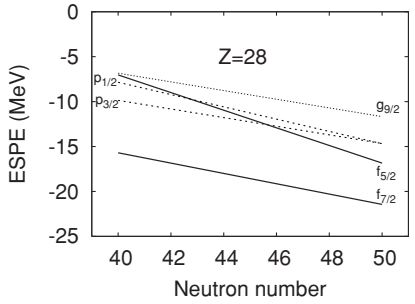

FIG. 1. Evolution of proton effective single-particle energies between ^{68}Ni and ^{78}Ni.

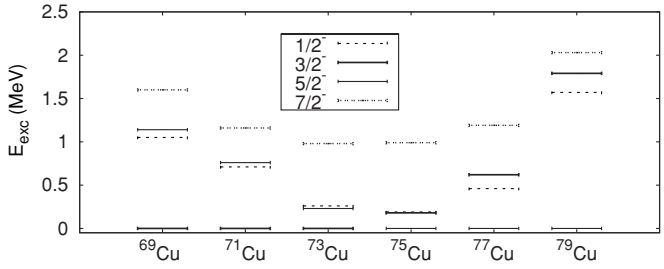

FIG. 2. Low-lying levels in copper isotopes resulting shell model calculations.

charge of 0.5 e the transition probability of 143 e^2 fm^4, in good agreement with the experimental value of 150(32) e^2 fm^4. The calculated correlated gaps amount to 5.7 and to 5.0 MeV in ^{68}Ni and ^{78}Ni, respectively. The corresponding reduction of the gaps in ESPE, observed in Fig. 1, is from 5.8 MeV in ^{68}Ni (the gap between $f_{7/2}$ and $p_{3/2}$ orbits) to 4.6 MeV (between $f_{7/2}$ and $f_{5/2}$ orbits) in ^{78}Ni. The reduction of the proton gap points to the necessity of taking into account the proton core excitations when approaching the neutron shell closure. One should notice, however, our prediction of a larger gap as compared to that of Ref. [15], where the value of 3.5 MeV has been deduced from the systematics. The rigidity of the gaps in ^{78}Ni is an important issue for the astrophysics because this nucleus is one of the waiting points in the r-process. Future experiments, especially mass measurements, will hopefully allow for precise verification of the size of the gaps in ^{78}Ni.

The resemblance of the proton ESPE in Fig. 1 to the ones calculated in Ref. [2] using a schematic tensor force is conspicuous, indirectly giving evidence for the role of the first-order tensor effects in the monopole drift, as noticed in Refs. [2,16]. In addition to the reduction of the gap between spin-orbit partners $f_{7/2}$ and $f_{5/2}$, a second important feature is observed in the proton ESPE, that is, the rapidly descending $f_{5/2}$ orbital that crosses the $p_{3/2}$ orbital in the middle of the shell. This single-particle level crossing should manifest itself in the low spin structure of copper isotopes, which have only one proton above the $f_{7/2}$ proton orbital. As mentioned, a sharp decrease in the energy of the first excited $5/2^-$ level between $N = 40$ and $N = 50$ was considered as an indication for monopole migration [8,17] and recent measurements established that $5/2^-$ becomes the ground state in ^{75}Cu [7]. The SM calculations presented in the same work, performed assuming a ^{56}Ni core, revealed a considerable deficiency in reproducing both the collectivity of the $1/2^-$ state and the systematics of the magnetic moments. We show in the following that this ill behavior is the effect of the truncation of the valence space, which eliminates the important proton degrees of freedom.

The low-lying level systematics in coppers is shown in Fig. 2. Our SM calculations reproduce correctly the change of the ground state in ^{75}Cu and, moreover, the pronounced lowering of the $1/2^-$ level that we obtain at the same excitation energy as the $3/2^-$ level. One should note that the ordering of these two levels has not been uniquely established in the experiment so far [6]. The collective nature of the $1/2^-$ level can be deduced from experimental $B(E2; 1/2^- \rightarrow 3/2^-)$ transition rates, which reach around 20 W.u. in ^{71,73}Cu compared with $B(E2; 5/2^- \rightarrow 3/2^-)$ transition rates of about 4 W.u. in the same nuclei. The electromagnetic transition rates calculated in our model have been recently published in another work [6] and appear to agree fairly with the known experimental values, which together with the results for magnetic moments presented later in this article confirm the realistic character of the calculated wave functions.

In Fig. 3 the proton occupations of the single-particle orbitals in the lowest calculated states are depicted. In the case of the $7/2^-$ state, the number of holes in the $f_{7/2}$ orbit is reported. It is apparent from the figure that the nature of the low-lying states evolves a lot with the filling of the neutron $g_{9/2}$ orbital.

It is also worth noticing that the excitations through the neutron gap are unblocked at $N = 40$. In the calculations of Ref. [12] it was pointed out that the $N = 40$ harmonic oscillator shell is not a rigid shell closure and that ^{68}Ni has a mixed character of a superfluid and closed-shell nucleus in its ground state, with an extra occupancy of the $\nu g_{9/2}$ orbital of 1.19. This additional occupancy is then lowered in heavier nickels due to the Pauli blocking and the same behavior is observed here in copper isotopes for which the extra occupancies of the $g_{9/2}$ orbital are listed in Table I.

One can now see from Fig. 3 and Table I that at the neutron shell closure $N = 40$ the occupancy of the $p_{3/2}$ orbital is close to 1.0 and the extra occupancy of the neutron $g_{9/2}$ orbit is 0.84: this information confirms the single-particle character of the $3/2^-$ level, which has the $\pi p^1_{3/2} \otimes \nu 0^+$ structure. This is no longer the case for $1/2^-$ and $5/2^-$ states whose neutron occupancies resemble those of the 2^+ state in ^{68}Ni [12], and the occupancies of the proton single-particle orbitals ($p_{1/2}$ in $1/2^-$ and $f_{5/2}$ in $5/2^-$) are much lower. The $3/2^-$

TABLE I. The extra occupancy of the neutron $g_{9/2}$ orbital in the low-lying states in neutron-rich copper isotopes.

A	$1/2^-$	$3/2^-$	$5/2^-$	$7/2^-$
69	2.15	0.87	2.27	2.21
71	0.98	0.60	1.11	0.44
73	0.42	0.37	0.52	0.21
75	0.18	0.17	0.23	0.09
77	0.05	0.05	0.12	0.02
79	0.0	0.0	0.0	0.0

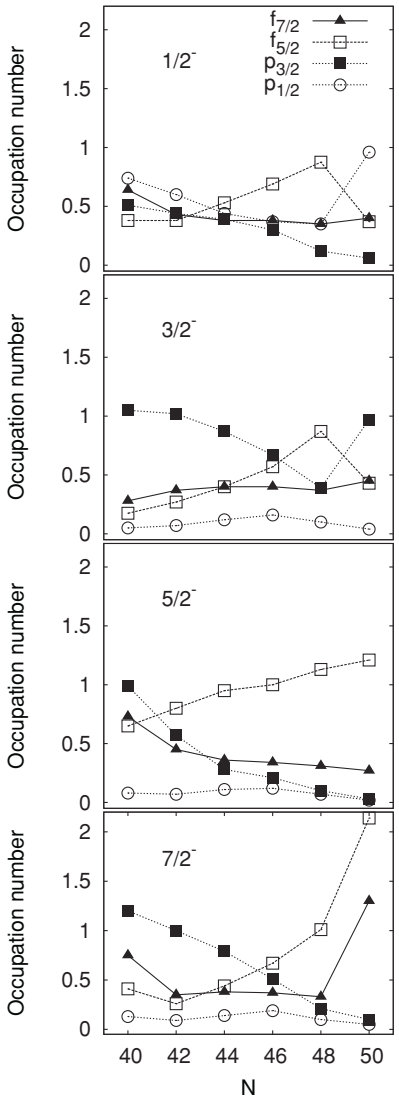

FIG. 3. Occupation of proton single-particle levels in the lowest calculated levels along the copper chain. In the case of the $f_{7/2}$ orbital the number of holes is plotted.

state loses, however, its single-particle character very quickly with the filling of the $g_{9/2}$ shell. Similarly, the $1/2^-$ level gains in collectivity with increasing neutron number, and the occupation of the $p_{1/2}$ drops twice when the middle of the shell is reached, to be enhanced again closer to the $N = 50$ closure. One observes that the sudden lowering of the $7/2^-$ state between ^{69}Cu and ^{71}Cu is also due to its change of the proton structure from ∼70% of a single-hole structure to a more collective one. Interestingly, the behavior of the hole number in the $f_{7/2}$ orbital in the $7/2^-$ level resembles the parabolic trend of the $p_{1/2}$ particles in the $1/2^-$ state. Finally, one observes that the occupation of the $f_{5/2}$ orbital in the lowest $5/2^-$ increases linearly when the neutron shell is filled. This behavior reflects clearly the crossing of the single-particle levels caused by the difference in the strength of the $V_{g_{9/2}\text{-}p_{3/2}}$ and $V_{g_{9/2}\text{-}f_{5/2}}$ proton-neutron interactions.

Finally, let us show the impact of the core excitations on the description of magnetic moments. In Fig. 4, the experimental

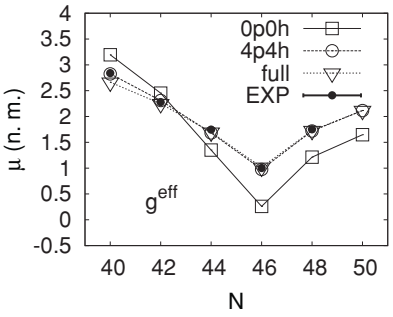

FIG. 4. Experimental (solid symbols) and theoretical (open symbols) magnetic moments of neutron-rich copper isotopes ($Z = 29$). SM calculations are shown without (0p0h) and with configuration mixing at the 4p4h level and in a full space calculation.

data from Refs. [7,18] are plotted in comparison to calculated values. Three theoretical curves are shown: without configuration mixing (0p0h), allowing for four particle-four holes excitations (4p4h), and a full space diagonalization calculation (or 8p8h in the case of ^{69}Cu). A standard effective $M1$ operator is used in the calculation with the quenching factor 0.75 of the spin g factors and orbital g factors equal to 1.1 for protons and −0.1 for neutrons [19–21].

One can see that the magnetic moments are converged basically at the 4p4h level and that the agreement with experiment is excellent when particle-hole excitations are allowed, contrary to the 0p0h case. It could come as a surprise that the improvement in our model is maximal in the middle of the shell, where the proton $f_{5/2}$, $p_{3/2}$ single-particle orbitals cross and a $5/2^-$ level becomes the single-particle-like ground state. Nonetheless, one should bare in mind that in our model the attractive $f_{5/2}$-$g_{9/2}$ monopole interaction tends to purify the single-particle nature of the $5/2^-$ state and the occupancy of the $f_{5/2}$ shell increases when correlations are taken into account.

One should also stress that the calculations with the ^{56}Ni core [7] reproduce experimental values only in ^{69}Cu and ^{75}Cu, where the ground states ($3/2^-$ and $5/2^-$, respectively) calculated in our model reveal the most clean, single-particle-type of structure. This observation proves the necessity of the proton core excitations that allow for mixing of proton configurations, apparently inevitable for a realistic composition of the calculated wave functions. Let us acknowledge, in passing, the very insightful role of the measurements of the magnetic moments for the understanding of the nuclear structure and testing in detail the calculated wave functions.

In Fig. 5 we distinguish also the proton and neutron contributions from the orbital and spin parts to the ground-state magnetic moments obtained in full SM calculations with effective g factors presented in Fig. 4. The most important message of this decomposition is that the magnetic moments are clearly dominated by the proton components. The magnetic moment of the $5/2^-$ state ($N = 46$–50) arises from a destructive superposition of a smaller negative proton spin part and a large proton orbital part. The magnetic moment of the $3/2^-$ state ($N = 40$–44) consists of positive, nearly equal proton spin and orbital components. The neutron spin and orbital

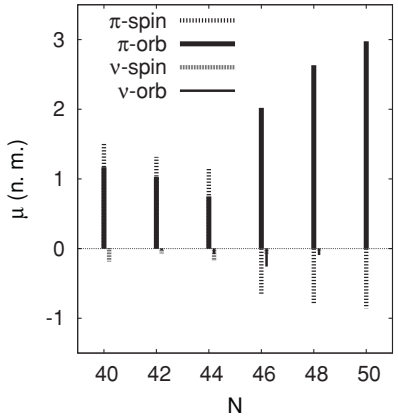

FIG. 5. Proton and neutron contributions from orbital and spin components to the magnetic moments of the ground states of copper isotopes.

components remain negative all along the chain but, as stated, their total contribution to the magnetic moment is negligible.

Finally, let us comment on the g factors used in the calculations. The need of effective g factors in the SM studies is well understood as ones performs calculations in a limited model space where an *effective* operator needs to act. While the effective Hamiltonians for the model spaces are derived nowadays in a perturbative scheme [22,23], the effective transition operators are introduced in a bare form with a renormalization factor, for the sake of simplicity. It has been shown in Refs. [19–21] that spin operators are to be quenched by a factor 0.75, as only ∼70% of the Gamow-Teller (GT) strength resides in the model space, while the other 30% rests outside [20]. The enhancement of the orbital g factors has been proven necessary to redistribute the orbital strength in sd, pf, and gds shells [24–26]. In Fig. 6 we show, however, the calculations with the bare g factors for an explanatory purpose: One sees that though the discrepancies between theory

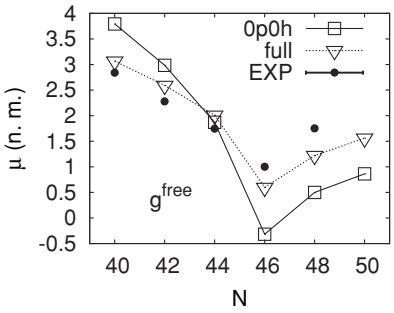

FIG. 6. Magnetic moments calculated with bare g factors. Full space diagonalization results (open triangles) are compared with the ones without configuration mixing (open squares) and available experimental data (solid circles).

and experiment are now larger (as expected) the correct systematics preserves and the agreement between experiment and theory improves the same way as in Fig. 4, once the particle-hole excitations are allowed. This result rules out any speculation whether the correct reproduction of the experimental systematics may be related to a specific choice of the gyromagnetic factors in the particular case of $^{69-77}$Cu.

In conclusion, we have presented SM calculations in an enlarged model space outside the ^{48}Ca core for the copper isotopic chain. A correct systematics of the low-lying levels and magnetic moments have been obtained for the first time in SM calculations. This appeared due to the inclusion of proton degrees of freedom omitted in previous SM calculations in limited valence spaces outside the ^{56}Ni core. We have also discussed the underlying proton shell evolution between ^{68}Ni and ^{78}Ni. The calculations have indicated that the $Z = 28$ shell closure gets reduced by about 0.7 MeV when filling the neutron $g_{9/2}$ orbital. This implies that the proton core excitations are an indispensable ingredient in understanding the structure of neutron-rich nuclei toward ^{78}Ni.

[1] B. Bastin *et al.*, Phys. Rev. Lett. **99**, 022503 (2007).
[2] T. Otsuka, T. Matsuo, and D. Abe, Phys. Rev. Lett. **97**, 162501 (2006).
[3] J. Leske *et al.*, Phys. Rev. C **71**, 034303 (2005).
[4] O. Perru *et al.*, Phys. Rev. Lett. **96**, 232501 (2006).
[5] I. Stefanescu *et al.*, Phys. Rev. Lett. **100**, 112502 (2008).
[6] J. Daugas *et al.*, Phys. Rev. C **81**, 034304 (2010).
[7] K. Flanagan *et al.*, Phys. Rev. Lett. **103**, 142501 (2009).
[8] S. Franchoo *et al.*, Phys. Rev. Lett. **81**, 3100 (1998).
[9] N. A. Smirnova, A. De Maesschalck, A. Van Dyck, and K. Heyde, Phys. Rev. C **69**, 044306 (2004).
[10] A. F. Lisetskiy, B. A. Brown, M. Horoi, and H. Grawe, Phys. Rev. C **70**, 044314 (2004).
[11] M. Honma, T. Otsuka, T. Mizusaki, and M. Hjorth-Jensen, Phys. Rev. C **80**, 064323 (2009).
[12] O. Sorlin *et al.*, Phys. Rev. Lett. **88**, 092501 (2002).
[13] E. Caurier and F. Nowacki, Acta Phys. Pol. B **30**, 705 (1999).
[14] J. Van de Walle *et al.*, Phys. Rev. C **79**, 014309 (2009).
[15] O. Sorlin and M.-G. Porquet, Prog. Part. Nucl. Phys. **61**, 602 (2008).
[16] N. Smirnova, B. Bally, K. Heyde, F. Nowacki, and K. Sieja, Phys. Lett. B **686**, 109 (2010).
[17] S. Franchoo *et al.*, Phys. Rev. C **64**, 054308 (2001).
[18] N. J. Stone *et al.*, Phys. Rev. C **77**, 014315 (2008).
[19] E. Caurier, G. Martinez-Pinedo, F. Nowacki, A. Poves, and A. P. Zuker, Rev. Mod. Phys. **77**, 427 (2005).
[20] E. Caurier, A. Poves, and A. P. Zuker, Phys. Rev. Lett. **74**, 1517 (1995).
[21] P. von Neumann-Cosel, A. Poves, J. Retamosa, and A. Richter, Phys. Lett. B **443**, 1 (1998).
[22] M. Hjorth-Jensen, T. T. S. Kuo, and E. Osnes, Phys. Rep. **261**, 125 (1995).
[23] M. Hjorth-Jensen, T. Kuo, and E. Osnes, Phys. Rep. **261**, 125 (1995).
[24] G. Jakob *et al.*, Phys. Rev. C **65**, 024316 (2002).
[25] B. A. Brown and B. H. Wildenthal, Annu. Rev. Nucl. Part. Sci. **38**, 29 (1988).
[26] E. Caurier, A. Poves, and A. Zuker, Phys. Lett. B **256**, 301 (1991).

PHYSICAL REVIEW C **85**, 051301(R) (2012)

Three-body forces and persistence of spin-orbit shell gaps in medium-mass nuclei: Toward the doubly magic ^{78}Ni

K. Sieja and F. Nowacki

Université de Strasbourg, IPHC, 23 rue du Loess 67037 Strasbourg, France and CNRS, UMR7178, 67037 Strasbourg, France

(Received 27 January 2012; published 7 May 2012)

We present state-of-the-art shell-model calculations in a large model space (pf for protons, $fpgd$ for neutrons), which allows us to study simultaneously excitations across the $Z = 28$ and $N = 50$ shell gaps. We explore the region in the vicinity of ^{78}Ni, which is a subject of intense experimental investigations. Our calculations correctly account for the known low-lying excited states in this region, including those which may correspond to cross-shell excitations. We observe the minimum of the $N = 50$ mass gap at $Z = 32$ consistent with experimental data and its further increase toward $Z = 28$, indicating a robustness of the $N = 50$ gap in ^{78}Ni. The evolution of the $N = 50$ gap along the nickel chain is shown to bear similarities to what is known in oxygen and calcium chains, providing a new opportunity for the studies of three-body monopole effects in medium-mass nuclei.

DOI: 10.1103/PhysRevC.85.051301 PACS number(s): 21.60.Cs, 21.30.−x, 21.45.Ff, 23.20.Lv

The search for the breaking of shell closures known at the stability valley when going toward the drip lines is one of the problems of contemporary nuclear structure studies. Recent decades have provided many cases of unexpected shell erosions, ^{42}Si being a famous example [1], and of appearances of deformed intruders in supposedly semimagic nuclei known as the phenomena of *islands of inversions* [2,3]. The issue of the occurrence of shell quenching in connection with astrophysical scenarios has been widely debated, in particular for $N = 50$ and $N = 82$ around the r-process waiting points [4–7].

Experimental progress allows for the study of more and more exotic systems, including the nuclear structure toward the still unknown, possibly doubly magic nucleus ^{78}Ni. The region around it is interesting for several reasons: very neutron rich nuclei play an important role in r-process nucleosynthesis, and ^{78}Ni is one of its possible waiting points [8–10]. From the nuclear structure point of view, ^{78}Ni, with the largest N/Z ratio in a doubly magic nucleus, represents a unique possibility of exploring the properties of very neutron-rich nuclei. The evolution of the $N = 50$ gap between ^{68}Ni and ^{78}Ni may be due to the repulsive character of the effective three-body force, in analogy to what has been found in oxygen and calcium chains [11,12]. Thus, constraining its size is of paramount importance for future developments and tests of state-of-the-art effective interactions with the inclusion of many-body forces, as well as for validation of empirical *universal monopole* interactions, such as those proposed in Refs. [13–15]. The knowledge of single-particle energies of ^{78}Ni is also crucial for shell-model studies which utilize this nucleus as a core [16–20] and which allow exploration of the properties of $A = 80$–90 neutron-rich nuclei, including those lying on the r-process path.

Though a lot of experimental evidence in this region has been accumulated, the data, or to be precise the conclusions drawn by different authors, seem contradictory. The possibility of the weakening of the $N = 50$ closure has been anticipated, e.g., in Refs. [21–23], while the contrary has been deduced by other authors, e.g., in Refs. [24–26]. One should notice, however, that experimentally it is still not possible to reach ^{78}Ni itself and since the shell effects manifest themselves suddenly at the shell closures, while being hindered by correlations in semimagic nuclei, it is not possible to conclude firmly on the rigidity of ^{78}Ni based on the currently available data alone. To shed light on the physics of this nucleus one needs a theory capable of reproducing the spectroscopic details of the region and robust enough to extrapolate to the yet unknown regions. As crucial information about the underlying shell evolution can be extracted from the structure of odd nuclei, the large-scale shell model, currently the only nuclear theory model treating on the same footing even and odd systems, is a tool of choice to explore the shell evolution in the vicinity of ^{78}Ni.

Recently, we have addressed the problem of the possible quenching of the $Z = 28$ gap in the shell-model framework, using a large valence space containing pf orbitals for protons and $pf_{5/2}g_{9/2}$ orbitals for neutrons [27]. In this Rapid Communication we present calculations that are performed in an even larger model space, which contains pf-shell orbitals for protons and $f_{5/2}$, p, $g_{9/2}$, $d_{5/2}$ orbitals for neutrons, allowing thus for simultaneous excitations across $Z = 28$ and $N = 50$ gaps. The detailed spectroscopy of $N = 49$–50 nuclei and the evolution of the neutron $N = 50$ gap with the proton number between ^{78}Ni and ^{86}Kr and with the neutron number between ^{68}Ni and ^{78}Ni is discussed.

The effective interaction used in this work is based on realistic G matrices with a number of experimental constraints taken into account to improve the properties of the monopole part of the Hamiltonian, as commonly practiced in the shell model [28]. A detailed description of this effective interaction can be found in Ref. [3]. In this work, however, we have introduced additional monopole adjustments with respect to Ref. [3], in order to constrain the proton gap evolution from ^{68}Ni to ^{78}Ni [27]. To probe reliability of such an interaction, we investigate the low-lying states of even-even $N = 50$ nuclei between ^{78}Ni and ^{84}Se, as well as even-odd $N = 49$ isotones between ^{79}Zn and ^{85}Kr, which correspond to cross-shell excitations. We discuss also the evolution of neutron shells along the nickel chain and provide predictions for the structure of ^{78}Ni. The calculations are performed using the m-scheme code ANTOINE [28,29].

TABLE I. Experimental vs theoretical excitations energies and calculated occupation numbers in the wave functions of low-lying excited states in ^{82}Ge. Given in bold are the neutron occupancies in the states corresponding to the 1p-1h excitations across the $N = 50$ shell gap.

Expt.		Theor.		Protons			Neutrons	
J^π	E (MeV)	J^π	E (MeV)	$f_{7/2}$	$f_{5/2}$	p	$g_{9/2}$	$d_{5/2}$
0^+	0.0	0^+	0.0	7.64	3.74	0.41	9.65	0.37
2^+	1.35	2^+	1.40	7.77	3.73	0.33	9.60	0.42
4^+	2.28	4^+	2.21	7.84	3.79	0.23	9.6	0.36
$(5^+, 6^+)$	2.93	5^+_1	3.17	7.59	3.61	0.50	**8.53**	**1.48**
(6^+)	3.23	6^+_1	3.37	7.59	3.62	0.49	**8.57**	**1.44**
		5^+_2	4.22	7.79	3.01	0.81	9.52	0.49
		6^+_2	4.32	7.82	3.04	1.02	9.64	0.37

Let us start the discussion with a reminder of the current status of experimental knowledge on the structure of $N = 49$ and $N = 50$ isotones. In the low-lying spectra of $N = 49$ nuclei one observes the low-lying negative parity states corresponding to the holes in the $p_{1/2}$ orbital, as well as positive parity states, among which the lowest excited $5/2^+$ may correspond to a 1p-1h excitation across the $N = 50$ gap, and can be thus addressed in our model space which encompasses the $d_{5/2}$ neutron orbital. The systematics of $5/2^+$ states in $N = 49$ isotones is known up to ^{81}Ge (four protons away from ^{79}Ni) but experimental data should be soon available as far as ^{79}Zn (two protons away from ^{79}Ni) [30]. The states corresponding to the excitations across the $N = 50$ gap serve as a perfect test for its size in our interaction in the vicinity of ^{78}Ni. In the spectra of even-even nuclei, 1p-1h excitation can form the first excited $5^+, 6^+$ states. They are known experimentally up to ^{82}Ge and the relatively low excitation energy of these states at $Z = 32$ has lead the authors of Ref. [22] to anticipate the possible weakening of the $N = 50$ closure. We start thus the presentation of our results with the example of ^{82}Ge. In Table I we show the spectra calculated in our approach compared to experimental data for the case of ^{82}Ge and the wave functions of the calculated levels. The known energy levels $2^+, 4^+$ are reproduced with great accuracy, and theoretical counterparts for the experimental candidates of $5^+, 6^+$ spins are located within 200 keV. The first excited $2^+, 4^+$ states are clearly of a proton nature. In contrast, it is seen that the lowest calculated $5^+, 6^+$ levels correspond indeed to the 1p-1h excitations to the $\nu d_{5/2}$ orbital, as proposed in Ref. [22]. The second calculated $5^+, 6^+$ states, located at around 4 MeV, are again of proton nature, having nearly the same occupations of the neutron $g_{9/2}, d_{5/2}$ orbitals as the ground state.

In Fig. 1 we present the systematics of lowest excited $5^+, 6^+$ states from $Z = 28$ to $Z = 36$ compared to the known experimental data, which probes the evolution of the gap when moving away from $Z = 32$. Our calculations match well the decreasing trend observed from Kr to Ge, but the increase of the excitation energy is predicted toward Ni. In addition, we present in the same figure the systematics of the calculated and experimentally known $5/2^+$ states in $N = 49$ isotones. These states are correctly reproduced and, similarly to the case of even-even nuclei, the increase of the $5/2^+$ is observed toward Ni. In both systematics a minimum appears around $Z = 32$. Such a minimum however does not reflect any changes in the spherical mean-field in these nuclei. This is illustrated in Figs. 1(b) and 2. The former shows the correlated gap, i.e., the gap obtained from binding energies

$$\Delta = BE(Z, N+1) + BE(Z, N-1) - 2BE(Z, N). \quad (1)$$

The latter is the shell-model prediction for the evolution of the effective single-particle energies (ESPE). The ESPE are obtained as the differences of energies of closed shell and closed shell ± 1 particle configurations which, by definition, contain no correlations [28]. Thus the splitting of the ESPE defines the uncorrelated shell gap and allows us to separate the spherical mean-field from correlation effects contained in Δ. One should also add that the ESPE represent schematically the evolution of the monopole field in nuclei, which is not an observable itself. In particular, it assumes a given filling ordering scheme, which in reality is broken by the residual interaction, but for many years the monopole Hamiltonian has been used successfully to investigate and visualize the shell evolution in nuclei.

It is seen in Fig. 2 that there is no clear variation of the ESPE between ^{78}Ni and ^{86}Kr. At the same time, the gap calculated from shell-model masses varies from 4.7 MeV in ^{78}Ni to only 3.6 MeV in ^{82}Ge and then increases again toward ^{86}Kr as shown in Fig. 1(b). This indicates that the

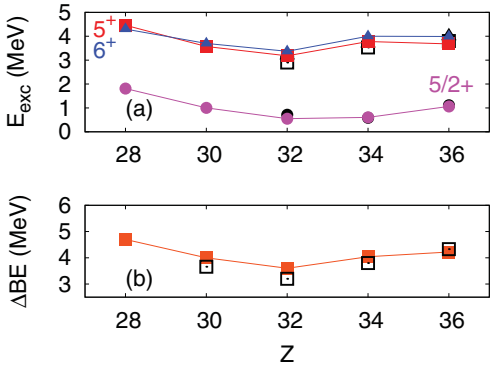

FIG. 1. (Color online) Systematics of the low-lying 1p-1h states in $N = 50$ and $N = 49$ isotones (a) and the evolution of the $N = 50$ gap calculated from masses (b). Color symbols stand for shell-model (SM) results; black (open) symbols represent the experimental data from Refs. [7,31,32].

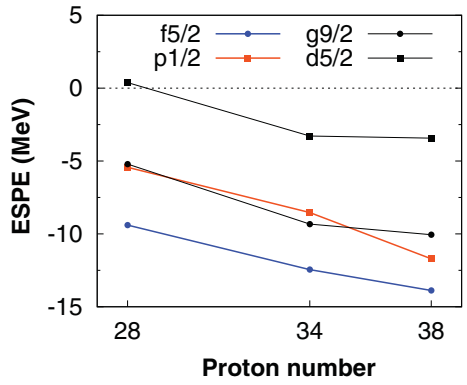

FIG. 2. (Color online) Evolution of the neutron effective single-particle energies with the proton number at $N = 50$.

correlation effects lead to a minimum in the mass gap at $Z = 32$, which explains the observed pattern of the excited states; but at the same time no indication for the weakening of the spherical gap toward ^{78}Ni is found. One should note that the majority of other microscopic models used in nuclear structure calculations fail to reproduce the $N = 50$ gap size and trend in the experimentally known region, and deviate substantially in their predictions toward ^{78}Ni (See Fig. 4 of Ref. [32]).

One of the key issues in nuclear structure is knowledge of the shell closure formation in nuclei. For a long time, it was not understood why nucleon-nucleon (NN) realistic interactions fail to reproduce spin-orbit shell closures, such as those in ^{48}Ca and ^{56}Ni. A deeper insight came when the importance of the monopole field was emphasized in the mechanism of shell drift [33] and later, when the connection with missing three-nucleon monopole forces in nuclear structure calculations was suggested [34]. The evolution of such gaps can be placed in a general context of fundamental problems of nuclear structure: when the largest orbit in a major shell fills, it binds itself and contributes to the binding of the largest orbits in neighboring shells in a way that NN forces fail to reproduce. As the largest orbit in the oscillator shell n is the one that is expelled to become an intruder in an orbit $n - 1$, it follows that the pure two-body forces are unable to produce the spin-orbit shell closures at $N, Z = 14, 28, 50, 82$, and 126. Only recently the first attempts of shell-model (SM) calculations with effective three-body forces based on the chiral next-to-next-to-leading order potential became available [11,12], for the time being exclusively in the $T = 1$ channel. These calculations suggest that at least some of the missing repulsion between $d_{5/2}$ and $s_{1/2}$ orbitals in oxygen and between $f_{7/2}$ and $p_{3/2}$ orbitals in calcium can be gained by including the three-body contribution of two valence and one core particles in the two-body matrix elements. If the three-body effects can explain the spin-orbit shell closures observed experimentally in $Z = 8$ isotopes ($n = 1$ harmonic oscillator shell closure) and $Z = 20$ isotopes ($n = 2$), one could search for similar effects at $Z = 40$ ($n = 3$) around ^{80}Zr. However, the proton shell closure appears as well at $Z = 28$, making the next place in the Segrè chart available for such studies already between ^{68}Ni and ^{78}Ni, where the neutron $N = 50$ shell closure may appear due to the filling of the $g_{9/2}$ orbital.

We would like to discuss now the $g_{9/2}$-$d_{5/2}$ splitting along the nickel chain. In Fig. 3 we show the evolution of neutron effective single- particle energies in the region considered in this work, in comparison to analogous ESPE in sd and fp shells obtained with empirical interactions: USDb [35] and LNPS [3]. In addition, the ESPE obtained with V_{lowk} effective interactions with 2.0 fm^{-2} cutoff based on charge-dependent Bonn potentials [36] are plotted for each case. For transparency, only the first two orbits in a harmonic oscillator shell are plotted, and we arbitrarily normalized the starting energy of the large shell to zero. Apparently, with empirical interactions a shell gap is created when filling the large orbit, leading to 14, 28, and 50 closures in the subsequent shells. The behavior given by the realistic force is incompatible with empirical ESPE, and, in particular, there is nearly no variation of the gap with the filling of the large orbital. Additionally, the V_{lowk} forces predict degeneracy (sd, pf) or even inversion (gd) of the $f_{7/2}$-$p_{3/2}$, $d_{5/2}$-$s_{1/2}$, and $g_{9/2}$-$d_{5/2}$ orbitals, inconsistent with their experimental ordering at $N = 8$, 20, and 40 [37]. As has been shown in Refs. [11,12], the inclusion of the effective three-body forces in sd and fp shells can separate the single-particle levels and provide at least a part of the repulsion necessary to pull apart the orbitals with the filling of the large shell. Thus the nickel chain offers another possibility for state-of-the-art derivations of the three-body monopole interactions, the present work providing a precious benchmark for such studies. It has to be noted that this qualitatively analogous behavior of the $N = 50$ gap has not been imposed in our model but results solely

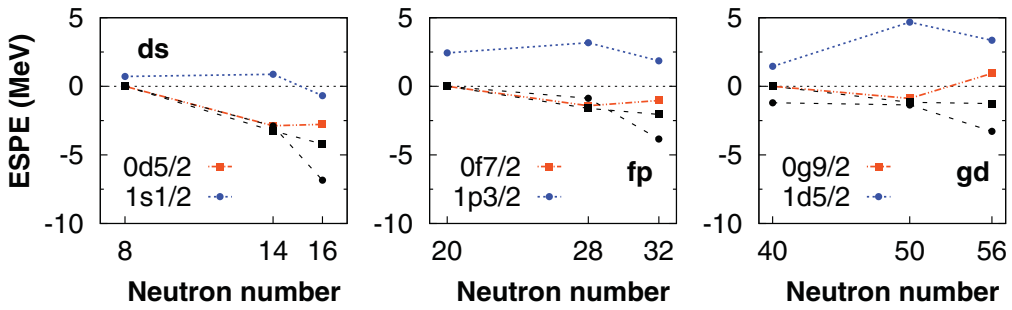

FIG. 3. (Color online) Evolution of the neutron effective single-particle energies with neutron filling in sd, fp, and gd shells. Only orbitals of interest are plotted between which the spin-orbit gap is created. Color lines correspond to empirical interactions and black lines to realistic V_{lowk} interactions; see text for more details.

from the spectroscopic description of the island of inversion around ^{64}Cr studied in Ref. [3] and of $N = 49$–50 isotones.

Finally, let us comment on the structure of ^{78}Ni itself, resulting from the shell-model calculations. Its ground state is calculated to have 79% of the closed shell configuration, the largest value in the whole nickel chain (around 60% of closed shell is found in pf calculations in ^{56}Ni with various interactions and only 50% in ^{68}Ni, here or in previous SM studies [3,38]). The first 2^+ state in ^{78}Ni is predicted at nearly 4 MeV, a value analogous to the 2^+ state of its "big sister" ^{132}Sn. This first excited state is of a neutron nature, having 1.35 particle in the $d_{5/2}$ orbital (0.16 particle in the 0^+ state). The gaps estimated from calculated mass differences in ^{78}Ni are 4.7 MeV for neutrons and 5.0 MeV for protons. These prediction appears much more robust than recent extrapolations from two-neutron separation energies of ground and isomeric states [39].

In summary, we have performed large-scale shell-model calculations in the $\pi(fp)$-$\nu(fpgd)$ model space in the vicinity of ^{78}Ni. We have studied the evolution of the $N = 50$ shell gap due to the proton-neutron interaction between ^{86}Kr and ^{78}Ni. The calculations point to a minimum of the mass gap in ^{82}Ge consistent with data and its increase toward ^{78}Ni. We predict the location of the first excited $5/2^+$ in ^{79}Ni at nearly 2 MeV and a high-lying 2^+ (4 MeV) in ^{78}Ni. We thus conclude on the robustness of both $Z = 28$ and $N = 50$ gaps in ^{78}Ni. The evolution of the $N = 50$ gap due to the $T = 1$ interaction is shown to be analogous to what has been attributed to the action of the effective three-body forces in oxygen and calcium chains, providing a new opportunity for exploring further the three-body effects in medium-mass nuclei. The developments of this work open a possibility of microscopic evaluations of (n, γ) cross sections around $A = 80$, where due to the low level density statistical approaches cannot be employed.

[1] B. Bastin *et al.*, Phys. Rev. Lett. **99**, 022503 (2007).
[2] Y. Utsuno, T. Otsuka, T. Mizusaki, and M. Honma, Phys. Rev. C **60**, 054315 (1999).
[3] S. M. Lenzi, F. Nowacki, A. Poves, and K. Sieja, Phys. Rev. C **82**, 054301 (2010).
[4] I. Dillmann *et al.* (ISOLDE Collaboration), Phys. Rev. Lett. **91**, 162503 (2003).
[5] A. Jungclaus *et al.*, Phys. Rev. Lett. **99**, 132501 (2007).
[6] L. Cáceres *et al.*, Phys. Rev. C **79**, 011301(R) (2009).
[7] S. Baruah *et al.*, Phys. Rev. Lett. **101**, 262501 (2008).
[8] M. Terasawa, K. Sumiyoshi, T. Kajino, G. J. Mathews, and I. Tanihata, Astrophys. J. **562**, 470 (2001).
[9] S. Wanajo *et al.*, Astrophys. J. **593**, 968 (2003).
[10] P. T. Hosmer *et al.*, Phys. Rev. Lett. **94**, 112501 (2005).
[11] T. Otsuka, T. Suzuki, J. D. Holt, A. Schwenk, and Y. Akaishi, Phys. Rev. Lett. **105**, 032501 (2010).
[12] J. D. Holt, T. Otsuka, A. Schwenk, and T. Suzuki, e-print arXiv:1009.5984.
[13] J. Duflo and A. P. Zuker, Phys. Rev. C **59**, R2347R (1999).
[14] T. Otsuka, T. Matsuo, and D. Abe, Phys. Rev. Lett. **97**, 162501 (2006).
[15] T. Otsuka, T. Suzuki, M. Honma, Y. Utsuno, N. Tsunoda, K. Tsukiyama, and M. Hjorth-Jensen, Phys. Rev. Lett. **104**, 012501 (2010).
[16] K. Sieja, F. Nowacki, K. Langanke, and G. Martinez-Pinedo, Phys. Rev. C **79**, 064310 (2009).
[17] G. S. Simpson, W. Urban, K. Sieja, J. A. Dare, J. Jolie, A. Linneman, R. Orlandi, A. Scherillo, A. G. Smith, T. Soldner *et al.*, Phys. Rev. C **82**, 024302 (2010).
[18] W. Urban, K. Sieja, G. S. Simpson, T. Soldner, T. Rzaca-Urban, A. Złomaniec, I. Tsekhanovich, J. A. Dare, A. G. Smith, J. L. Durell *et al.*, Phys. Rev. C **85**, 014329 (2012).
[19] W. Urban, K. Sieja, G. S. Simpson, H. Faust, T. Rzaca-Urban, A. Złomaniec, M. Łukasiewicz, A. G. Smith, J. L. Durell, J. F. Smith *et al.*, Phys. Rev. C **79**, 044304 (2009).
[20] T. Rzaca-Urban, K. Sieja, W. Urban, F. Nowacki, J. L. Durell, A. G. Smith, and I. Ahmad, Phys. Rev. C **79**, 024319 (2009).
[21] J. Krumlinde and P. Moeller, Nucl. Phys. A **417**, 419 (1984).
[22] T. Rzaca-Urban, W. Urban, J. L. Durell, A. G. Smith, and I. Ahmad, Phys. Rev. C **76**, 027302 (2007).
[23] J. A. Winger *et al.*, Phys. Rev. C **81**, 044303 (2010).
[24] D. Verney *et al.* (PARRNe Collaboration), Phys. Rev. C **76**, 054312 (2007).
[25] G. de Angelis, Nucl. Phys. A **787**, 74 (2007).
[26] J. Van de Walle *et al.* , Phys. Rev. C **79**, 014309 (2009).
[27] K. Sieja and F. Nowacki, Phys. Rev. C **81**, 061303 (2010).
[28] E. Caurier, G. Martinez-Pinedo, F. Nowacki, A. Poves, and A. P. Zuker, Rev. Mod. Phys. **77**, 427 (2005).
[29] E. Caurier and F. Nowacki, Acta Phys. Pol. B **30**, 705 (1999).
[30] R. Orlandi, presented in the conference on Advances in Radioactive Isotope Science 2011.
[31] G. Audi, A. Wapstra, and C. Thibault, Nucl. Phys. A **729**, 129 (2003).
[32] J. Hakala *et al.*, Phys. Rev. Lett. **101**, 052502 (2008).
[33] A. Poves and A. Zuker, Phys. Rep. **70**, 235 (1981).
[34] A. P. Zuker, Phys. Rev. Lett. **90**, 042502 (2003).
[35] B. A. Brown and W. A. Richter, Phys. Rev. C **74**, 034315 (2006).
[36] R. Machleidt, Phys. Rev. C **63**, 024001 (2001).
[37] A. Schwenk and A. P. Zuker, Phys. Rev. C **74**, 061302 (2006).
[38] O. Sorlin *et al.*, Phys. Rev. Lett. **88**, 092501 (2002).
[39] M.-G. Porquet and O. Sorlin, Phys. Rev. C **85**, 014307 (2012).

Chapter 8

Publication list

8.1 Publications

- Theoretical articles

1. **K. Sieja**, *Low energy enhancement of dipole radiation in medium mass nuclei*, in preparation.
2. **K. Sieja**, T.R. Rodriguez, K. Kolos, D. Verney, *Laboratory versus intrinsic description of non-axial nuclei above* ^{78}Ni, Phys. Rev. C88 (2013) 034327.
3. Q. Zhi, E. Caurier, J.J. Cuenca-Garcia, K. Langanke, G. Martinez-Pinedo and **K. Sieja**, *Shell model half-lives of r-process waiting point nuclei including first-forbidden contributions*, Phys.Rev. C87 (2013) 025803.
4. N. Smirnova, B. Bally, K. Heyde, F. Nowacki and **K. Sieja**, *Nuclear shell evolution and in-medium NN interaction*, Phys. Rev. C86 (2012) 034314.
5. **K. Sieja** and F. Nowacki, *Three body forces and persistence of spin-orbit shell gaps: towards the doubly-magic* ^{78}Ni, Phys. Rev. C85 (2012) 051301R.
6. H. P. Loens, K. Langanke, G. Martinez-Pinedo and **K. Sieja**, *M1 strength functions from large scale shell model calculations and their impact on astrophysical neutron capture cross sections*, Eur. Phys. Jour. A48 (2012) 34.
7. **K. Sieja** and F. Nowacki, *Core polarization effects and effective interactions far from stability*, Nucl. Phys. A857 (2011) 9-15.
8. Q. Zhi, K. Langanke, G. Martinez-Pinedo, F. Nowacki and **K. Sieja**, *Importance of Gamow-Teller strength on* ^{76}Se *for stellar electron capture rates*, Nucl. Phys. A859 (2011) 172-184.
9. E. Caurier, F. Nowacki, A. Poves and **K. Sieja**, *Collectivity in light xenon isotopes: a shell model study*, Phys. Rev. C82 (2010) 064304.
10. S. Lenzi, F. Nowacki, A. Poves and **K. Sieja**, *Island of inversion around* ^{64}Cr, Phys. Rev. C82 (2010) 054301. **Featured in Physics.**

11. **K. Sieja** and F. Nowacki, *Shell quenching in ^{78}Ni: a hint from structure of neutron rich copper isotopes*, Phys. Rev. C81 (2010) 061303R.
12. N.A. Smirnova, B. Bally, K. Heyde, F. Nowacki and **K. Sieja**, *Disentangling different terms of the nuclear interaction in shell evolution*, Phys. Lett. B686 (2010) 109-113.
13. **K. Sieja**, G. Martínez-Pinedo, L. Coquard and N. Pietralla, *Shell model description of the proton-neutron mixed-symmetry states in the ^{132}Sn region*, Phys. Rev. C80 (2009) 054311.
14. **K. Sieja**, F. Nowacki, G. Martínez-Pinedo and K. Langanke, *Shell model description of zirconium isotopes*, Phys. Rev. C79, (2009) 064310; Erratum Phys. Rev. C79 (2009) 064310.
15. L. Bonneau, P. Quentin and **K. Sieja**, *Properties of N=Z deformed nuclei in HF+BCS and HTDA methods* Phys. Rev. C76, 014304 (2007).
16. A. Baran, Z. Lojewski, **K. Sieja** and M. Kowal, *Global properties of even-even superheavy elements in macroscopic-microscopic models*, Phys. Rev. C72, 004310 (2005) 1–13.
17. **K. Sieja** and A. Baran, *State dependent delta-pairing force with Nilsson models: nuclear shapes, radii, masses*, Phys. Rev. C68, 044308 (2003) 1–12.
18. **K. Sieja**, A. Baran and K. Pomorski, *Delta-pairing forces and collective pairing vibrations*, EPJ A20, (2004) 413–418.

- Experimental articles

1. W. Urban, **K. Sieja** et al., *Low spin structure of ^{86}Br and ^{86}Kr nuclei. The role of the $g_{7/2}$ orbital*, Phys. Rev. C94 (2016) 044328.
2. W. Urban, **K. Sieja** et al., *First evidence of γ collectivity close to the doubly magic core ^{132}Sn*, Phys. Rev. C93 (2016) 035805.
3. M. Czerwinski, T. Rzaca-Urban, W. Urban, P. Baczyk, **K. Sieja** et al., *Neutron-proton multiplets in the nucleus ^{90}Rb*, Phys. Rev. C93 (2016) 034318.
4. Z. Meisel,...,**K. Sieja**, et al., *Time-of-flight measurements of neutron-rich chromium isotopes up to N=40 and implications for the accreted neutron star crust*, Phys. Rev. C93 (2016) 035805.
5. P.-A. Sörderstorm, S. Nishimura, Z.Y. Xu, **K. Sieja** et al., *Two-hole structure outside ^{78}Ni: Existence of μs isomer in ^{76}Co and β decay into ^{76}Ni*, Phys. Rev. C92 (2015) 051305R.
6. P. Morfouace, S. Franchoo, **K. Sieja** et al., *Single-particle strength in neutron rich ^{69}Cu from the (d, ^{3}He) proton pick-up reaction*, Phys. Rev. C93 (2016) 064308.
7. P. Morfouace, S. Franchoo, **K. Sieja** et al., *Evolution of single-particle strength in ^{71}Cu*, Phys. Lett. B751 (2015) 306.

8. J. Litzinger, A. Blazhev, A. Dewald, F. Didierjean, G. Duchene, C. Fransen, R. Lozeva, **K. Sieja**, et al., *Transition probabilities in neutron-rich* $^{84,86}Se$, Phys. Rev. C92 (2015) 064322.

9. T. Materna, W. Urban, **K. Sieja** et al., *Low spin structure of* ^{86}Se*: confirmation of* γ*-collectivity at N=52*, Phys. Rev. C92 (2015) 034305.

10. M. Czerwinski, T. Rzaca-Urban, W. Urban, P. Baczyk, **K. Sieja** et al., *Neutron-proton multiplets in the nucleus* ^{88}Br, Phys. Rev. C92 (2015) 014328.

11. E. Sahin, M. Doncel, **K. Sieja** et al., *Shell evolution beyond N=40:* $^{69,71,73}Cu$, Phys. Rev. C91 (2015) 034302.

12. R. Orlandi, ..., **K. Sieja** et al., *Single-neutron orbits near 78Ni: Spectroscopy of the N=49 isotope 79Zn*, Phys. Lett. B740 (2015) 298-302.

13. G. Simpson, G. Gey, A. Jungclaus, J. Taprogge, S. Nishimura, **K. Sieja** et al., *Yrast 6+ Seniority Isomers of 136-138Sn*, Phys. Rev. Lett. 113 (2014) 132502.

14. J. Diriken, ..., **K. Sieja** et al., *Study of the deformation-driving* $\nu d_{5/2}$ *orbital in* ^{67}Ni *using one-neutron transfer reactions*, Phys. Lett. B 736 (2014) 533.

15. M. L. Bissel, J. Papuga, H. Naidja, K. Kreim, K. Blaum, M. de Rydt, R.F. Garcia-Ruiz, H. Heylen, M. Kowalska, R. Neugart, G. Neyens, F. Nowacki, M.M. Rajabali, R. Sanczez, **K. Sieja**, D.T. Yordanov, *Proton-Neutron Pairing Correlations in the Self-Conjugate Nucleus* ^{38}K *Probed via a direct Measurement of the Isomer Shift*, Phys. Rev. Lett. 113 (2014) 052502.

16. G.J. Kumbartzki, ..., **K. Sieja**, et al., *Transition from collectivity to single-particle degrees of freedom from magnetic moment measurements on* ^{82}Sr *and* ^{90}Sr, Phys. Rev. C89 (2014) 064305. **Editor's suggestion**.

17. A. Gade, ..., **K. Sieja** et al., *Nuclear structure towards N=40* ^{60}Ca*: In-beam gamma-ray spectroscopy of 58-60Ti*, Phys. Rev. Lett. 112 (2014) 112503.

18. A. Korgul, K.P. Rykaczewski, R. Grzywacz, H. Sliwinska, ..., **K. Sieja** et al., *Experimental study of the beta-gamma and beta-n-gamma decay of neutron-rich nucleus 85Ga*, Phys. Rev. C88 (2013) 044330.

19. V. Modamio, ..., **K. Sieja**, et al., *Lifetime measurements in neutron-rich* $^{63,65}Co$ *isotopes using AGATA demonstrator*, Phys. Rev. C88 (2013) 044326.

20. M. Czerwinski, T. Rzaca-Urban, **K. Sieja** et al., *Yrast excitations in the neutron-rich N=52 isotones*, Phys. Rev. C88 (2013) 044314.

21. K. Kolos, D. Verney, F. Ibrahim, F. Le Blanc, S. Franchoo, **K. Sieja** et al., *Probing nuclear structures in the vicinity of* ^{78}Ni *with* β *and* β*-n decay spectroscopy of* ^{84}Ga, Phys. Rev. C88 (2013) 047301.

22. T. Rzaca-Urban, M. Czerwinski, W. Urban, A.G. Smith, I. Ahmad, F. Nowacki and **K. Sieja**, *First observation of excited states in 87Se: Collectivity and j-1 anomally at N=53*, Phys. Rev. C88 (2013) 034302.

23. G. Gustafalla, D.D. DiJulio, M. Gorska, J. Cederkall, P. Boutachkov, P. Golubev, S. Pietri, H. Grawe, F. Nowacki, **K. Sieja** et al.,*Coulomb Excitation of ^{104}Sn and the strength of ^{100}Sn Shell Closure*, Phys. Rev. Lett.110 (2013) 172501.

24. M. Palacz, J. Nyberg, H. Grawe, **K. Sieja** et al. *N=50 core excited states in the ^{96}Pd nucleus*, Phys. Rev. C86 (2012) 014318.

25. A. Korgul, ..., **K. Sieja** et al., *Beta-gamma and beta-delayed neutron-gamma decay of neutron rich copper isotopes*, Phys. Rev. C86 (2012) 024307.

26. C. Hinke, M. Bohmer, P. Boutachkov, T. Faestermann, H. Geissel, J. Gerl, R. Gernhauser, M. Gorska, A. Gottardo, H. Grawe, J.L. Grebosz, R. Kruecken, N. Kurz, Z. Liu, L. Maier, F. Nowacki, S. Pietri, Zs. Podolyak, **K. Sieja** et al., *Superallowed Gamow-Teller decay of doubly magic ^{100}Sn*, **Nature** 486 (2012) 341.

27. E. Fiori, ..., **K. Sieja**, et al., *First g(2+) measurement on neutron-rich ^{72}Zn, and the high-velocity transient field technique for radioactive heavy-ion beams* , Phys. Rev. C85 (2012) 034334.

28. A. Dijon, ..., **K. Sieja** et al., *Discovery of a new isomeric state in ^{68}Ni: Evidence for a highly deformed proton intruder state*, Phys. Rev. C85 (2012) 031301R.

29. W. Urban, **K. Sieja** et al., *Isomeric levels in ^{92}Rb and the structure of neutron-rich, odd-odd Rb isotopes*, Phys. Rev. C85 (2012) 014329.

30. E. Rapisarda, ..., **K. Sieja** et al., *Coulomb excitation of the 3- isomer in ^{70}Cu*, Phys. Rev. C84 (2011) 064323.

31. B.S. Nara Singh et al., and **K. Sieja**, 16^+ *Spin-gap isomer in ^{96}Cd*, Phys. Rev. Lett. 107 (2011) 172502.

32. P. Boutachkov et al. and **K. Sieja**, *High spin isomers in ^{96}Ag: Excitations across the Z=38 and Z=50, N=50 closed shells*, Phys. Rev. C84 (2011) 044311.

33. F. Naqvi, M. Gorska, L. Caceres, A. jungclaus, M. Pfutzner, H. Grawe, F. Nowacki, **K. Sieja** et al., *Isomer spectroscopy of ^{127}Cd*, Phys. Rev. C82 (2010) 034323.

34. G. Simpson, W. Urban, **K. Sieja**, et al., *Near-yrast, medium-spin exitations in ^{91}Rb, ^{93}Rb and ^{95}Rb*, PRC82 (2010) 024302.

35. J. Ljungvall, ..., **K. Sieja**, et al., *Onset of collectivity in neutron rich Fe isotopes: Toward a new island of inversion?*, Phys. Rev. C81 (2010) 061301R.

36. J.M. Daugas et al. and **K. Sieja** and F. Nowacki, *Low-lying isomeric levels in ^{75}Cu*, Phys. Rev. C81 (2010) 034304.

37. A. Shrivastava, M. Caamano, M. Rejmund, A. Navin, A. Lemasson, C. Schmitt, L. Gaudefroy, **K. Sieja**, et al., *Prompt γ spectroscopy of isotopically identified fission fragments*, PRC 80, 051305(R) (2009).

38. W. Urban, **K. Sieja**, G. Simpson, H. Faust, T. Rzaca-Urban, A. Złomaniec, *et.al. New isomers and medium-spin structure of the* ^{95}Y *nucleus*, Phys. Rev. C79 (2009) 044304.
39. L. Cáceres, M. Górska, M. Pfützner, A. Jungclaus, H. Grawe, F. Nowacki, **K. Sieja**, S. Pietri *et al. Spherical proton-neutron structure of isomeric states in* ^{128}Cd, Phys. Rev. C79 (2009) 011301 (R).
40. T. Rzaca-Urban, **K. Sieja**, W. Urban, F. Nowacki, J.L. Durell, A.G. Smith and I. Ahmad, *The* $(h_{11/2}, g_{7/2})_{9^-}$ *excitations in Sr isotopes*, Phys. Rev. C79 (2009) 024319.
41. E.-W.Grewe, C. Bäumer, H. Dohmann, D. Frekers, M.N. Harakeh, H. Johansson, K. Langanke, G. Martínez-Pinedo, F. Nowacki, I. Petermann, L. Popescu, S. Rakers, D. Savran, **K. Sieja**, H. Simon, J.H. Thies, A.M. van den Berg, H.J. Wörthe and A. Zilges, *Studies on the double-beta decay nucleus* ^{64}Zn *using the (d,* ^2He*)-reaction*, Phys. Rev. C77 (2008) 064303.

- Refereed conference proceedings

1. **K. Sieja**, *Low energy dipole strength from large scale shell model calculations*, submitted to Eur. Phys. J. A.
2. **K. Sieja**, *Collectivity above the closed* ^{78}Ni *and* ^{132}Sn *cores*, Acta Phys. Polonica B247 (2016) 883.
3. H. Naidja, F. Nowacki, **K. Sieja**, *Recent Advances in the Shell Model Calculations of the Spectroscopic Properties of* $^{134-138}Sn$, Acta. Phys. Pol. B46 (2015) 669.
4. H. Naidja, F. Nowacki, **K. Sieja**, *Spectroscopic properties of neutron rich nuclei beyond* ^{132}Sn *and seniority mixing*, J. Phys. Conf. Ser. 580 (2015) 012030.
5. A. Poves, F. Nowacki, **K. Sieja**, A.P. Zuker and S. M. Lenzi, *From N=2Z in* ^{60}Ca *to N=Z in* ^{80}Zr*: Connecting the driplines*, J. Phys. Conf. Ser. 580 (2015) 012007.
6. M. Palacz et al., *Odd-parity,* ^{100}Sn *core excitations*, Acta Phys. Polonica B44 (2013) 491.
7. F. Recchia et al., *Spectroscopy of neutron-rich Co nuclei populated in the Zn70+U238 reactions*, Journal of Physics Conference Series 381 (2012) 012082.
8. F. Recchia et al., *Toward the N=40 sub-shell closure in Co isotopes and the new island of inversion*, Phys. Scripta T150 (2012) 014034.
9. B. Nara Singh et al., *Spin-gap isomer in Cd96*, Journal of Physics Conference Series 381 (2012) 012074.
10. B. Nara Singh et al., *Exotic nuclear studies around and below A=100*, AIP Conf. Proc. 1409, 19-24 (2011).

11. A. Poves, E. Caurier, F. Nowacki and **K. Sieja**, *The Shell model towards the driplines*, Phys. Scripta. T150 (2012) 014030.
12. M. Moukaddam et al., *Search for 2d5/2 neutron states in ^{69}Ni*, Acta Phys. Pol. B42 (2011) 541.
13. W. Urban, H. Faust, M. Jentschel, U. Köster, J. Krempel, Th. Materna, P. Mutti, T. Soldner, J. Genevey, J.A. Pinston, G. Simpson, T. Rzaca-Urban, A. Złomaniec, M. Łukasiewicz, **K. Sieja**, F. Nowacki, *et.al.* , *Isomers in fission fragments*, AIP Conf. Proc. 1090 (2009) 494.
14. **K. Sieja**, T.L. Ha, P.Quentin and A. Baran, *Particle number conserving approach to correlations*, Int. J. Mod. Phys. E16 (2007) 289–297.
15. Andrzej Baran, Zdzislaw Łojewski and **Kamila Sieja**, *Pairing and α decay*, Int. J. Mod. Phys. E16 (2007) 320–327.
16. **Kamila Sieja** and Andrzej Baran, *Proton-neutron pairing in Lipkin-Nogami approach*, Acta Phys. Pol. B37 (2006) 107–113.
17. Andrzej Baran, Zdzislaw Łojewski and **Kamila Sieja**, *Superheavy nuclei in different pairing models*, Int. J. Mod. Phys. E15 (2006) 452–456.
18. **K. Sieja**, A. Baran and P. Quentin, *Skyrme force-like extension of nuclear pairing interaction*, Phys. Scr. T125 (2006) 220–221.
19. A. Baran, Z. Łojewski and **K. Sieja**, *Masses and half-lives of superheavy elements*, Acta. Phys. Pol. B36 (2005) 1369–1372.
20. A. Baran, Z. Łojewski and **K. Sieja**, *Ground state properties of superheavy elements in macroscopic-microscopic models*, EPJ A Direct (2005) DOI: 10.1140/epjad/i2005-06-006-4.
21. A. Baran, M. Kowal, Z. Łojewski and **K. Sieja**, *Properties of superheavy nuclei in various macroscopic-microscopic models*, Int. J. Mod. Phys. E14 (2005) 365–372.
22. Andrzej Baran and **Kamila Sieja**, *Neutron-proton pairing in 64Ge*, Int. J. Mod. Phys. E14 (2005) 445–450.
23. Andrzej Baran and **Kamila Sieja**, *Comparison of delta- and Gogny-type pairing interactions*, Acta Phys. Pol. B35, no3 (2004) 1291–1298.
24. Andrzej Baran and **Kamila Sieja**, *Delta-pairing forces and nuclear masses*, Int. J. Mod. Phys. E13 (2004) 113–116.
25. A. Baran, Z. Łojewski and **K. Sieja**, *State-dependent delta-pairing and spontaneous fission*, Int. J. Mod. Phys. E13 (2004) 353–356.

- Other

1. **K. Sieja**, F. Nowacki and G. Martinez-Pinedo, *Shell Model as Unified View of Nuclear Structure*, meeting report, Nuclear Physics News International 23 (2013) 36-37.

2. Q. Zhi, E. Caurier, J.J. Cuenca-Garcia, K. Langanke, G. Martinez-Pinedo and **K. Sieja**, *Shell model half-lives for r-process nuclei*, GSI Scientific Report 2013.
3. J.J. Cuenca-Garcia, E. Caurier, K. Langanke, G. Martínez-Pinedo, F. Nowacki, **K. Sieja**, *Shell model First-Forbidden beta decays for N=82 nuclei*, GSI Scientific report 2008, p168.
4. **K. Sieja**, W. Urban, G. Martínez-Pinedo and F. Nowacki, *Shell model description of isomers in mass A$\sim$ 95 region*, GSI Scientific report 2008, p167.
5. I. Petermann, K. Langanke, G. Martínez-Pinedo, **K. Sieja**, *Breaking of the SU(4) symmetry in the pf-shell nuclei*, GSI Scientific Report 2007, p129.

Chapter 9

Detailed CV

Kamila Sieja, M. Sc., PhD

9.1 Contact information

IPHC
23 rue du Loess
67037 Strasbourg Cedex
tel : (+33) 03.88.10.61.67
fax : (+33) 03.88.10.62.02
mail : Kamila.Sieja@iphc.cnrs.fr

Correspondence address: IPHC
23 rue du Loess
67037 Strasbourg Cedex

9.2 Personal informations

Date of birth	15.12.1978
Place of birth	Tarnobrzeg, Poland
Nationality	polish

9.3 Employment

- October 2012-present, Chargé de recherche CNRS (CR1), theory group, IPHC Strasbourg, France.

- December 2009-September 2012, post-doctoral researcher (CDD), theory group, Insitute Pluridisciplinaire Hubert Curien, Strasbourg, France.
- 2008-2009: post-doctoral research fellow, theoyr group, Helmholtz International Centrum for FAIR and Institut für Kernphysik, Technische Universität Darmstadt, Germany
- 2007-2008: post-doctoral research fellow, theory group, Gesellschaft für Schwerionenforschung, Darmstadt, Germany.

9.4 Education

- February 26, 2007: PhD in Maria Curie-Skłodowska University, Lublin, Poland and Université Bordeaux 1, Bordeaux, France.
  PhD thesis on 'Extended approach to correlations beyond mean-field in atomic nuclei' under supervision of Prof. A. Baran (UMCS) and Prof. P. Quentin (CENBG).
- June 21, 2002: Master of Science in Maria Curie-Skłodowska University, Lublin, Poland.
  Diploma on 'Collective pairing vibrations with delta-pairing forces' under supervision of Prof. B. Pomorska.

9.5 Research area

9.5.1 Research topics and tools developed

-2007- present

- Statistical properties of nuclei.
- Structure of exotic nuclei, shell evolution far from stability.
- Nuclear structure and weak decays in interface with astrophysics.
- Many-body forces in nuclear systems.
- Large scale shell model codes and empirical interactions.

-2002-2007

- Correlations beyond the mean-field: proton-neutron pairing, pairing vibrations.
- Pairing properties of rare-earth and superheavy nuclei.
- Higher Tamm-Dancoff Approximation, BCS and Lipkin-Nogami methods.
- Macroscopic-microscopic approaches.

9.6 Experience

9.6.1 Invited seminars

1. Warsaw University, Warsaw, Poland, January 2017:
   Shell model studies around close cores of ^{78}Ni and ^{132}Sn.

2. Consortium de Physique Théorique de Strasbourg, Strasbourg, France, January 2013:
   Shell Model as a Unified View of Nuclear Structure.

3. Institute de Physique Nuclèaire, Orsay, France, February 2010:
   Recent shell model studies of exotic nuclei.

4. Centre d'Etudes Nucléaires de Bordeaux Gradignan, Bordeaux, France, June 2009:
   Recent shell model studies of nuclei from Ni56 to Sn132.

5. Institut Pluridisciplinaire Hubert Curien, Strasbourg, France, March 2009: *Recent shell model studies of nuclei from Ni56 to Sn132.*

6. Institut Laue-Langevin, Grenoble, France, June 2008:
   Recent shell-model developments for medium-mass nuclei.

7. Sérvice de Physique Nuclèaire, CEA/DAM, Bruyéres-le-Châtel, France, June 2007:
   Ground state properties of $N = Z$ nuclei in HFBCS and HTDA descriptions.

8. Institute de Physique Nuclèaire, Orsay, France, January 2007:
   Proton-neutron pairing in the particle number conserving approaches.

9.6.2 Invited presentations in international conferences

1. International Collaborations in Nuclear Theory: Theory for open-shell nuclei near the limits of stability, Michigan State University, USA, 2015:
   Shell evolution and collectivity in model spaces above ^{78}Ni and ^{132}Sn cores.

2. FUSTIPEN topical meeting "Recent advances in the nuclear shell model", GANIL, France, 2014:
   Several recent SM results and their interest for nuclear astrophysics.

3. 11th Russbach School on Nuclear Astrophysics, Russbach, Austria, 2014:
   Recent developments in the large scale shell model and their interest for nuclear astrophysics.

4. 22 Congrès de la Société Francaise de Physique, Marseille, France, 2013:
   Recent developments in the nuclear shell model.

5. XLI International Workshop on Gross Properties of Nuclei and Nuclear Excitations, Hirschegg, Austria, 2013:
   Dipole excitations in the islands of inversions.

6. NUPNET-Sarfen Collaboration Meeting, Trento, Italy, 2012:
   Strasbourg-Madrid Shell Model Collaboration.

7. The first conference on Advances in Radioactive Isotope Science (joined ENAM and RIB conferences) Leuven, Belgium, 2011:
   Shell model studies along Z=28 and N=50 shell closures.

8. 1 Day Experiment and Theory at SPIRAL2, GANIL, France, 2010:
   New land of deformation south of ^{68}Ni.

9. 2nd EMMI-EFES workshop on Neutron-rich nuclear matter, nuclear structure and nuclear astrophysics, RIKEN-Wako, Japan, 2010:
   New land of deformation south of ^{68}Ni.

10. Workshop on shell effects, ESNT, Paris, France, 2010:
    Shell evolution towards and beyond ^{78}Ni.

11. Confrontation and convergence in nuclear theory, Trento, Italy, 2009:
    Shell evolution towards and beyond ^{78}Ni.

12. Workshop on Nuclear structure of the neutron-rich region around Z=28 towards and beyond N=50, Leuven, Belgium, 2009:
    Shell-model studies of N=40–50 region.

9.6.3 Contributed conferences and workshops

1. Nuclear Data, Bruges, Belgium, 2016:
   Dipole strength functions from LSSM in medium-mass nuclei.

2. Statistical Properties of Nuclei, ECT* Trento, Italy, 2016:
   Dipole strength functions from LSSM in medium-mass nuclei.

3. 19th Colloque GANIL, Angelet, France, 2015:
   Shell evolution and collectivity in the vicinity of ^{78}Ni.

4. Collective Motion in Nuclei under Extreme Conditions (COMEX), Krakow, Poland, 2015:
   Strength functions from the large scale shell model and their interest for nuclear astrophysics.

5. XXIV Mazurian Lakes Conference on Physics, Piaski, Poland, 2015:
   Shell evolution and collectivity in the vicinity of ^{78}Ni.

6. EGAN 2014 workshop, Darmstadt, Germany, 2014.

7. Workshop "The structure of 68Ni, current knowledge and open questions", Leuven, Belgium, 2014.

8. XVIII Colloque GANIL, Port en Bassin, France, 2013.

9. Zakopane Conference on Nuclear Physics, Zakopane, Poland, 2012:
Toward a universal monopole description of atomic nuclei.

10. Facets of Strong-Interaction Physics, Hirschegg, Austria, 2012.

11. Colloque GANIL, Belgodore, France, 2011:
Dipole excitations in the islands of inversion.

12. European Gamma and Ancillary Detectors Network workshop, Padova, Italy, 2011:
Shell model studies along Z=28 and N=50 lines.

13. FUSTIPEN inauguration workshop, GANIL, France, 2011:
Strasbourg-Madrid Shell Model collaboration.

14. Zakopane Conference on Nuclear Physics, Zakopane, Poland, 2010:
E1 excitations on nickel isotopes.

15. 10th International Spring Seminar on Nuclear Physics, Vietri, Italy, 2010:
Shell evolution and core excitations in semi-magic nickel and tin isotopes.

16. SPIRAL2 week, Caen, France, 2010:
Shell model and exotic nuclei.

17. XVI Colloque GANIL, Giens, France, 2009:
New island of inversion around N=40.

18. 6th Russbach Workshop on Nuclear Astrophysics, Russbach, Austria, 2009:
Shell-model half-lives for r-process nuclei at N=50, 82..

19. Workshop on Nuclear Physics, Havana, Cuba, 2009.

20. Zakopane Conference on Nuclear Physics, Zakopane, Poland, 2008:
Recent shell-model developments for medium-mass nuclei from ^{56}Ni to ^{132}Sn.

21. From quarks to nuclear many-body problem, Eivind Osnes 70th birtday, Oslo, Norway, 2008:
Shell model description of the shape transition in Zirconium isotopes.

22. Cross-fertilizations between shell-model and density functional theory, Saclay, France, 2008.

23. Deutsche Physikallische Gesellschaft Tagung, Darmstadt, Germany, 2008:
Shell model description of the shape transition in Zirconium isotopes.

24. Modern Aspects in Nuclear Structure and Reactions, Hirschegg, Austria, 2008.

25. Doctoral Training Programme, Trento, Italy, 2007:
Extended appraoch to correlations beyond mean-field in atomic nuclei.

26. XIII Theoretical Nuclear Workshop 'Marie and Pierre Curie', Kazimierz Dolny, Poland, 2006:
Particle number conserving treatment of correlations.

27. XXI Zakopane Conference on Nuclear Physics, Zakopane, Poland, 2006:
Particle number conserving treatment of correlations.

28. XII Theoretical Nuclear Workshop 'Marie and Pierre Curie', Kazimierz Dolny, Poland, 2005:
Proton-neutron pairing in Lipkin-Nogami approach.

29. XXIX Mazurian Lakes School on Physics, Piaski, Poland, 2005:
State-dependent proton-neutron pairing -restoration of particle number symmetry.

30. International Conference on Finite Fermionic Systems Nilsson Model 50 Years, Lund, Sweden, 2005:
Skyrme-force like extension of nuclear pairing interaction.

31. XI Theoretical Nuclear Workshop 'Marie and Pierre Curie', Kazimierz Dolny, Poland, 2004:
Proton-neutron pairing in RMF model.

32. The Fourth International Conference on Exotic Nuclei and Atomic Masses (ENAM'04), Callaway Gardens, Pine Mountian, USA, 2004:
Ground State properties of superheavy elements.

33. XXXIX Zakopane School of Physics, Zakopane, Poland, 2004:
Masses and half-lives of superheavy elements.

34. 3^{eme} Workshop de Physique Teorique, Strasbourg, France, 2003.

35. X Theoretical Nuclear Workshop 'Marie and Pierre Curie', Kazimierz Dolny, Poland, 2003:
Delta-pairing forces and nuclear masses.

36. XXVIII Mazurian Lakes Conference on Physics, Krzyze, Poland, 2003:
Comparison of Gogny and delta-type pairing interactions.

37. IX Theoretical Nuclear Workshop, Kazimierz Dolny, Poland, 2002:
Delta-pairing forces and collective vibrations.

9.6.4 Teaching experience

- CERN Geneva, October 2013, lectures and computing sessions in the ISOLDE Shell Model Course for Non-Practitionners (22hrs).
- Ecole Joliot-Curie September 2011, shadow lecturer in the shell model course.
- INFN Legnaro, October 2010- lectures and computing sessions in the Workshop on Shell Model Applications in Nuclear Spectroscopy (22hrs).
- GANIL Cean, December 2009- lectures and computing sessions in the Workshop on Shell Model Applications in Nuclear Spectroscopy (22hrs).
- IPHC Strasbourg, June 2009- European Summer University, tutor in computing sessions.
- GSI Darmstadt, Summer 2008- tutor in the Summer Student Programme.
- UMCS Lublin, 2005/2006- classes of quantum mechanics (40 hrs, ranked 4.75/5.0 by students).
- UMCS Lublin, 2002-2005- classes of elementary physics and electrodynamics (120hrs).

9.6.5 Tutor of students/post-docs

- IPHC Strasbourg, 2013-2014, H. Naidja (post-doc), 2 associated publications in Phys. Rev. Lett. and 1 in Phys. Rev. C.
- IPHC Strasbourg, 2012-2013, H. Sliwinska (PhD), 2 publications in Phys. Rev. C.
- GSI Darmstadt, 2008-2010, J.J. Cuenca-Garcia, (PhD), 1 publication in Phys. Rev. C.

9.6.6 Tutor of experimental PhD students for theory part of their work

1. K. Kolos, IPN Orsay, 2 publications in Phys. Rev. C.
2. P. Morfouace, IPN Orsay, 2 publications in Phys. Lett. B and Phys. Rev. C.
3. G. Gey, LPSC Grenoble, 1 publication in Phys. Rev. Lett.

9.6.7 Referee work

- since 2013, referee for Physical Review Letters.
- since 2012, referee for European Journal of Physics A.
- since 2012, referee for International Journal of Modern Physics E.
- since 2011, referee for Nuclear Physics A.
- since 2010, referee for Physical Review C.

9.6.8 Member of committees and expert

- 2015-2019, member of governing board of French -US Theory Institute for Physics with Exotic Nuclei (FUSTIPEN).
- since 2016, member of the Thesis Monitoring Committee (CST) in IPHC.
- since 2012, member of Scientific Council of Ecole Joliot-Curie.
- 2012, invited member of PhD jury of M. Moukaddam, IPHC Strasbourg.
- 2011, member (examiner) of the PhD jury of B. Tastet, IPNO Orsay.

9.6.9 Organization of conferences, seminars, colloquia

- 2015, organization of nuclear physics colloquia in XXIII General Congres of French Physical Society, Strasbourg, France.
- 2014, Chairman, Rencontres Jeunes Chercheurs, Strasbourg, France.
- 2013, member of Organizing Committee of Journées de Jeunes Chercheurs, France.
- 2013, member of Organizing Committee of XVIII Colloque GANIL, France.
- 2012, member of Organizing Committee of Ecole Joliot-Curie, Fréjus, France.
- 2012-2014, co-organization of Colloquia of Subatomic Department in IPHC.
- 2012, organization of workshop "Shell model as a unified view of nuclear structure", IPHC Strasbourg.
- 2010-2014, organization of seminars on nuclear physics in IPHC.
- 2009-2010, organization of SMANS2009 (GANIL, France) and SMANS2010 (INFN, Italy) workshops.
- 2004, editor of the special issue of the International Journal of Modern Physics E, proceedings of X Theoretical Nuclear Workshop 'Marie and Pierre Curie', Kazimierz Dolny, Poland, 2003.

9.7 Grants, scholarships, awards

- 2014-2018 Prime d'Excellence Scientifique CNRS.
- 2014, 36 months grant of Polish National Science Centre under the contract DEC-2013/09/B/ST2/03485, participation as theory expert.
- 2007, 3 months Marie Curie scholarship for the Doctoral Training Programme in ECT, Trento, Italy.
- 2005, 24 months grant of the Committee of Scientific Research (KBN) of the Polish Ministry of Science and Education, contract No. 1P03B13028.
- 2004, 15 months scholarship of The French Government for the realization of the PhD thesis in collaboration with prof. P. Quentin (CENBG) (thèse en co-tutelle).
- 2004, conference scholarship of Fundacja na Rzecz Nauki Polskiej (The Foundation for Polish Science).

9.8 Proficiency in languages

- polish : native
- english, french : conversational
- german, spanish : basic